

**“ A comparative petrological and geochemical study of garnetiferous
rocks associated with base metal deposits in the Kanmantoo Trough:
meta-exhalites or synmetamorphic alteration zones?”**

Marnie Kate Smith, BSc.

NATIONAL GRID REFERENCE

S1-54
Echunga
6627-I
(1:50000)

Thesis submitted as partial fulfilment of the requirements for the
Honours Degree of Bachelor of Science

December 1998

Department of Geology and Geophysics

The University of Adelaide

ABSTRACT

Garnetiferous rocks show a spatial association with several base metal deposits in the Early Cambrian Kanmantoo Trough. These rocks include cotiules (garnet-quartz rocks) and banded iron formation (BIF) and are hosted by pelitic metasediments of the Tapanappa Formation. Petrological and geochemical investigations have been made of garnetiferous rocks associated with the Scotts Creek Ag-Pb-Zn and Angas Pb-Zn deposits and in the vicinity of the Kanmantoo Cu deposit.

Geochemical features indicate variations between cotiules from the three localities but general similarities with cotiules from Broken Hill, N.S.W. BIF from the Kanmantoo area is also comparable to the equivalent lithologies in the Willyama Complex, at Olary and Broken Hill. Geochemical diagrams ($Fe-Mn-(Co+Cu+Ni)$, $Al/(Al+Fe+Mn)$ vs Fe/Ti , TiO_2 vs. Al_2O_3 and chondrite-normalised rare earth element (REE)) for cotiules and iron formations suggest variable contributions of detrital and hydrothermal components. The hydrothermal component, is generally 30 to 50 wt. percent for cotiules, and >70 wt percent for BIF.

The stratigraphic position, layer parallel banding and unusual geochemistry suggest the cotiules associated with Scotts Creek, Kanmantoo and Angas deposits are exhalative in origin, and may be termed "meta-exhalites". The Kanmantoo BIF appears to have formed from high temperature submarine hydrothermal fluids and metalliferous sediments analogous to those of the Red Sea and the East Pacific Rise.

Cotiules and BIFs are indicators of hydrothermal activity and may be local guides to base-metal mineralisation. The Mn content of garnet in cotiules reflects proximity to Pb-Zn ore, and may be a useful exploration tool.

TABLE OF CONTENTS

ABSTRACT

Page

LIST OF FIGURES PLATES AND TABLES

CHAPTER 1

INTRODUCTION

1.1 Preamble	1
1.2 Previous work	2
1.3 Project Aims and Methods	3

CHAPTER 2

GEOLOGICAL SETTING

2.1 Regional Geology	5
2.2 Mineralisation	6

CHAPTER 3

SCOTTS CREEK Ag-Pb-Zn DEPOSIT

3.1 Introduction	8
3.2 Structure	8
3.3 Mineralisation and Host Rocks	9
3.3.1 Coticules	9
3.3.2 Biotite-microcline-garnet schist	10
3.3.3 Biotite-Garnet schist	10
3.4 Electron Microprobe Mineral Analyses of Garnet	10
3.4.1 Results	10
3.5 Whole-rock Geochemistry	11
3.5.1 Introduction	11
3.5.2 Results	12

3.6 REE Geochemistry	12
3.6.1 Introduction	12
3.6.2 Results	13
3.7 Interpretation and Discussion	13

CHAPTER 4

KANMANTOO GARNETIFEROUS ASSEMBLAGES

4.1 Introduction	16
4.2 Petrological Investigations	17
4.3 Electron Microprobe Mineral Analyses of Garnet	18
4.4 Whole-rock Geochemistry	19
4.4.1 Results	19
4.5 REE Geochemistry	19
4.5.1 Results	20
4.6 Interpretation and Discussion	20

CHAPTER 5

ANGAS Pb-Zn DEPOSIT AND GARNET RICH BANDS

5.1 Introduction	23
5.2 Petrological Investigation of Garnet Rich Bands	23
5.3 Electron Microprobe Mineral Analyses of Garnet	24
5.3.1 Results	24
5.4 Whole-rock Geochemistry	25
5.5 REE Geochemistry	25
5.6 Interpretation and Discussion	26

CHAPTER 6

DISCUSSION AND CONCLUSIONS

6.1 Comparative Discussion of Garnetiferous Assemblages27
6.2 Petrogenesis of the Garnetiferous Rocks29
6.3 Conclusions31
 6.3.1 Further investigations33

ACKNOWLEDGMENTS35

REFERENCES

APPENDICES:

- Appendix A: Hand Specimen and petrological description of samples
- Appendix B: XRF analysis – major and trace elements
- Appendix C: Electron microprobe analysis of garnet

LIST OF FIGURES

Figure No.

- 1 Location map of base metal sulphide deposits in the Kanmantoo Group, south eastern Mount Lofty Fold Thrust Belt. Modified from Flöttmann, Haines and Gum, (1996)
- 2 1:1000 structural map of Scotts Creek shear zone
- 3 Photos and photomicrographs of minerals from Scotts Creek
- 3a Example of open style fold from Scotts Creek with prominent axial planar foliation typical of first major deformational event. (Spry et al. 1988, D₂)
- 3b Type 2 fold of psammite and pelite layers within Scotts Creek shear zone indicating axial planar cleavage
- 3c Refolded earlier foliation of muscovite grains forming crenulation cleavage (S₂) in shear zone, Scotts Creek, note folded sulphide layer
- 3d Photomicrograph of layered mineralisation within a host rock of fine grained spessartine garnet coticule. Note the deformed layers, Scotts Creek
- 3e Outcrop of coticule within a finely laminated quartz-biotite schist, Scotts Creek
- 3f Photomicrograph of almandine rich garnets in garnetiferous schist, Scotts Creek. Note size of garnet grains compared to coticule garnets from same area.
- 4 Ternary diagram of electron microprobe analyses of garnets plotted in terms of Sp (spessartine), Alm + Pyr (almandine + pyrope) and Gr (grossular) endmembers
- 5a Histogram showing endmember composition of garnets from Scotts Creek, Broken Hill (Spry, 1990) and from control sample 1113-282
- 5b Histogram showing endmember composition of garnets from Angas prospect, Broken Hill (Spry, 1990) and from control sample 1113-282
- 5c Histogram showing endmember composition of garnets from Kanmantoo field area, Broken Hill (Spry, 1990) and from control sample 1113-282
- 6a REE pattern for coticules from field areas (stippled) compared with REE patterns from unaltered Tapanappa Formation metasediment, and garnetiferous schist control sample
- 6b REE pattern for coticules from field areas compared with REE patterns of Broken Hill coticules (stippled) (Spry *et al.* in press)
- 6c REE pattern for BIF from Kanmantoo (stippled) compared with REE patterns of unaltered Tapanappa Formation metasediment, and garnetiferous schist control sample
- 6d REE pattern for BIF from Kanmantoo field area compared with REE patterns of BIF from Broken Hill and Olary Block, Willyama Complex (stippled) (Spry *et al.*, in press)
- 7a Ternary plot of Fe-Mn-(Cu+Co+Ni) x 10 for coticules and BIF from field areas (Wonder *et al.*, 1988)

- 7b Ternary plot of Fe-Mn-(Cu+Co+Ni) x 10 for coticles and BIF from Broken Hill, Australia (Spry, 1990)
- 8a Fe/Ti versus Al/Al+Fe+Mn plot for BIFs, coticles and sulphide rich garnet-muscovite-quartz-biotite schist from the study areas (Spry *et al.*, in press)
- 8b Fe/Ti versus Al/Al+Fe+Mn plot for BIFs and coticles from Broken Hill, Australia (Spry *et al.*, in press)
- 9a Al₂O₃ wt% versus TiO₂ wt % for metasedimentary rocks and coticles from Scotts Creek (Spry *et al.*, in press)
- 9b Al₂O₃ wt% versus TiO₂ plot for metasedimentary rocks and coticles from Broken Hill, Australia. (Spry *et al.*, in press)
- 10a REE pattern for hydrogenous, hydrothermal and mixed Mn sediments compared with REE patterns of coticles from the field areas (stippled) (Spry, 1990)
- 10b REE pattern for hydrogenous, hydrothermal, and mixed Mn sediments compared with REE patterns of BIF from Kanmantoo field area (stippled) (Spry, 1990)
- 11 Interpretive stratigraphic map of the Kanmantoo Field area. 1:5000 scale
- 12a Very fine grained coticle (sample 1113-283) from boudinaged layer south east of Kanmantoo mine
- 12b Microphotograph of sample 1113-283 illustrating very altered fine grained garnets in a matrix of quartz, with trace chlorite
- 12c Photograph of Kanmantoo BIF in thin section illustrating fine quartz and magnetite bands. No garnet present in this sample
- 12d 'Background' almandine type garnets with inclusion rich cores in a matrix of quartz, biotite and staurolite
- 12e "Background" sample 1113-282 showing typical garnetiferous schist devoid of mineralisation in the Kanmantoo region
- 12f Pale pink garnet rich coticle band from DDH 31, sample no. 1113-90. Located within garnetiferous envelope from Angas Pb-Zn deposit.
- 12g Photomicrograph of garnet rich coticle band indicating fine grained pale pink garnets with relatively inclusion free cores.
- 12h Surface coticle sample 1113-281 in a matrix of quartz, relict andalusite and staurolite.
- 13 Schematic cross section and open pit plan of Kanmantoo Cu mine (Seccombe *et al.* 1985)
- 14 Generalised cross section of Angas prospect showing garnetiferous envelope

Chapter 1

INTRODUCTION

1.1 Preamble

The south-eastern flank of the Mount Lofty Ranges, South Australia, is composed of regionally metamorphosed and multiply deformed schists of the Cambrian Kanmantoo Group, which host several small base metal sulphide deposits (Fig. 1). Spatially associated with the base metal deposits are stratabound zones of metamorphic rocks with comparatively unusual mineral assemblages, and/or with abnormal concentrations of garnet, including coticles and banded iron formation (BIF) which are confined to the Tapanappa Formation (Toteff, in press), a sequence of metasediments devoid of volcanics, within the Kanmantoo Group (Parker, 1986; Preiss, 1987).

The term coticle was originally coined by Renard (1878) to describe a rock containing essentially spessartine garnet in a matrix of sericite and/or quartz. It has since been modified by Spry *et al.* (in press) to include all garnet-quartz rocks regardless of garnet composition, since intimate spatial relationships among spessartine-quartz-rich rocks, almandine-rich rocks, and grossular-quartz rich rocks occur in various localities (e.g., Broken Hill, Australia, Spry and Wonder, 1989). Garnet content is variable although garnet and quartz are the dominant phases and minor amounts of other minerals such as gahnite, magnetite, apatite, biotite and muscovite may be present.

Coticles have been reported within, above or beneath many metamorphosed massive sulfide deposits (e.g. Stumpfl, 1979; Spry, 1988). Examples include: Broken Hill and Pegmont, Australia (Vaughan and Stanton, 1986; Spry and Wonder, 1989; Lottermoser, 1989), Aggeneys, and Gamsberg, South Africa (Rosendaal and Stumpfl, 1984; Ryan *et al.*, 1986; Spry, 1988) and the Sullivan and North Star deposits, British Columbia (Slack *et al.*, 1998).

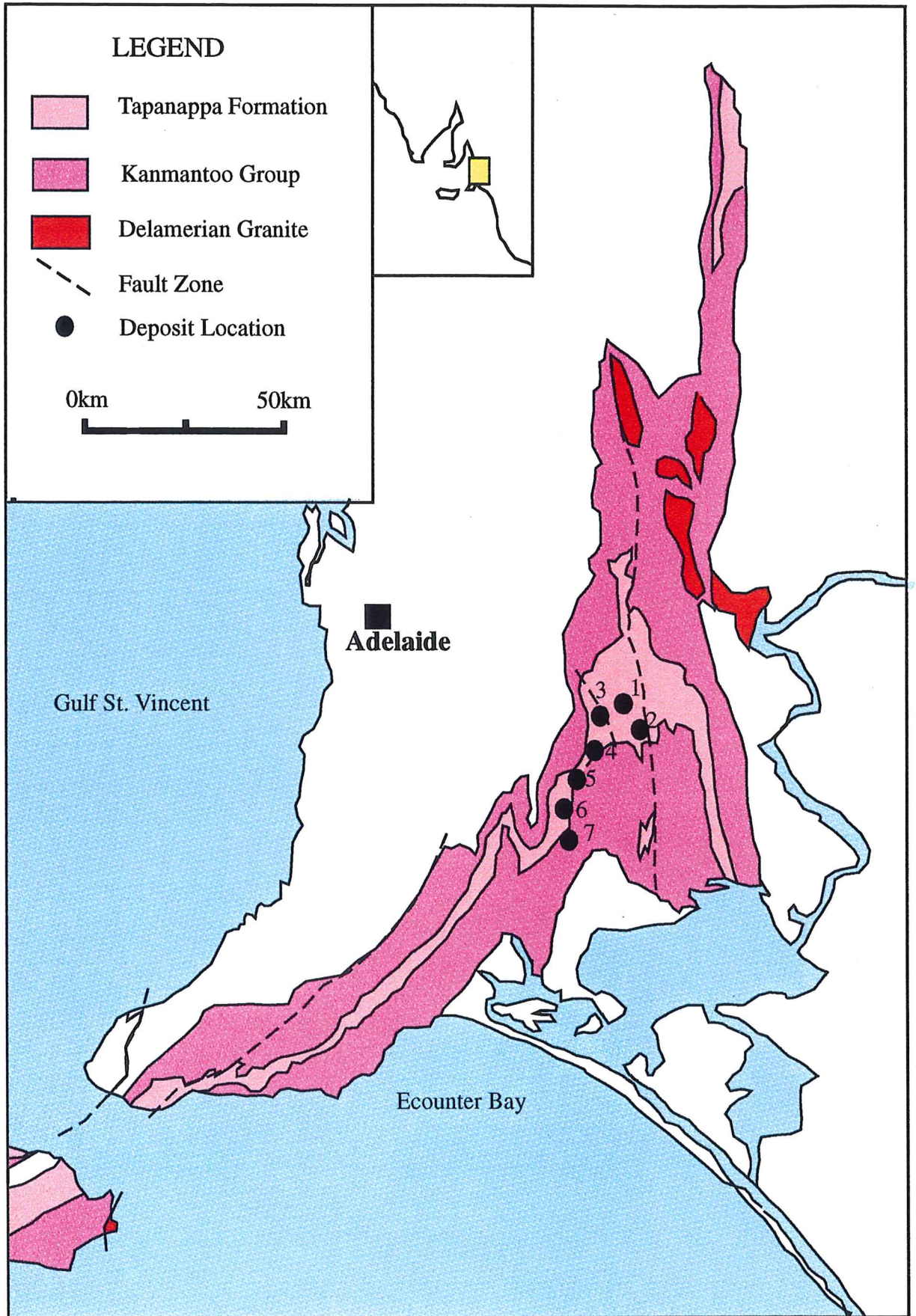


Fig.1. Regional geology of Kanmantoo Group, showing extent of Tapanappa Formation and locations of main mineral deposits. 1. Kanmantoo, 2. Bremer, 3. Scotts Creek, 4. Aclare, 5. Wheel Ellen, 6. Strathalbyn, 7. Angas. From Both et al. 1995. Locations 1, 3 and 7 represent location of field areas.

Coticules associated with ore deposits are generally regarded as having a submarine exhalative origin, and are referred to as 'meta-exhalites' (Wonder *et al.*, 1988; Spry *et al.*, in press). Other examples of meta-exhalites associated with sulphide ores are tourmalinite, apatite-rich rocks, quartz-gahnite rocks, zincian staurolite-bearing rock and barite-rich rocks (Spry *et al.*, in press).

Iron formations are also found in close spatial association with many sulphide ores (e.g. Appel, 1979; Hoy *et al.*, 1984; Troop, 1984) and have been interpreted as ore-equivalent facies at Broken Hill and Pegmont, Australia (Richards, 1966; Stanton and Vaughan, 1979). Iron formations are considered to be indicators of palaeohydrothermal activity (Spry *et al.*, in press) and are therefore potential exploration tools for base metal mineralisation.

The garnetiferous assemblages associated with the Kanmantoo sulphide deposits are of significance to exploration in the region, yet debate still arises over whether they represent meta-exhalites, synmetamorphic alteration features, or metamorphosed alteration zones (e.g. Both *et al.*, 1995; Oliver *et al.*, 1998; Toteff, in press).

1.2 Previous Work

The enigmatic nature of the base metal deposits, due largely to metamorphic overprinting and deformation, has led to considerable speculation over the origin(s) of the Cu and Pb-Zn deposits. Previous ideas include:

- A syn-sedimentary origin for the Pb-Zn deposits in the Kanmantoo Group and a related pre-metamorphic, sub-seafloor origin for the Kanmantoo Cu deposit (Seccombe *et al.*, 1985).
- An epigenetic, fracture and lineament controlled origin of the deposits (Thomson, 1975; Parker, 1986) which has since been revived by Solomon and Groves (1994), who support a syn-metamorphic origin.
- A late syn-tectonic origin for the Kanmantoo Cu deposit proposed by Oliver *et al.* (1998).
- A "probabalistic approach" by Marshall and Spry (in press) who suggested pre-tectonic emplacement related to hydrothermal activity of the ore deposits in the Kanmantoo Group, which have been substantially modified by deformation and metamorphism.

Previous work on garnetiferous assemblages within the Kanmantoo Group include:

- An investigation of the garnet rich rocks surrounding the Kanmantoo Cu mine and various lead-zinc deposits in the Kanmantoo Group by Faulkner (1996), who interpreted them as exhalites.
- Geochemical observations of the garnet envelope associated with the Angas Pb-Zn prospect by McElhinney (1994) and Both *et al.* (1995), who interpreted the feature as meta-exhalite.
- Descriptions by Toteff (in press) of garnetiferous rocks including coticles associated with the Scotts Creek and Angas Pb-Zn deposits and the Kanmantoo Cu deposit and a BIF north of the Kanmantoo deposit – all of which he interpreted as meta-exhalites.
- Recognition of garnetiferous rocks by Oliver *et al.* (1998) within the Kanmantoo Cu Mine, close to the present field area, who related the phenomenon to metasomatic processes on the basis that the high garnet content (up to 95%) would be ‘very difficult to attain from metamorphism of normal sediments.’

1.3 Project Aims and Methods

The main aim of this study is to investigate the geological setting, mineralogy and geochemistry of coticles and iron formations spatially associated with base-metal sulphide deposits within the Kanmantoo Group, in order to establish the origin of these garnetiferous assemblages and determine any genetic relationship with the associated ore deposits.

For this study three field areas were chosen within the Kanmantoo-Strathalbyn region, situated approximately 50 kilometres east to southeast of Adelaide (Fig.1): viz. a zone of garnet rich lithologies north and east of the Kanmantoo copper (Cu) mine, the Angas lead-zinc (Pb-Zn) prospect, and the Scotts Creek silver-lead-zinc (Ag-Pb-Zn) deposit (see Fig. 1 for locations).

Excellent examples of garnet-quartz rocks are displayed in fresh drill core from the Angas prospect, and in relatively unweathered outcrop at Scotts Creek. Garnet-quartz rocks from the Kanmantoo vicinity, although substantially weathered and poorly outcropping exhibit more variation in mineralogy, and are associated with a BIF. The choice of three deposits enables a comparison to be made between the Pb-Zn deposits and with Cu deposits.

Methods used to assist in investigation of the above aim involved:

- Structural mapping of the Scotts Creek Shear Zone and interpretive stratigraphic mapping of the Kanmantoo garnetiferous lithologies.
- Sampling from the areas mentioned above and from drill core of the Angas prospect.
- A petrological investigation of polished thin sections selected from the three field areas.
- A geochemical study of the samples collected including whole rock (major, trace and REE) and electron microprobe mineral analyses.
- Research of similar literature examples to provide a comparative basis to the project.

Chapter 2

GEOLOGICAL SETTING

2.1 Regional Geology

The southern Adelaide Fold-Thrust belt consists of high grade crystalline basement inliers overlain by Neoproterozoic Adelaidean sediments and the Cambrian Kanmantoo Group (Fig. 1). The Kanmantoo Group is a thick succession of clastic flysh-like metasediments, comprised of predominantly psammitic rocks interlayered with aluminous pelites, black shales, minor carbonates and rare calc-silicate rocks (Mancktelow, 1979). The apparent thickness of the Kanmantoo Group is up to 15 km (Thomson, 1969) although thrusting may have resulted in repetition of units, suggesting the true thickness is approximately 7-8 km. (Haines *et al.*, 1996). The units were rapidly deposited between 526 and 518 Ma (Sandiford *et al.*, 1995) in the eastward-deepening, fault controlled Kanmantoo Basin (Flöttmann *et al.*, 1994; Flöttmann and Cockshell, 1996; Flöttmann and James, 1997), then subsequently deformed, metamorphosed and intruded by granitic magmas during the Delamerian Orogeny, (480-524 Ma) (Turner *et al.*, 1993; Foden *et al.*, in press).

The tectonic and structural evolution of the Adelaide Fold Thrust Belt has been widely investigated (e.g. Offler and Fleming, 1968; Manktelow 1979, 1990; Jenkins 1990; Jenkins and Sandiford, 1992; Flöttmann *et al.*, 1994). The region is dominated by an imbricate set of SW-NE trending thrust faults which dip approximately 15-35°SE. On the south eastern margin of the Mount Lofty Ranges, the metamorphosed sequences are folded around upright to gently inclined, symmetric structures (Offler and Fleming, 1968; Mancktelow, 1990). Complex foliation patterns associated with the development of these folds, particularly in the higher grade parts of the belt, suggest a number of phases of deformation which has led to numerous interpretations of the structural history of this region (Offler and Fleming, 1968; Mancktelow, 1990; Sandiford *et al.*, 1992; Preiss, 1995). The main upright fold structures are probably a second generation feature (denoted D2 by Spry *et al.* 1988; Preiss, 1995) which at least in the regions of highest grade metamorphism, overprint a primary developed layer-parallel foliation (denoted S1 by Spry *et al.* 1988; Preiss, 1995)(Fleming and White, 1984),

the significance of which remains controversial (Marlow and Etheridge, 1978; Steinhardt 1989; Mancktelow, 1990).

Mineral assemblages in pelitic rocks of the Kanmantoo Group indicate that regional metamorphism is of low pressure-intermediate temperature type and reached middle amphibolite facies grade. Maximum pressures and temperatures reached during metamorphism were between 530° and 630°C and between 2.2 and 5.4 kb (Spry *et al.*, 1988).

Mancktelow (1979) identified five progressive metamorphic zones, namely, biotite-muscovite-chlorite, andalusite (kyanite)-staurolite, fibrous sillimanite (fibrolite), sillimanite and migmatite, within the amphibolite facies and showed that the zone boundaries are discordant to the fold belt. Timing of metamorphism shows some subtle variations. Metamorphism in the migmatite zone commenced prior to the appearance of penetrative structures (Offler and Fleming, 1968), while at lower grades, metamorphic minerals overgrow developing S₂ (by Spry *et al.* 1988), suggesting that metamorphism was contemporary with deformation of the fold belt.

2.2 Mineralisation

The majority of mineralisation in the Kanmantoo Group in the Strathalbyn to Kanmantoo areas occurs within the Tapanappa Formation (Seccombe *et al.*, 1985; Both, 1990) (Table 1), which is conspicuously more pelitic than other formations in the Kanmantoo Group. The predominant host rocks are quartz-mica schist and/or quartz-mica-andalusite schist which are probably metamorphosed aluminous sediments of terrigenous origin. Garnet bearing metasediments such as sulphide bearing garnet-muscovite-quartz-biotite rock, quartz-garnet-gahnite rocks, very fine-grained cotiules and thick intervals of andalusite-quartz-biotite-garnet ± staurolite schist, along with BIF, form part of the host rock sequence.

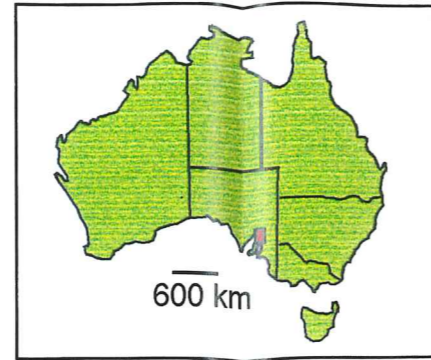
The relatively high-grade metamorphic conditions in the Strathalbyn-Kanmantoo area are indicated by the presence of andalusite or staurolite in rocks of appropriate composition, and are therefore assigned to the andalusite-staurolite metamorphic zone, with metastable fibrolitic sillimanite (Offler and Fleming, 1968; Mancktelow, 1990).

Table 1: Production data for the main mines in the Tapanappa Formation, Kanmantoo – Strathalbyn area (modified from Both, 1990; Flöttmann *et al.* 1998).

Historical Production Data							
Mine	Years of Operation	Ore Production (t)	Cu%	Pb%	Zn%	Other	References
Cu							
Kanmantoo	1971-1976	4,050,000	1				Seccombe et al.(1985)
Bremer	1850-1907 ^a	~35,000	~8				Dickinson (1942)
Scotts Creek	1848-1851	ore production and grade unknown					
Aclare	1859-1896 ^b	~14000 ^b		~7 ^b	~12 ^b	~680g/t Ag ^b	Chilman (1982)
						~2 g/t Au ^b	
Wheal Ellen	1857-1908 ^b	~75,000	<1	20 ^b	25 ^b	370 g/t Ag ^b 4.5 g/t Au ^b 49% As	Wade and Cochrane (1954). Askins (1968)
Strathalbyn	1848-1858	2000t ^c		18.5 ^c		500g/t Ag ^c	Seccombe et al. (1985)
Current Mineral Resources							
Deposit		Pre-Resource Estimate	Cu%	Pb%	Zn%	Ag g/t	
Kanmantoo		8,000,000	1.1				Seccombe et al. (1985)
Angas		1,000,000		4	10	60	Anderson (1993)
Mt Torrens		700,000		6.4	1.6	41	Anderson (1993)

a - production not continuous; b – grade of dressed ore; c – estimated values of grade (Brown,1908)

P-T estimates from coexisting sulphides provide direct evidence that the base metal sulphides were also subjected to peak metamorphic conditions. The sphalerite geobarometer, utilising Fe content of sphalerite, yields pressures of 4.1 ± 0.3 KB at the Wheal Ellen, Aclare and Brukungu deposits (Spry *et al.*, 1988). The arsenopyrite geothermometer indicates a minimum temperature of 500°C for ore at the Aclare mine, compared to minimum temperature estimates of approximately 500°C according to the garnet-biotite geothermometer for samples of metasediments from the Kanmantoo and Dawsley areas (Spry *et al.*, 1988).



ADELAIDE	ONKAPARINGA	TEPKO
NOARLUNGA	ECHUNGA	MONARTO
WILLUNGA	MILANG	ALEXANDRINA

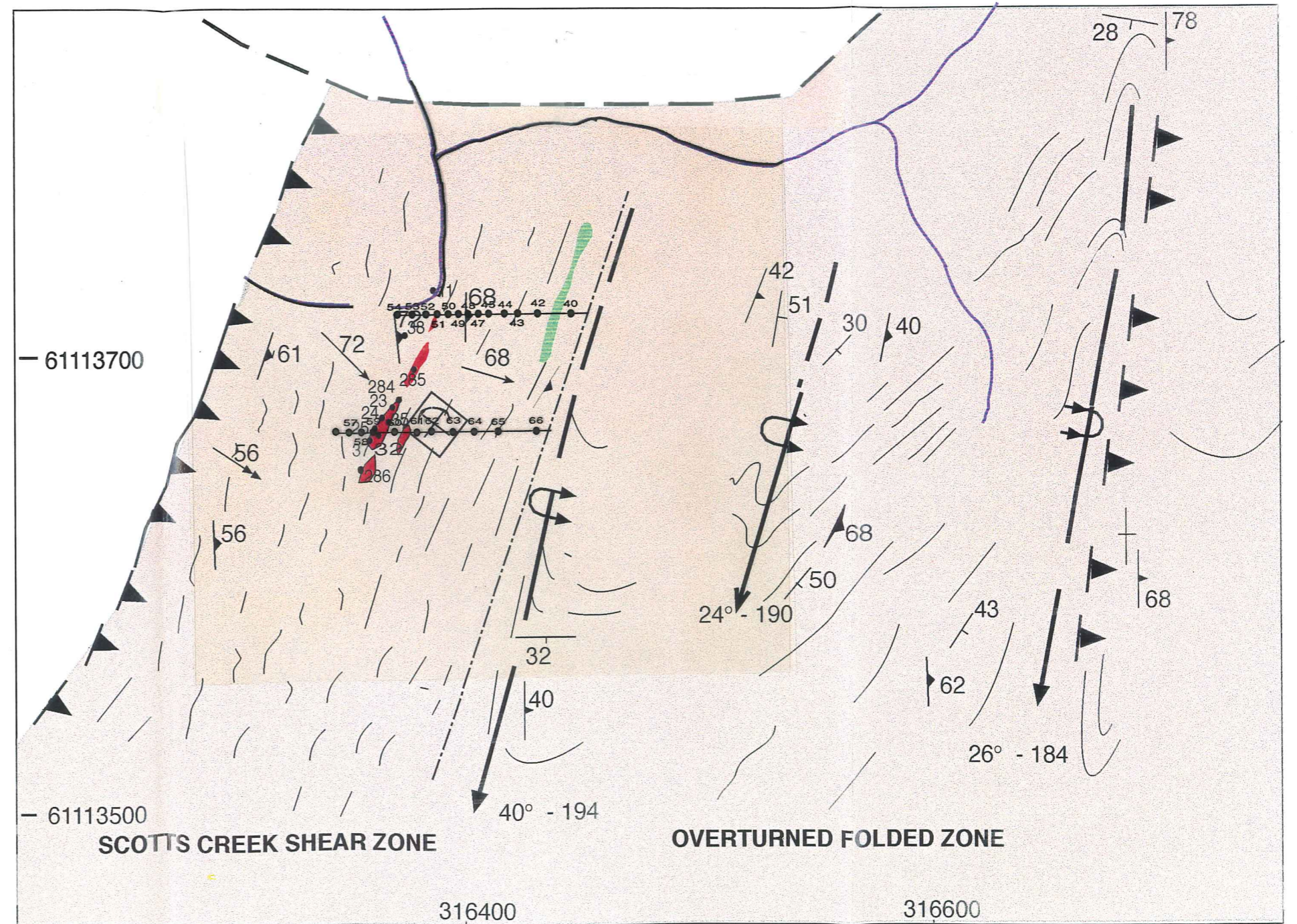
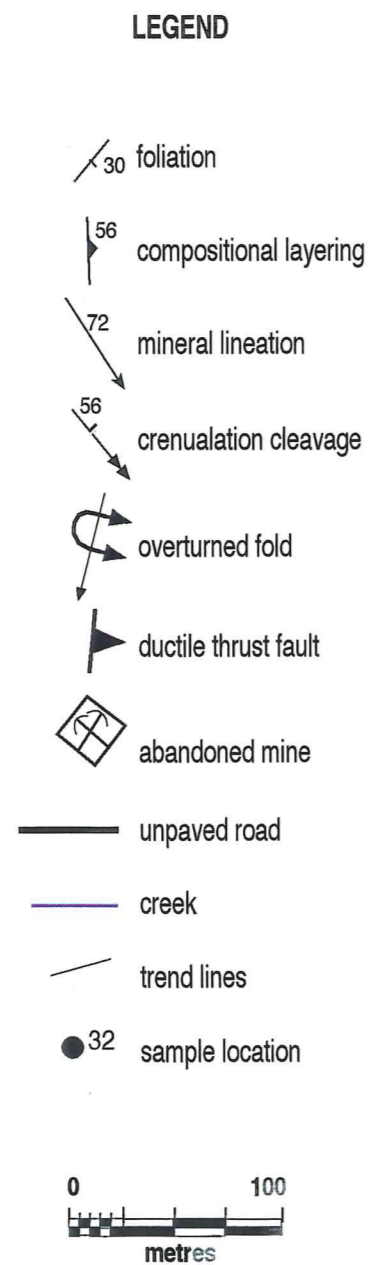
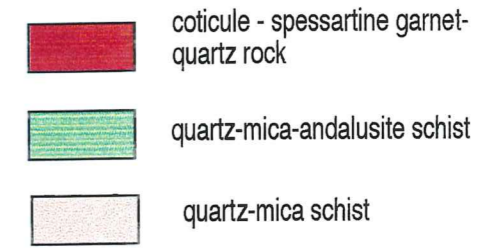


Figure 2. STRUCTURAL INTERPRETATION OF SCOTTS CREEK SHEAR ZONE

Chapter 3

SCOTTS CREEK Ag-Pb-Zn DEPOSIT

3.1 Introduction

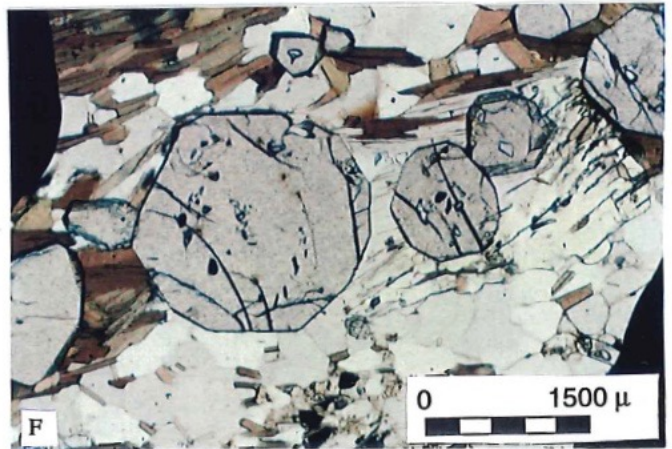
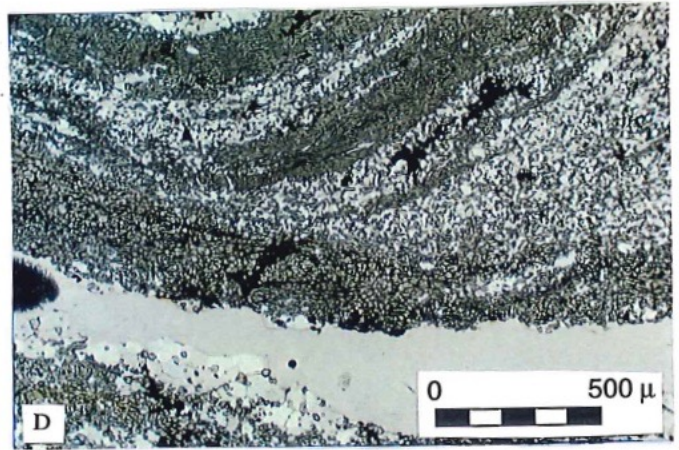
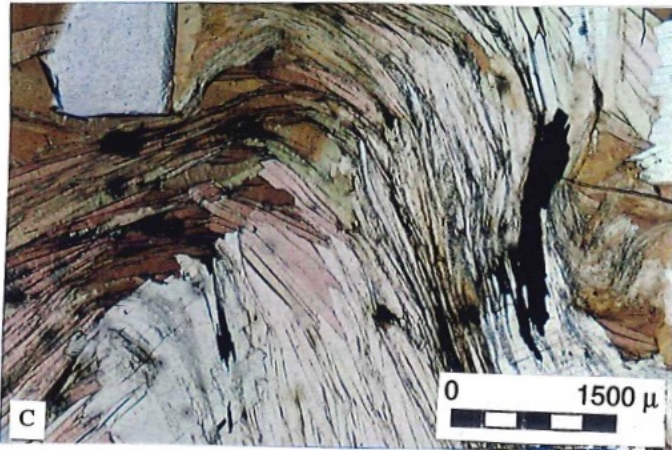
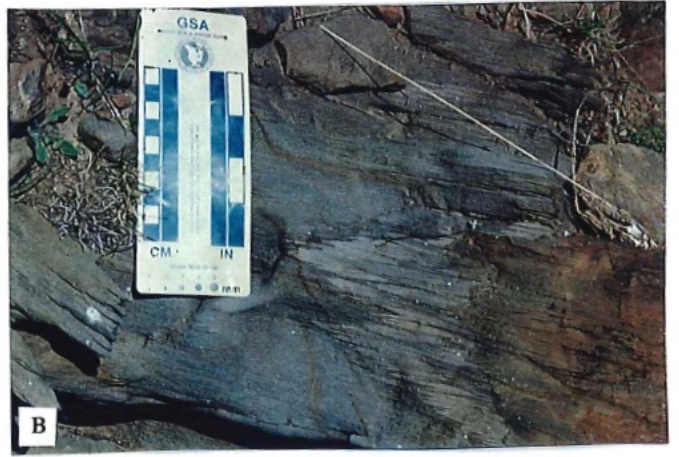
The Scotts Creek Ag-Pb-Zn deposit (Figs. 1, 2; Table 1) is located 5 km south of the Kanmantoo township and consists of three tabular bodies striking 010° and dipping 70° to the east. Ore production and grade has not been recorded, although Toteff (in press) recorded dressed ore grades of 50-60% Pb and 1500-2200 g/t Ag. Assaying of mineralisation in the mine dump material revealed 3-7% Pb, 0.5-2% Zn, 200-600 g/t Ag and 0.5 g/t Au (Toteff, in press). The host rocks consist of quartz-mica-andalusite schists and quartz-mica-schists with mineralisation occurring as layers within a fine grained garnet-quartz rock. This fine grained spessartine garnet-quartz rock associated with the Scotts Creek Ag-Pb-Zn orebody is a textbook example of a cotecule, as originally defined by Renard, 1878. This rock has been interpreted by Toteff (in press) and Spry *et al.* (in press) as a meta-exhalite, although shearing through the orebody suggests a possibility of syn-tectonic formation.

3.2 Structure

Three deformation periods are recognised at Scotts Creek. The first folding event is readily observed as open to tight overturned folds that generally strike N-S and plunge shallow to moderately south. Folding has resulted in the development of a dominant N-S striking axial planar foliation defined by alignment of platy biotite grains within the host quartz-biotite schist. The Scotts Creek Ag-Pb-Zn orebody occurs within the sheared out western limb of an overturned syncline. This forms the transitional zone of a ductile shear zone which strikes NE-SW and dips moderately to the SE and is evidenced by disharmonic type 2 folds developed where rocks have anisotropy due to alternate layers of andalusite-quartz-mica schists and quartz-biotite schists. Shearing is also evidenced by mullions, rodding lineation and boudinage quartz veins aligned parallel to foliation, and folded layers transected by a dominant axial planar cleavage (Fig. 3b). Intense elongation lineation indicates a W-WNW shear sense.

Figure 3

- A: Mesoscale close to open type 2 fold (limbs thinner than hinge) indicative of second generation deformation (D_2) in the Scotts Creek field area. Axial planar foliation (S_1) evident crosscutting bedding which is defined as compositional layering between coarse grained andalusite pelite layers and quartz-biotite psammite layers. Photo taken looking south.
- B: A tight to close, type 2 fold, from within the ductile shear zone at Scotts Creek. This style of fold is common within the shear zone, and is also present within upright shallow dipping eastern limbs of macroscale D_2 folds juxtaposing the shear zone. This common style present within the shear zone, and in the overturned folded zone of Scotts Creek presents evidence that the shear zone is a D_3 deformation feature. Prominent axial planar foliation is also indicated in the figure, where a folded psammite layer has been cross cut by foliation (S_2). Deformation feature is a synform, and photo has been taken looking south.
- C: Microphotograph of microscale deformation features of pelite within lower boundary thrust zone. Muscovite platy grains are original layer parallel foliation that have been folded around axial planar foliation to form crenulation folding and cleavage (S_2). Fibrolite present in left and right hand corners of photograph as dark grey fibrous material is also strongly deformed,. The fibrolite overgrows existing recrystallised minerals suggesting mineral growth was late syn D_3 deformation and most likely the product of shearing on the precursor mineral assemblage. Note folded sulphides (black) suggesting that both minerals formed pre or early syn shear deformation.
- D: Sample 1113-37 of a coticule taken proximal to the main shaft at Scotts Creek. Fine grained spessartine rich pale pink, disseminated and layered garnet occur within a granoblastic matrix of annealed quartz grains, minor apatite and layered sulphides. Dark beige bands constitute 100% garnet. Note folded layers of sulphides and garnet-quartz.
- E: Outcrop photo looking south at coticule band (approximately 20cm wide) situated west of the main shaft, Scotts Creek, within the shear zone. The lithology exhibits compositional layering indicated by darker and light bands. The darker bands consist of predominantly spessartine rich garnet. The coticule is layer parallel to host well laminated quartz-biotite schist and is also parallel to foliation.
- F: Microphotograph of large garnets within sample 1113-38, from a quartz-biotite-garnet-andalusite-staurolite schist located 30 metres west of main shaft at Scotts Creek, in a 50cm outcrop pod. Garnets are relatively inclusion free, align to foliation, or compositional banding (Both near parallel to each other) and are almandine rich. This reflects the precursor sediment chemistry away from the coticule bands and mineralisation, where Fe is becoming more predominant than Mn.



At the lower boundary of the thrust zone, extremely deformed pelite layers exhibit folded primary (S₁) foliation and the development of crenulation cleavage (S₂) (Fig. 3c). A third deformation period is observed in the area as isolated kink folds, which cross cut the shear zone in an E-W direction. The shear zone is interpreted as forming late D₃, using the structural nomenclature of Spry *et al.* (1988).

3.3 Mineralisation and Host Rocks

Samples taken from the waste dump at Scotts Creek indicate that the ore consists of deformed bands of disseminated galena and sphalerite with trace to minor chalcopyrite, pyrite and pyrrhotite (Fig. 3d). Galena is also present in local fracture veins indicating some remobilisation within the more brittle horizons. The mineralisation is hosted by a sequence of weakly to well laminated quartz-biotite and quartz-muscovite-biotite schists with rarer quartz-biotite-andalusite schists, which are parallel to the axial planar foliation. Detailed petrological descriptions are given in Appendix A.

3.3.1 Coticules

Approximately 12 metres west of the main shaft (Fig. 2), within the finely laminated quartz-biotite schist are rare, discontinuous layers of pale pink spessartine garnet-quartz rocks, or coticules, which reach a maximum width of 20 cm and crop out along strike for approximately 80 m before being lost under soil cover (Fig. 3f). The coticules consist of varying proportions of quartz and garnet (average ~ 60%, up to 100% in some bands) with trace amounts of muscovite, biotite, ilmenite, rutile, pyrite and apatite. Bedding on a fine scale is preserved as alternating bands (~2 mm width) composed of differing mineral assemblages, which in places, wraps an axial planar cleavage. Euhedral to subhedral garnets are generally fine grained and range from 10 µm to 100 µm in diameter. Inclusions of predominantly quartz and trace hematite, magnetite, ilmenite, and biotite are found in the garnet cores. Samples collected *in situ* from within the main shaft show that the immediate host to mineralisation is a well layered (> 2mm) coticule with accessory minerals muscovite, biotite, and microcline with lesser rutile, apatite and magnetite

3.3.2 *Biotite-microcline-garnet schist*

Immediately north of the mine and outcropping for approximately 5 m along strike (refer to Fig.2 for sample locations) is a finely laminated biotite-microcline-quartz-garnet schist (sample no. 1113-45). Recrystallised, highly strained microcline grains exhibit deformed twinning and occur as both axial planar veins and as a main component in the matrix. Larger euhedral crystals of garnet (~2 mm) which lack inclusions are concentrated near the vein selvage. Smaller, euhedral garnet crystals are present as folded bands about an axial planar foliation in sample no. 1113-50.

3.3.3 *Biotite-garnet schist*

At the base of the shear zone a lens of biotite-plagioclase-garnet schist with rare muscovite-andalusite-staurolite-fibrolite-chlorite and quartz outcrops for approximately 0.5 metres along strike and occurs in a local interval of quartz-mica \pm andalusite schist. Garnet occurs as both small (50 μ m) and larger euhedral crystals (3 mm) (Fig. 3f).

3.4 *Electron Microprobe Analyses of Garnet*

3.4.1 *Results*

Chemical compositions of garnets were determined from coticles (samples 1113-32, -35, -37) and other garnet bearing schists (1113-38, -45, -50, refer to Appendix C for data). Garnets in both coticles and other garnet-bearing rocks are dominated by spessartine and almandine components; grossular and pyrope components are present in lesser amounts (Fig.4). Garnets in coticles contain higher proportions of spessartine (up to 68 wt. %) than garnets in surrounding lithologies (the biotite-plagioclase-garnet schist and the biotite-microcline-quartz garnet schist), which have an average of ~15.3 wt % spessartine and when compared to garnets not associated with mineralisation (~3 wt % spessartine) (Fig.5a). The garnets not associated with mineralisation were sampled 5 km north of the Kanmantoo mine and herein, represent background analyses (sample 1113-282).

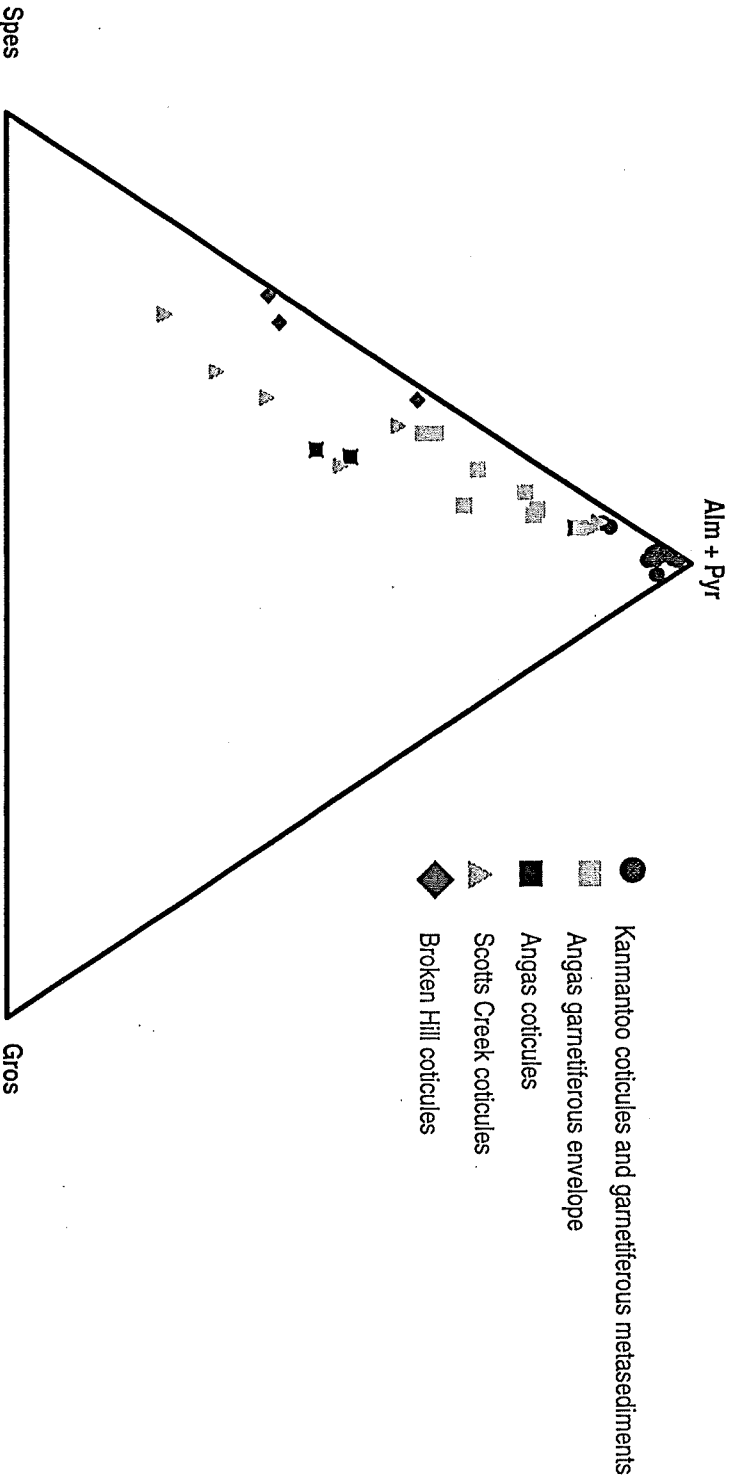


Fig.4 Ternary plot of electron microprobe analyses of garnets plotted in terms of spessartine (Spes) almandine and pyrope (Alm + Pyr) and grossular (Gros) endmember compositions

Figure 5

- a: Histogram of electron microprobe analyses of garnet from garnetiferous assemblages at Scotts Creek showing variation in content of garnet endmember components; almandine, spessartine, grossular and pyrope. Field samples have been compared to garnet composition from garnet in unmineralised andalusite-biotite-garnet-quartz-muscovite-staurolite (background) schist (sample no. 1113-282) and coticles from Broken Hill (Spry and Wonder, 1990) (sample nos. 43, 342, and 279). An antithetic relationship exists between the almandine and spessartine components of garnets in garnetiferous assemblages from Scotts Creek. Sample no. 1113-11 is approximately 100m north of the main shaft (refer to fig.2), and sample 37 is from the coticle layer immediately adjacent to the main shaft.
- b: Histogram of electron microprobe analyses of garnet from garnetiferous assemblages at Kanmantoo showing variation in content of garnet endmember components; almandine, spessartine, grossular and pyrope. Field samples have been compared to garnet composition from garnet in unmineralised andalusite-biotite-garnet-quartz-muscovite-staurolite (background) schist and coticles from Broken Hill (Spry and Wonder, 1990).
- c: Histogram of electron microprobe analyses of garnet from coticles in Angas drill core and surface sample 1113-281 showing variation in content of garnet endmember components; almandine, spessartine, grossular and pyrope. Field samples have been compared to garnet composition from garnet in unmineralised andalusite-biotite-garnet-quartz-muscovite-staurolite (background) schist, coticles from Broken Hill (Spry and Wonder, 1990) and analyses of garnet from the main host unit, upper host unit and lower host unit of the garnetiferous envelope (McElhinney, 1994).

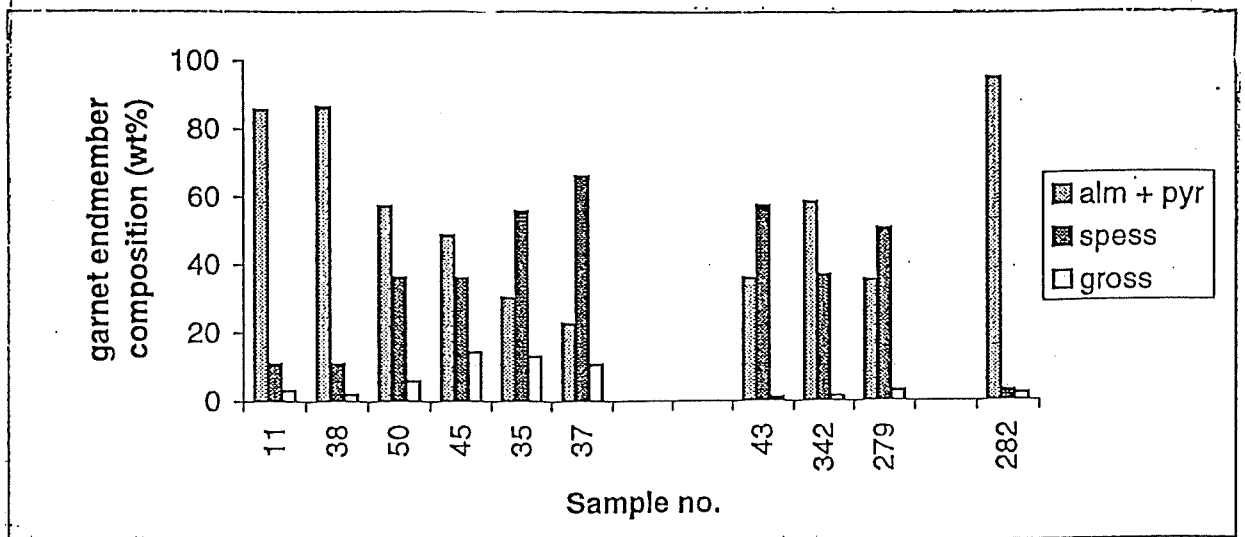


Fig. 5a Histogram of garnet composition from garnets at Scotts Creek

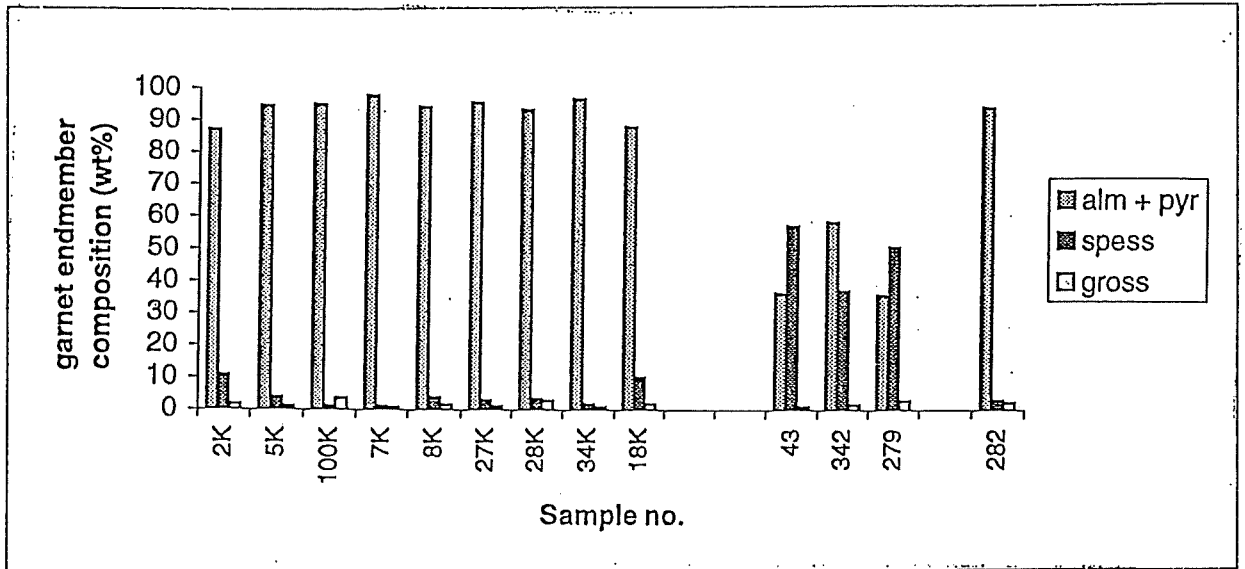


Fig. 5b. Histogram of garnet composition from garnets at Kánmántoo

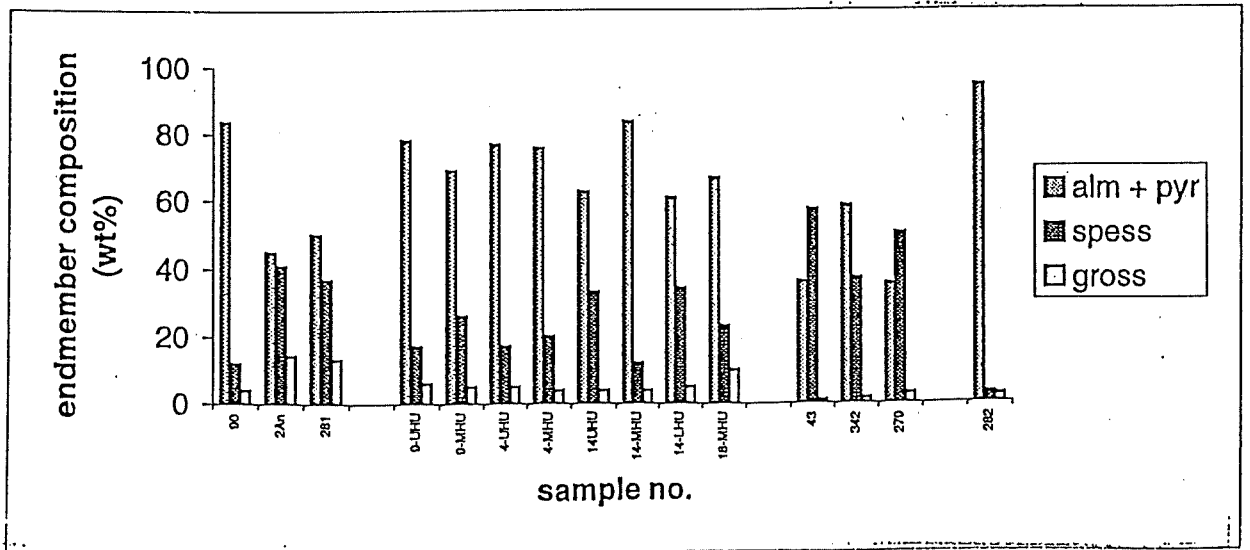


Fig. 5c Histogram of garnet composition from garnets at Angás

Microprobe analysis of the more almandine rich garnetiferous schists shows very slight normal zoning within individual grains, with Mn and Ca concentrated at the core of the grains and Fe and Mg concentrated at the rims.

These zoned garnets commonly have larger domains from which to derive the necessary elements, or are surrounded by other ferromagnesian silicates. Banded coticles from Scotts Creek show very little difference in garnet composition between the various layers and generally lack normal compositional zoning within individual grains.

The general lack of compositional zoning of the garnets is attributable to the segregation-depletion process (Hollister, 1966), which for coticles acts on a very small scale of a volume only a few times the volume of the garnet.

An antithetic relationship exists between Mn wt. % and Fe wt % in garnets north along strike of the orebody. A marked Mn wt % increase is observed in garnets proximal to the orebody (samples 1113-11 to 1113-37, Fig. 5a), which corresponds to a marked decrease in the Fe content of the garnets. This relationship is not apparent in whole rock analyses of the samples.

3.5 Whole-rock Geochemistry

3.5.1 Introduction

A variety of plots of analytical data have been used in the literature to determine the origin of coticles. Several authors have utilized the ternary plot of Fe-Mn-(Cu+Co+Ni) x 10 (e.g. Bonatti, 1975; Toth, 1980; Spry, 1990), and a plot of Fe/Ti versus Al/(Al+Fe+Mn) (e.g. Barrett, 1981; Spry, 1990). Bonatti *et al.* (1972) showed that Co, Cu and Ni are more concentrated in hydrogenous Fe-Mn sediments than in hydrothermal sediments, primarily because the accumulation rate of hydrogenous sediment is much slower than that of hydrothermal sediments, allowing scavenging of these elements by Fe and Mn mineral particles.

Due to their coherent geochemical behaviour, REE are also particularly useful in tracing igneous, sedimentary and metamorphic processes.

The behaviour of the REE in modern seafloor hydrothermal environments is sufficiently well known to make comparisons with ancient samples and therefore deduce past processes and/or sources that controlled their distribution. Rare earth elements in coticles and BIF can originate from hydrothermal, hydrogenous, and detrital sources.

Whole rock analyses were performed on 21 samples of quartz-biotite schist and 9 of the coticule, collected across strike of the main shaft, along approximately 100 m long E-W traverses. Whole rock analyses are shown in Table 1, Appendix B. Samples 1113-23, -24, -25, -284, -285 and -286 represent the coticule layer west of the orebody and samples 1113-61, -62, and -64 represent the coticule within which mineralisation occurs.

3.5.2 Results

In general the most abundant components in the coticles are SiO_2 (48.2-68.3 wt %), Al_2O_3 (11.2-16.8 wt %), $\text{Fe}_2\text{O}_3\text{T}$ (4.6-8.3 wt %) and MnO (5-12.5 wt %). These values are within the range of values compiled for coticles from various locations by Spry *et al.* (p. 24, in press) for SiO_2 (31.3-94.3 wt %), Al_2O_3 (1.3-21.1 wt %), $\text{Fe}_2\text{O}_3\text{T}$ (0.8-37.4 %) and MnO (0.2-18.2 wt %). The proportion of each element is largely dependent upon the relative amounts of quartz and garnet, the composition of the garnet and the variety of minerals in the matrix (Spry, 1990). The MnO wt % in the coticule is anomalously high when compared to the surrounding metasediments (average of 0.1 wt %) with an average of 7% in the layers west of the mine, and a maximum of 12.5% in the mineralised zone. Both metasediments and the coticule are deficient in alkalis. MgO is variable but rarely exceeds 3.5 wt % in the metasediments and 2.0 wt % in the coticule. The mineralised host rock sample, 1113-64 is high in CaO (12.83 wt %) due to the increased feldspar content. Fe_2O_3 content is essentially constant in all samples, with the exception of 1113-53 sampled from an almandine garnet rich layer, with 13.31 wt % compared to an average of 6.2 wt %. Anomalously high amounts of Ba (up to 1373 ppm), when compared to surrounding metasediments (Ba_{ave} 400 ppm), occur proximal to the mine in metasediments and the main coticule horizon and are associated with elevated levels of Cu, Pb and Zn

3.6 Rare Earth Element (REE) Geochemistry

3.6.1 Introduction

A suite of 5 rock samples from Scotts Creek were analysed for their REE contents. One sample was analysed from the coticule near the mineralised zone (1113-284) and four from along strike of the distinctive coticule layer west of the mineralised zone (1113-23, -24, -25, -286).

A garnet rich quartz-mica schist sample (1113-282) not associated with mineralisation, or affected by shearing was collected 5 km north of Kanmantoo mine has been included as a control for comparison, along with unaltered Tapanappa metasediments (from Turner *et al.*, 1992). Analytical results are presented in Table 1, Appendix B.

3.6.2 Results

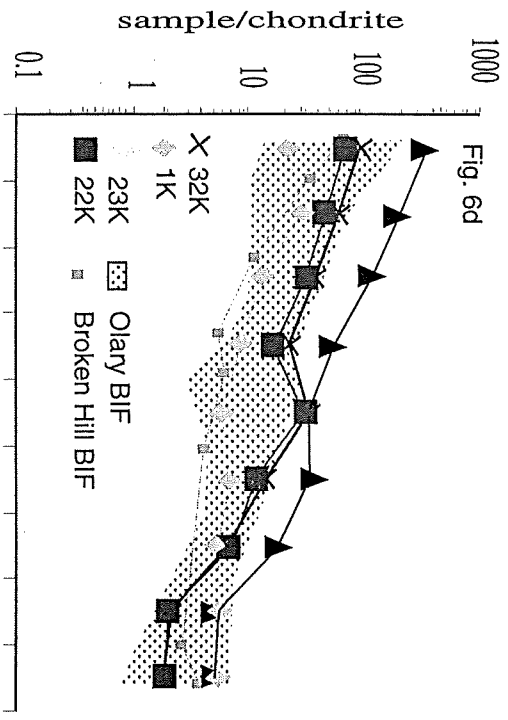
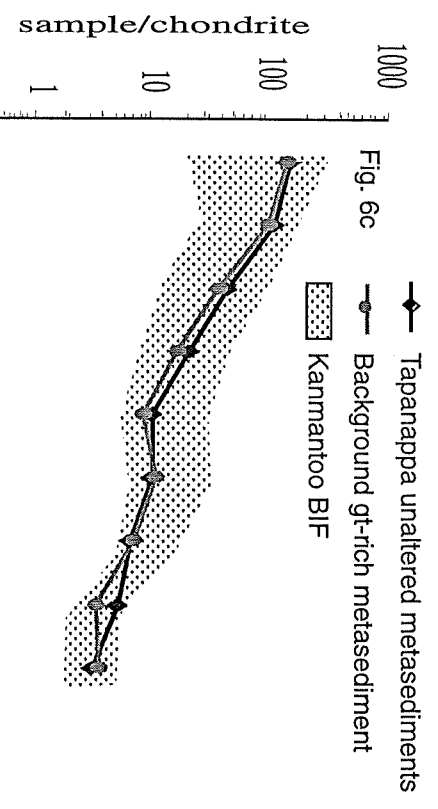
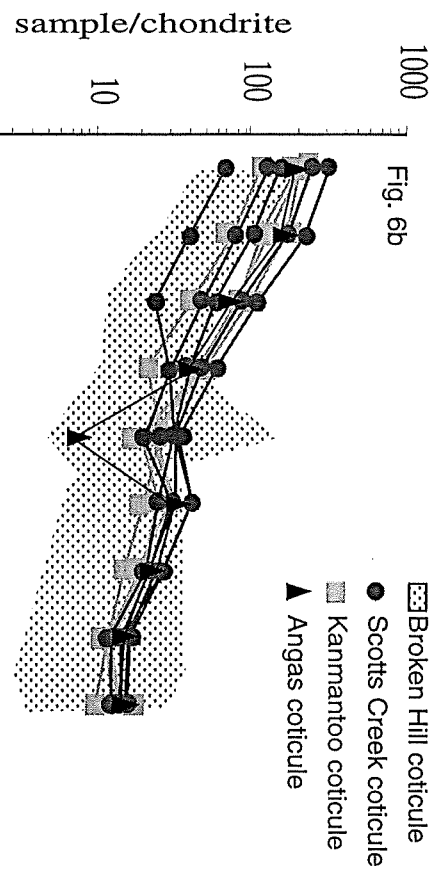
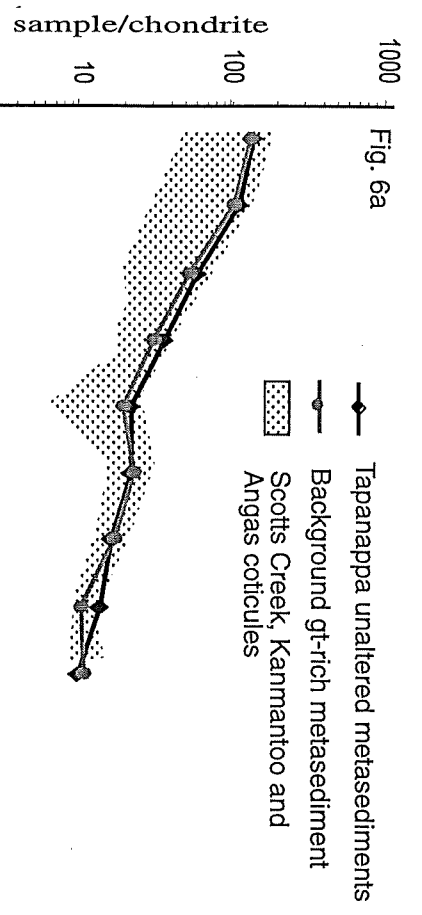
The coticules show moderate enrichment in LREE and depletion in HREE and generally exhibit a small negative Eu anomaly (Fig. 6b). None of the coticules exhibit chondrite-normalised patterns reminiscent of metamorphic garnets, namely, HREE-enriched and LREE-depleted profiles (Gravuch, 1989). The REE patterns of the coticules at Scotts Creek are similar to the pattern for unaltered Tapanappa Formation metasediments that host the Scotts Creek Ag-Pb-Zn deposit and the background pattern (Fig. 6a).

3.7 Interpretation and Discussion

The Scotts Creek coticules that lie within metasediments of the Tapanappa Formation are present in two forms: (1) as a layer that hosts mineralisation and (2) as a stratigraphic unit in the footwall of the orebody that is essentially devoid of mineralisation. Garnets from both areas are similar in size, shape and abundance. The garnets are predominantly spessartine rich and occur as fine grained, pale pink euhedral grains in bands. The garnets are set in a mineralogically simple matrix of quartz, apatite + biotite + rutile + ilmenite.

Figure 6:

- a: Comparison between chondrite normalised (Boyton, 1984) rare earth element (REE) signature of Scotts Creek cotiules (stippled area), REE signature of unaltered metasediments from the Host Tapanappa Formation (Foden *et al.*, 1992), and “background” unmineralised garnet rich quartz-biotite-andalusite \pm biotite schist, sampled 5 km N of the Kanmantoo field site.
- b: Chondrite normalised (Boyton, 1984) REE signatures of cotiules sampled from Scotts Creek (1113-286 from ore host cotiule, samples -23, -24, -284, -285 from strike length, lateral to the main shaft), Kanmantoo cotiules (sample 283 taken 150m SE of the Cu mine; samples 1113-24, -25, -26, -27 from 150m E of the deposit), and Angas surface cotiule (sample 1113-281), compared with REE signature of Broken Hill cotiules (stippled area) (data from Spry *et al.*, in press).
- c: Chondrite normalised REE signature (Boyton, 1984) of BIF from Kanmantoo and (stippled area) sulphide-rich garnet-muscovite-quartz-biotite rock stratigraphically overlying the BIF, compared with background and unaltered Tapanappa Formation samples.
- d: Chondrite normalised REE signatures (Boyton, 1984) of BIF (samples 1113-01, 1113-22, 1113-23 sampled N along strike; sample 1113-32) and sulphide-rich staurolite-muscovite-quartz-bioite rock stratigraphically overlying the BIF, compared with Broken Hill BIF (Spry *et al.*, in press) and BIF from the Olary Block (stippled area). Note positive Eu anomalies for samples 1113-22 and 1113-23 which are indicative of reduced hot fluids.



Atomic No.

Atomic No.

Electron microprobe studies have illustrated a spatial relationship between Mn content of garnet in the coticule layer and proximity to base metal mineralisation, indicating a genetic link between the coticule and the mineralisation.

Thin coticule bands observed tightly folded around a high-grade axial planar schistosity and boudinaged coticule bands, reflect competency differences with the enclosing quartz-biotite schists. A process which occurred during the high grade deformation manifest in the shear zone and provides evidence of a pre-metamorphic origin for the coticule.

A ternary plot of Fe-Mn-(Cu+Co+Ni) x 10 (Bonatti *et al.*, 1972) has been used to constrain the depositional environment for the coticules (Fig. 7a). The Scotts Creek coticules plot in the hydrothermal field and have a chemical signature characteristic of metalliferous sediments from hydrothermal deposits. These are consistent with coticules from Broken Hill, Australia (Fig. 7b).

Bostrom and Peterson, (1969) showed that hydrothermal sediments contain very little Al but have high Fe/Ti ratios. Spry *et al.* (in press) further suggested that Fe and Mn are indicators of fossil zones of hydrothermal activity, whereas Al and Ti are contributed by detrital clastic material. Contamination of hydrothermal sediments by normal deep sea sediments dilute the hydrothermal elements, resulting in an enrichment of detrital elements (*i.e.* Al and Ti). In a plot of Fe/Ti versus Al (Al+Mn+Fe), Bostrom (1973) demonstrated the use of this method as a test for the presence of hydrothermal metalliferous constituents in deep sea sediments. Coticules from Scotts Creek plot close to the mixing curve between pelagic clays/terrigenous sediments and hydrothermal metalliferous precipitates. Most of the Scotts Creek coticule samples plotted in Figure 8a possess < 40% hydrothermal sedimentary input and display considerable contamination from pelagic and terrigenous sources. As a comparison, data from coticules at Broken Hill (Spry and Wonder, 1990) were plotted and demonstrate a similar source origin to coticules from the field sites to Broken Hill coticules (Fig. 8b).

This is further supported by a plot of TiO₂ versus Al₂O₃ by Spry *et al.* (in press) who showed a strong correlation among coticules and unaltered metasediments in the Broken Hill deposit, N.S.W. (Fig. 8b). These correlations were believed (Slack *et al.*, 1998b) to reflect similar processes of detrital sedimentation for clays, ilmenite and rutile for both lithologies, and therefore support a major detrital contribution to the coticules.

Figure 7:

- A: Ternary plot of Fe-Mn-(Cu+Co+Ni) x 10 for cotiules from Scotts Creek, Kanmantoo and Angas field sites and BIF from Kanmantoo; garnet envelope samples from Angas (McElhinney, 1994) with comparative fields of Red Sea metalliferous sediments (Bonatti, 1975) hydrogenous and hydrothermal sediments (Bonatti et al., 1972), and Fe-Mn crusts (Toth, 1980).
- B: Ternary plot of Fe-Mn-(Cu+Co+Ni) x 10 for cotiule samples from Broken Hill (Spry, 1990) with comparative fields of Red Sea metalliferous sediments (Bonatti, 1975) hydrogenous and hydrothermal sediments (Bonatti et al., 1972), and Fe-Mn crusts (Toth, 1980).

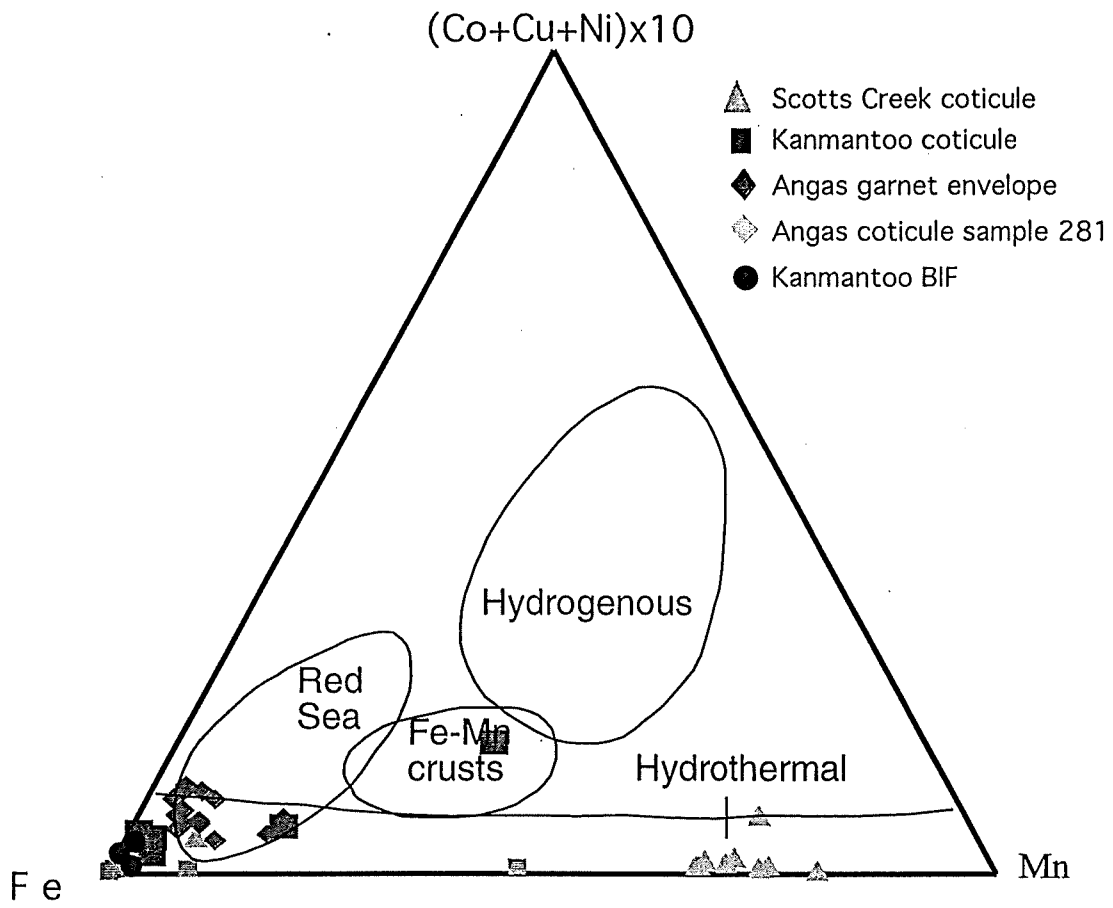


Figure 7a

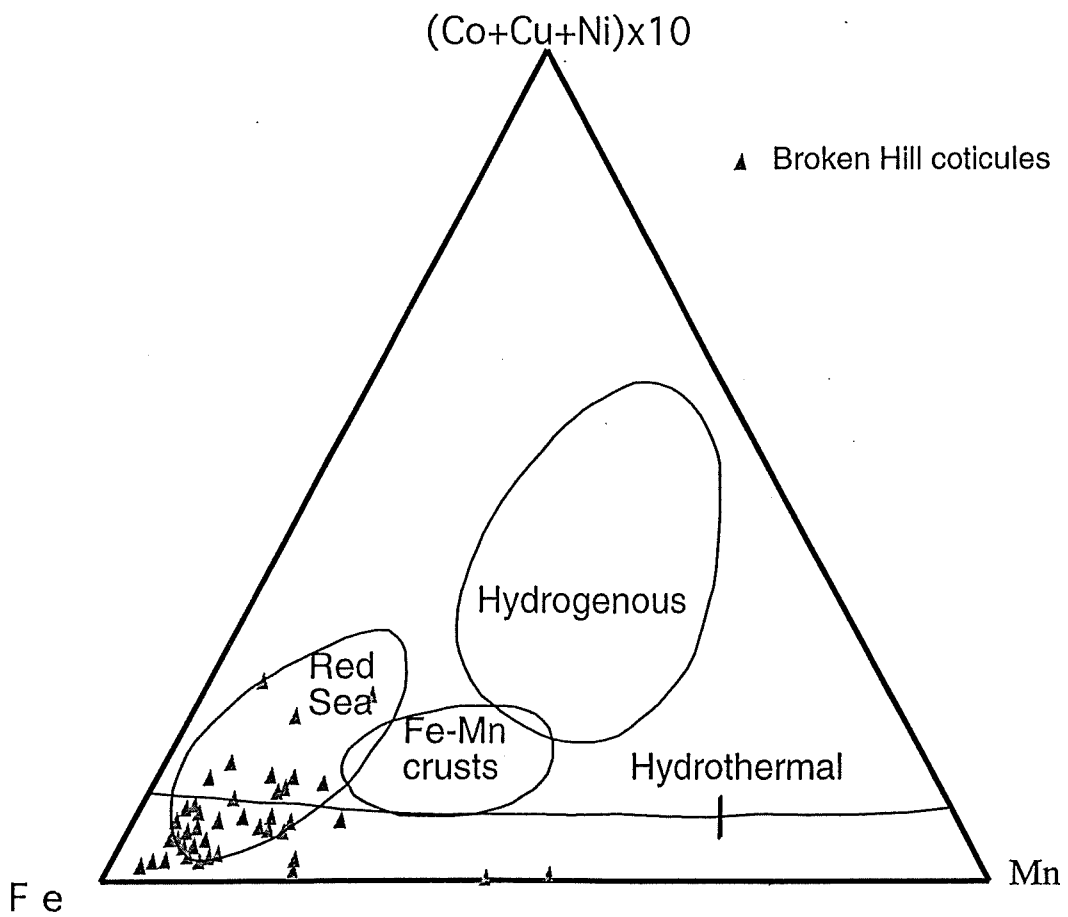


Figure 7b

Figure 8:

- a: Compositions of coticules and BIF from Scotts Creek, Kanmantoo and Angas and garnet envelope samples from Angas in terms of Fe/Ti versus $Al/(Al+Fe+Mn)$. Curves represent mixing of East Pacific Rise (EPR) and Red Sea (RS) sediment with terrigenous (TS) and pelagic sediment (PS). Numbers represent approximate amount of metalliferous sediment in the mixture (modified from Barrett, 1981).
- b: Compositions of coticules and BIF from Broken Hill (Spry et al., in press) in terms of Fe/Ti versus $Al/(Al+Fe+Mn)$. Curves represent mixing of East Pacific Rise (EPR) and Red Sea (RS) sediment with terrigenous (TS) and pelagic sediment (PS). Numbers represent approximate amount of metalliferous sediment in the mixture (modified from Barrett, 1981).

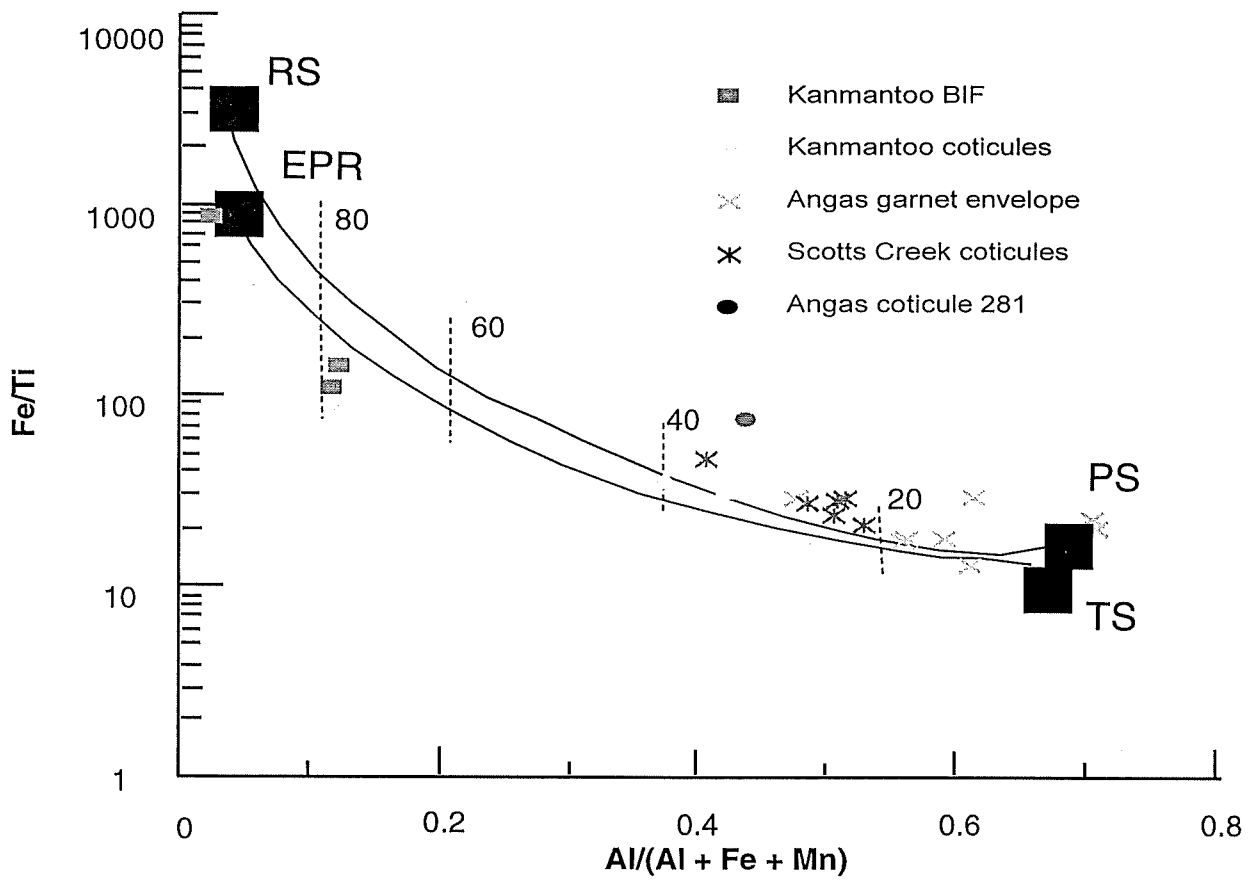


Figure 8a

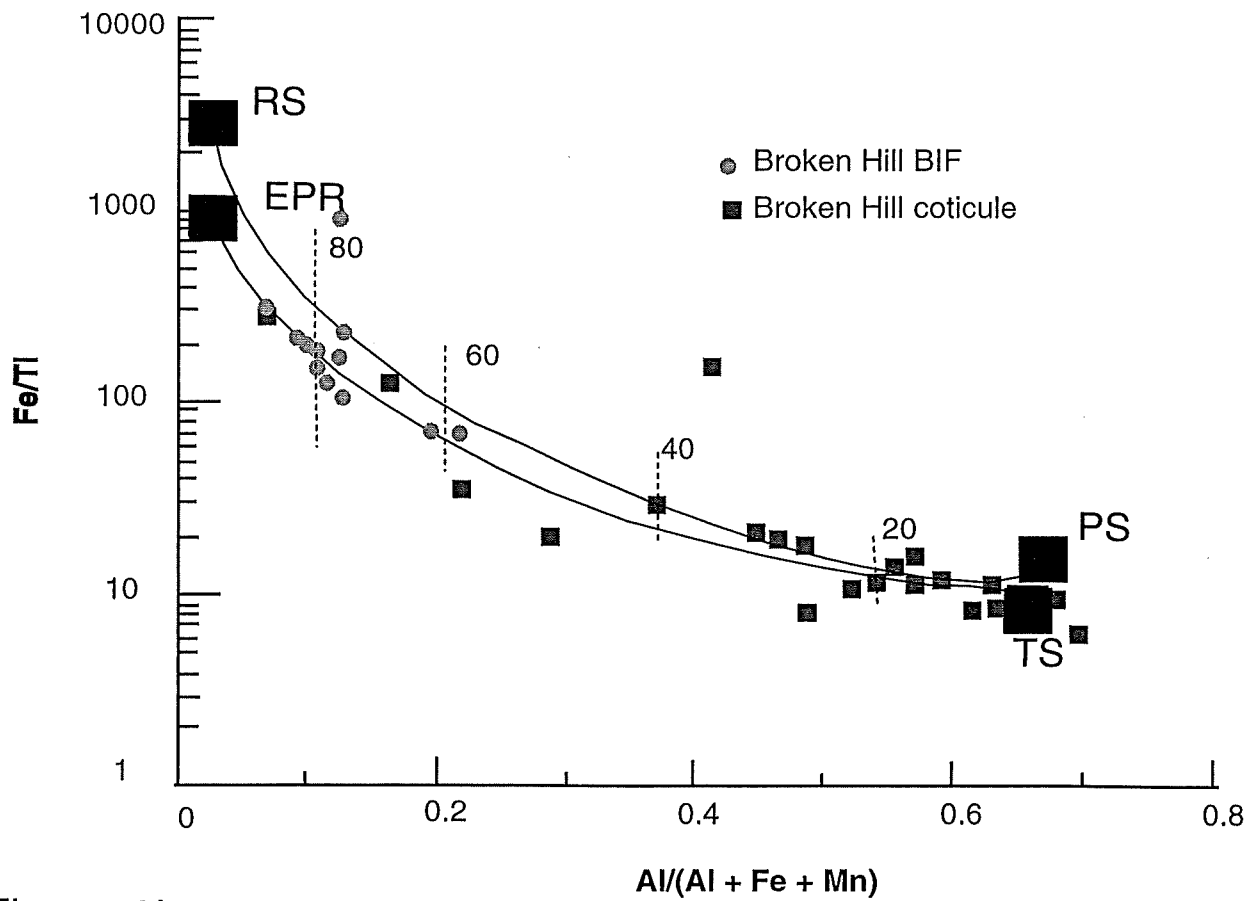


Figure 8b

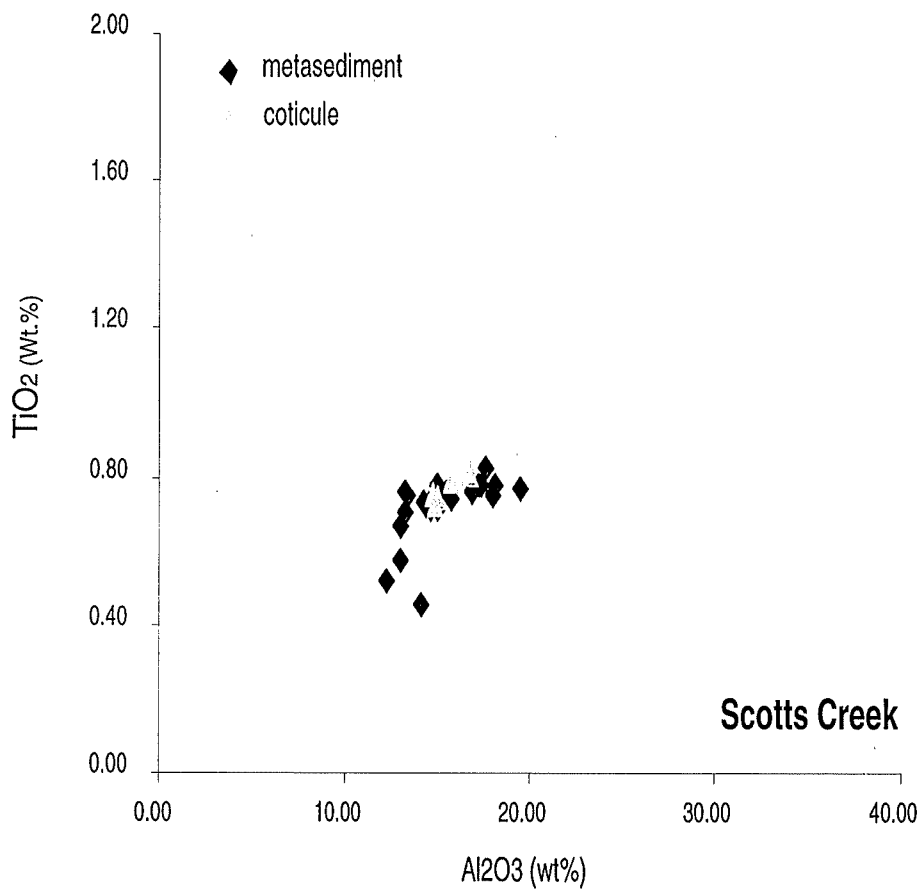


Fig. 9a Al_2O_3 versus TiO_2 plot for metasediments (stippled) hosting the Scotts Creek deposit and coticules from Scotts Creek.

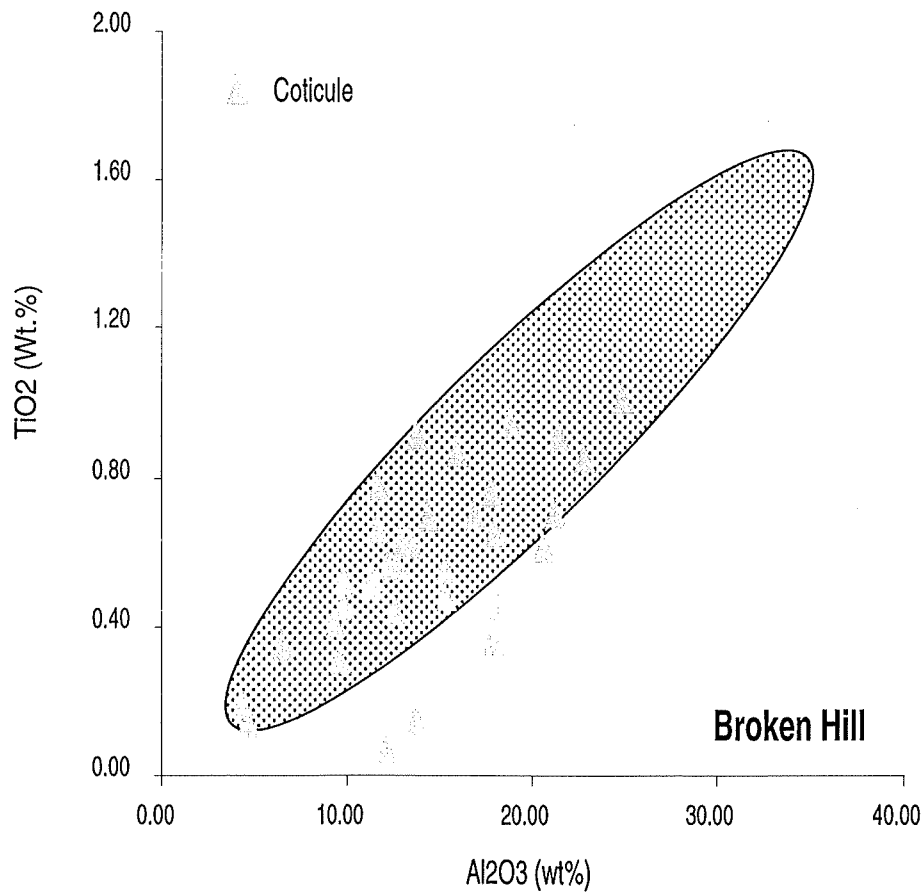


Fig 9b Al_2O_3 versus TiO_2 plot for metasediments and coticules from Broken Hill, Australia (Spry et al. in press) Compositions of clastic metasediments derived from Broken Hill area.

A similar positive correlation is observed between the Scotts Creek metasediments and coticules, suggesting a significant detrital contribution to the coticules (Fig.9a).

Hydrothermal and hydrogenous ferromanganese deposits have distinctly different REE characteristics (Ruhlin and Owen, 1986). Hydrogenous Fe-Mn nodules and crusts possess high enrichment factors for total REE, are enriched in LREE, with values mostly between 100 and 1000 times those of chondrites (Addy, 1979) and are characterised by positive Ce anomalies (Fig.10). In contrast, hydrothermal ferromanganese deposits contain lower concentrations of REE, mostly between 20 and 200 times chondrite (Bonatti, 1975), and are also enriched in light REE but display negative Ce anomalies (Fig. 10a). REE analyses of coticules from this study indicate concentrations between 20 and 200 times those of chondrites which is indicative of a hydrothermal source (Fig 10a).

On chondrite normalised REE plots, average continentally derived sediments are LREE enriched, depleted in HREE and have negative Eu anomalies. Peter and Good fellow (1996) noted that > 30 wt % detritus in the depositional environment of the coticules should produce this signature. This is observed in the Scotts Creek coticule REE pattern. The Fe/Ti versus Al/(Al+Fe+Mn) data shown in Figure 8a also supports a minimum of 30 wt % detritus in the source environment. This feature is similarly observed in samples from Broken Hill (Fig. 8b) (Spry *et al.* in press).

It is possible that if there was significant REE movement during metamorphism and equilibrium conditions were achieved then rocks of similar mineralogy would be expected to have similar homogenised REE signatures (Parr, 1992). However, data collected show that rocks with variable mineralogies are most commonly LREE enriched and have HREE content more consistent with background pelite/psammite contents suggesting there was not significant REE movement during metamorphism.

Figure 10

- a: Chondrite normalised (Boyton, 1984) REE data for cotiules from Scotts Creek, Angas and Kanmantoo field areas (stippled) and hydrogenous (Mn nodule average), hydrothermal and mixed Mn sediments. Data: Mn nodule average (Haskin et al., 1966), pelagic clay (Addy, 1979), hydrothermal sediment (Ruhlin and Owen, 1986), Bauer Basin nodules (Elderfield and Greaves, 1981), and Juan de Fuca crusts (Toth, 1980).
- b: Chondrite normalised (Boyton, 1984) REE data for BIF and sulphide rich garnet-muscovite-quartz-biotite rock from the Kanmantoo field area (stippled) and hydrogenous (Mn nodule average), hydrothermal and mixed Mn sediments. Data: Mn nodule average (Haskin et al., 1966), pelagic clay (Addy, 1979), hydrothermal sediment (Ruhlin and Owen, 1986), Bauer Basin nodules (Elderfield and Greaves, 1981), and Juan de Fuca crusts (Toth, 1980).

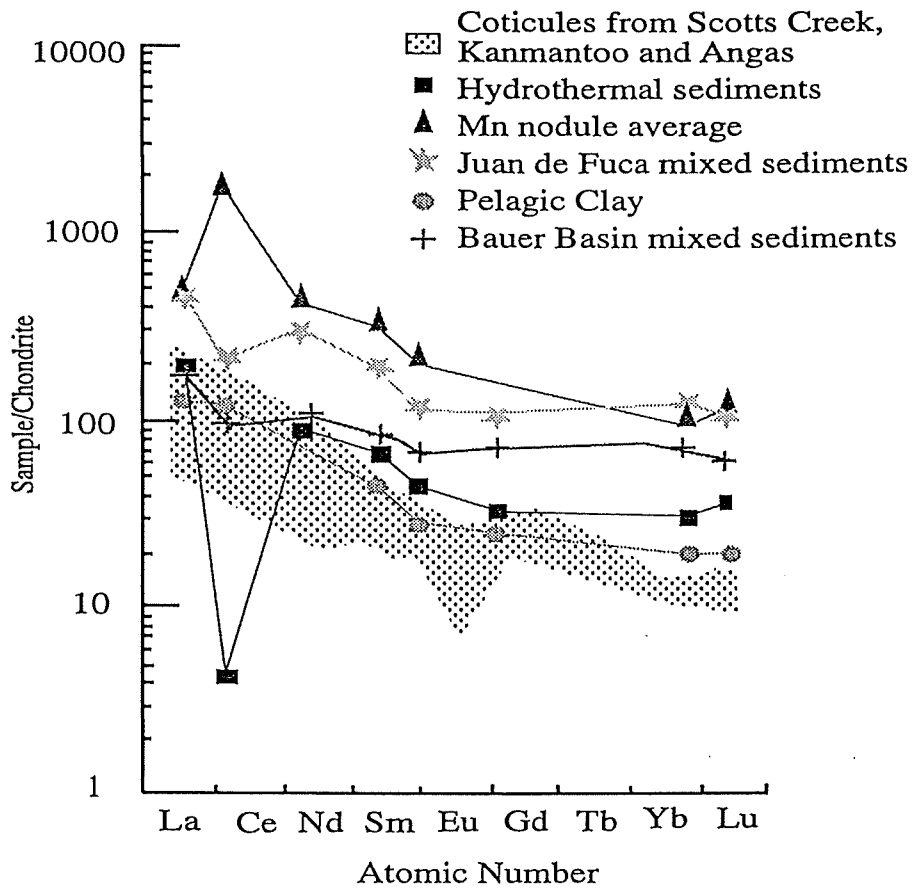


Fig. 10a

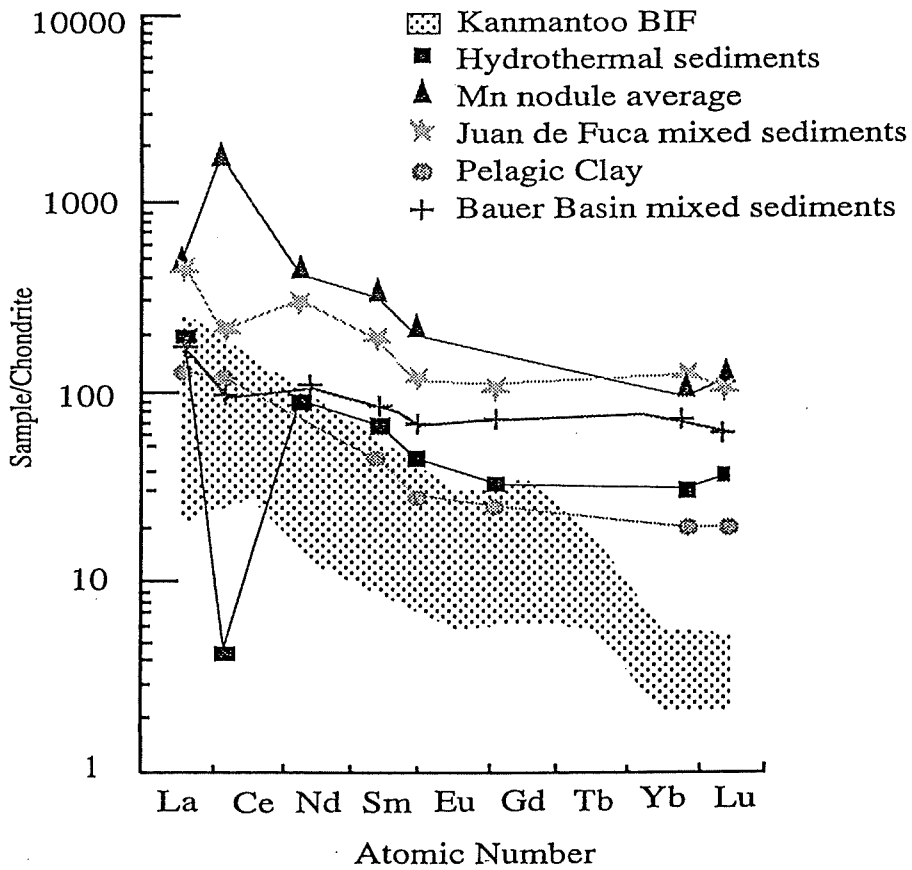


Fig. 10b

Chapter 4

KANMANTOO GARNETIFEROUS ASSEMBLAGES

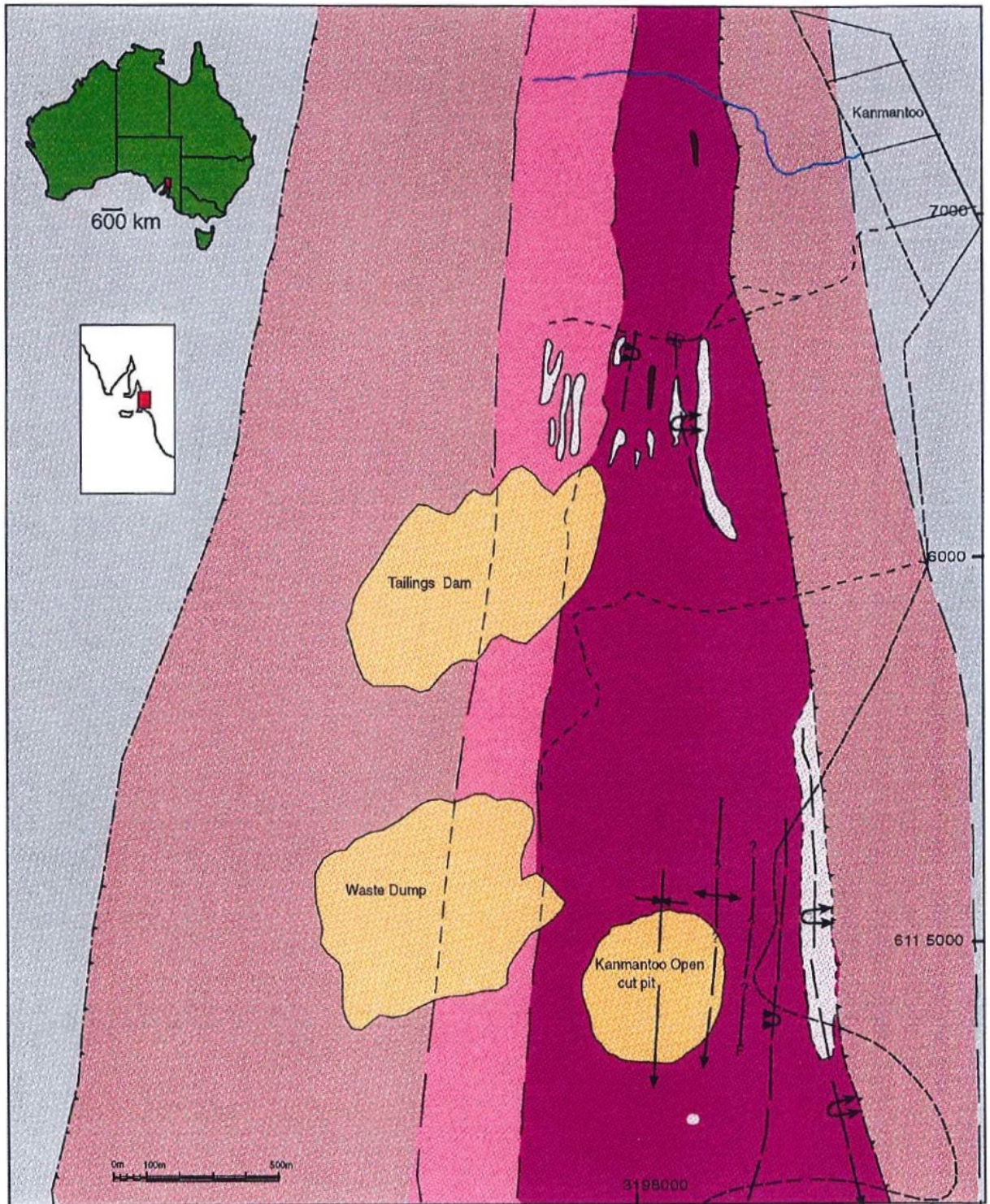
4.1 Introduction

The Kanmantoo Cu deposit has an overall pipe-like shape with several sulphide lenses. The lenses and the axis of the pipe are discordant to bedding, but parallel to a prominent schistosity which has been designated S_2 (Seccombe *et al.*, 1985; Preiss, 1995). The mineralisation consists of chalcopyrite + pyrrhotite + magnetite \pm pyrite, as veinlets, layers and disseminations within a quartz + chlorite + garnet schist, locally referred to as the 'lode schist' (Verwoerd and Cleghorn, 1975) which is spatially associated with a massive andalusite + quartz + biotite + garnet + staurolite rock. The ore body and host rock lie in the western limb of an overturned south plunging syncline (Seccombe *et al.*, 1985) (Figs. 11 & 13).

Within the study area, Spry *et al.* (1988) recognised planar inclusion trails (denoted S_1) in porphyroblasts, which were discordant to the matrix schistosity wrapping the porphyroblasts (denoted S_2). These observations are consistent with that of Mancktelow (1979) who proposed, as a result of a structural study of the southern Mount Lofty Ranges, that the widespread regional schistosity was S_1 and S_2 only developed in some areas, of which the present study area is one.

East and north of the Kanmantoo Cu mine, for approximately 2 km, rocks with unusual mineral assemblages crop out discontinuously (Fig. 11). The intermittent nature of the exposure is due mainly to soil cover and substantial weathering of the rocks. Bedding is difficult to observe in outcrop due to it being obscured by deformation and metamorphism. Compared to the adjacent country rock quartz-mica schists and quartz-mica-andalusite schists, these rocks are extremely garnetiferous and have high variance assemblages not commonly associated with the host rocks.



Fig. 11:KANMANTOO GARNETIFEROUS HORIZON - INTERPRETIVE GEOLOGY



LITHOLOGY

	Quartz-Mica Schist
	Quartz-Mica-Andalusite Schist + garnet + feldspar/Quartz-Mica Schist
	Quartz-Mica-Garnet Schist / Quartz-Mica-Andalusite Schist / Garnet-Andalusite Schist
	Garnet-Andalusite Schist
	Garnet-Quartz rock + garnite + cummingtonite + feldspar
	Banded Iron Formation

LEGEND

	Fault/thrust (inferred,observed)
	geological boundary
	Fold axis/plunge direction
	overturned fold
	unpaved road
	river
	road
	8k sample location

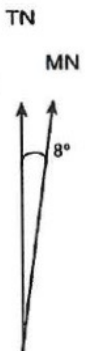
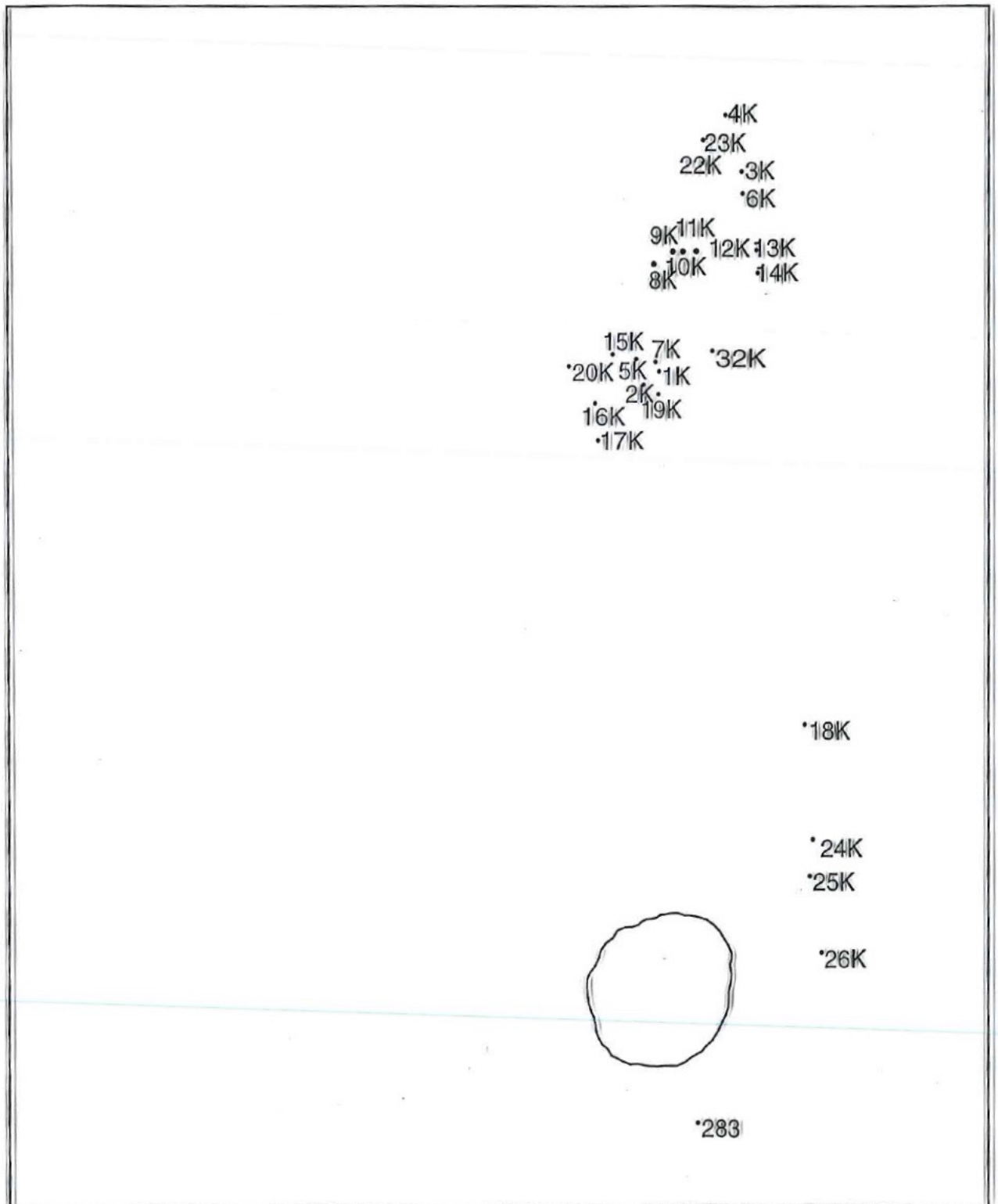


Fig. 11: KANMANTOO GARNETIFEROUS HORIZON - INTERPRETIVE GEOLOGY



The Kanmantoo garnetiferous assemblages are hosted by similar rock types as the Scotts Creek coticule yet exhibit a larger pelitic component. The interpretation of the Scotts Creek coticule has provided a comparative basis for the petrological and geochemical investigation of the coticule, the andalusite-quartz-garnet \pm staurolite schist and the apparent BIF, east and north of the Kanmantoo mine. The aim of establishing whether they are similar or different to Scotts Creek coticules will have important implications on the interpretation of the origin of the garnetiferous rocks.

4.2 Petrological Investigation

Surrounding the Kanmantoo mine, and extending in a north-south direction for several kilometres (Fig. 11), is a garnetiferous schist zone with coarse abundant andalusite, typically with considerable staurolite. The garnets within these rocks have inclusion rich cores (mainly of quartz) and make up 10 to 50% of the matrix. According to Spry *et al's* (in press) definition, these rocks are not considered coticules due to garnet and quartz not being the dominant minerals (samples 1113-5K, 1113-7K, 1113-8K, 1113-12K, 1113-28K, 1113-34K). Petrological descriptions of polished thin sections of the Kanmantoo field area are recorded in Appendix. A.

An iron-stained gahnite-bearing quartz-mica schist is exposed in a small pit ~ 700 m northeast of the mine and is accompanied by very fine-grained manganese-stained coticule with accessory minerals staurolite \pm adularia \pm biotite \pm muscovite \pm K feldspar \pm fibrolite \pm andalusite and disseminated sulphides (sample 1113-18K).

A similar, pale grey, fine-grained coticule was sampled 150 m southeast of the Kanmantoo mine, from a folded and boundinaged unit surrounded by laminated quartz-mica schist (sample 1113-283). The coticule contains up to 50 modal % very fine pale pink euhedral garnets which exhibit alteration in the cores (Fig. 12a, 12b). The surrounding granoblastic matrix is predominantly quartz and chlorite. Texturally, this fine-grained rock differs from those associated with copper mineralisation in the main garnet envelope, but it is similar in respect to the garnet rocks associated with Ag-Pb-Zn mineralisation at Scotts Creek and the Angas Pb-Zn prospect.

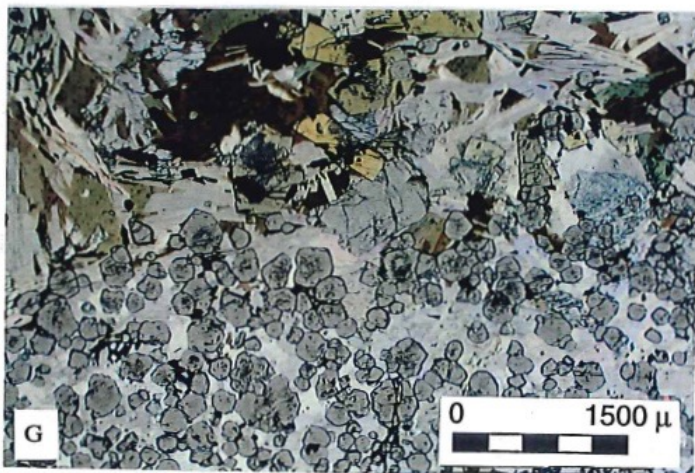
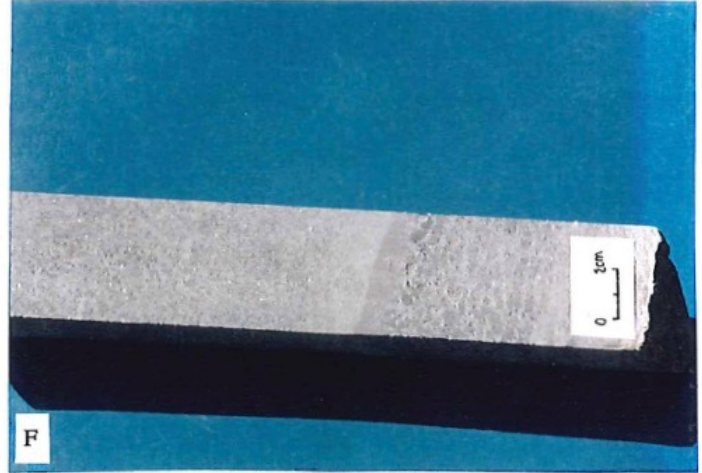
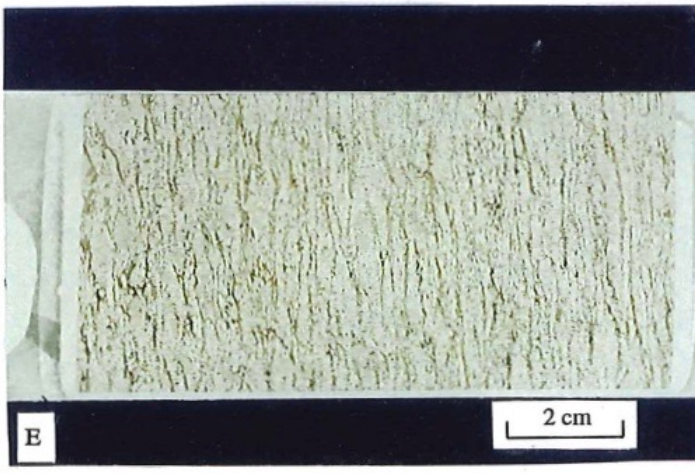
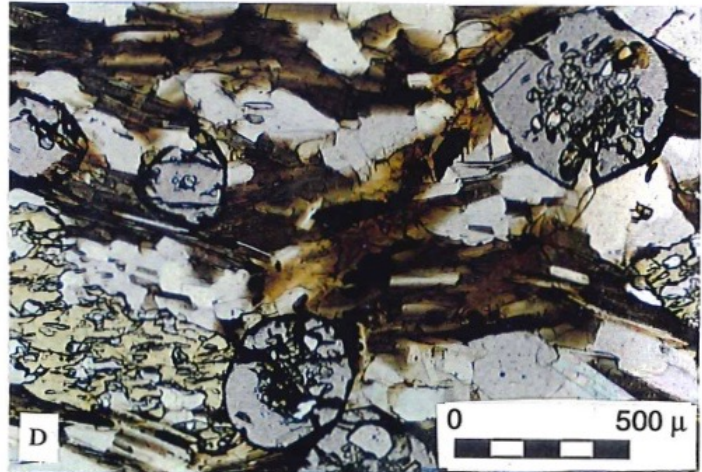
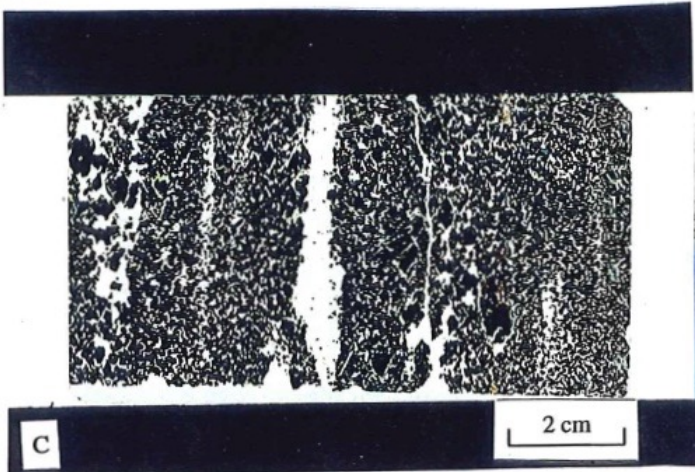
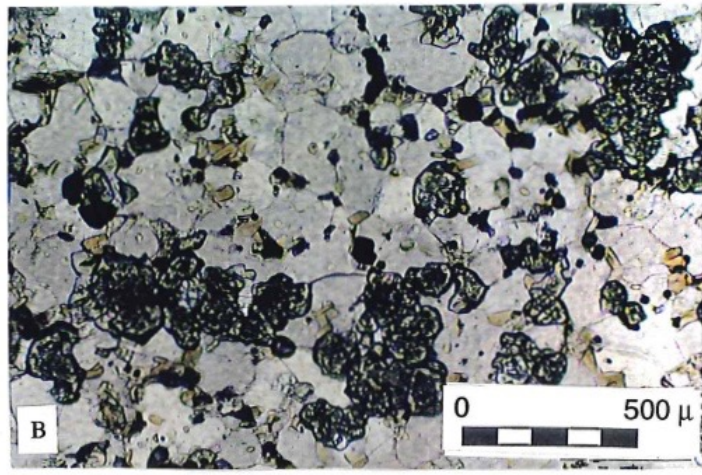
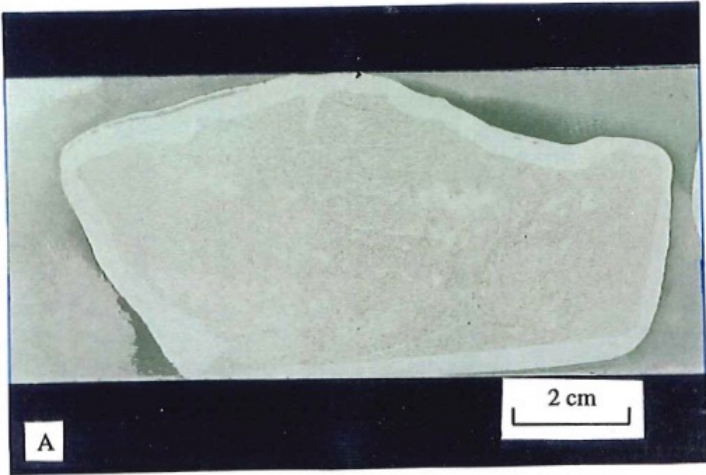
Figure 12

Kanmantoo field area:

- A: Sample 1113-283 from a boudinaged coticule within a well laminated quartz-biotite schist. Thin section displays very fine grained pale pink garnet-quartz coticule.
- B: Photomicrograph of the above sample 1113-283 displaying extremely altered garnet with inclusion rich cores, within a matrix of quartz, minor very fine grained biotite and apatite.
- C: Photograph of Kanmantoo BIF in thin section (sample no. 1113-1K) showing alternating layers of quartz and magnetite. Pelite may also interlay the quartz and magnetite, and garnet can be found confined to the quartz layers in other samples, but not indicated here.
- D: Photomicrograph of 'background' unmineralised garnetiferous schist, sampled 5 km north of the Kanmantoo field area (sample no. 1113-282). The mineral assemblage is dominated by quartz-biotite-andalusite-garnet-muscovite and staurolite. The sample is medium grained compared to the more altered garnetiferous schist proximal to the Kanmantoo mine which contains very large porphyroblasts of andalusite, and considerably more garnet and staurolite.
- E: Photo of thin section of 'background' unmineralised quartz-biotite-andalusite garnetiferous schist (sample no. 1113-282). Foliation evident is due to the alignment of platy biotite minerals.

Angas field area:

- F: Drill core sample (1113-90) from DDH 28, 194.4m depth showing 10mm coticule band of fine grained dense pale pink euhedral garnet (>80%) with a mineralogically simple matrix of quartz with minor muscovite, apatite, staurolite and biotite. Aligned parallel to compositional banding indicating younging direction to the right in the photo, and right way up in the drill core.
- G: Microphotograph of garnet-quartz coticule band illustrating relatively inclusion free cores in some grains, and inclusion rich cores in others (Inclusions are predominantly quartz and biotite). No gradational decrease is seen in garnet content either side of the band, nor is there evidence of alteration. A very sharp contact exists (1113-90).
- H: Microphotograph of surface coticule sample 1113-281. Garnet content is > 50% with no layering or banding of the garnet evident in hand specimen. Garnet appears disseminated through matrix of quartz, relict andalusite, staurolite and minor biotite. Some garnets exhibit inclusion rich cores of predominantly quartz and biotite, where as others are inclusion free. This may suggest two periods of garnet growth?



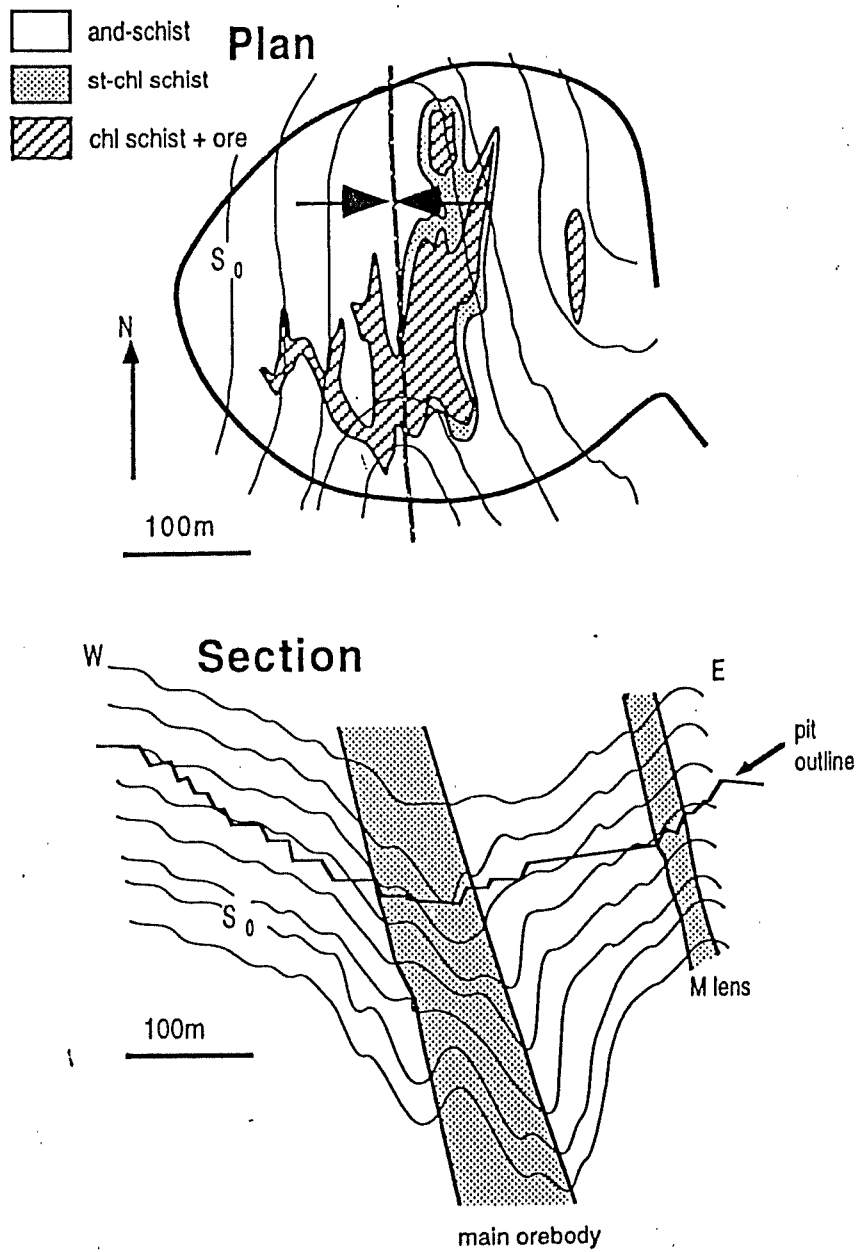


Fig. 13. Top - open pit plan at 500 ft level, and bottom - schematic cross section at 12000N (mine grid reference) From Seccombe *et al.* 1985

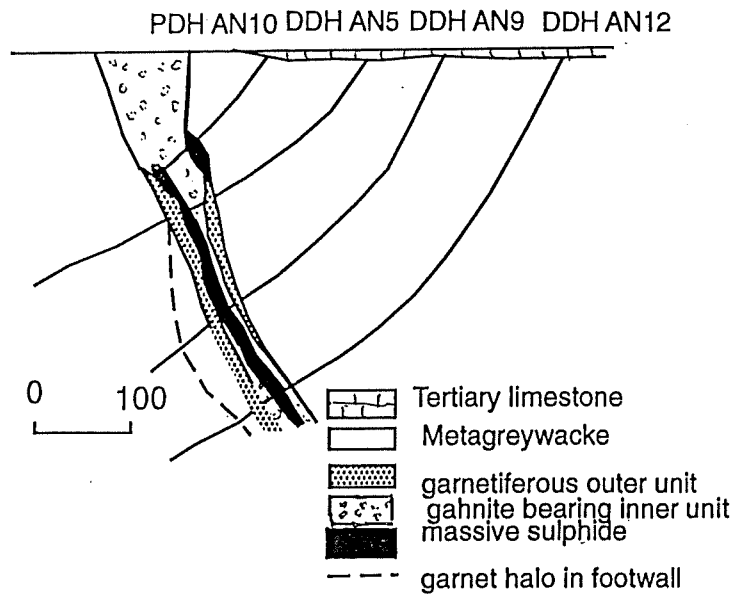


Fig. 14. Generalized cross section of Angas prospect showing garnetiferous envelope. Modified from Both *et al.* 1995

Approximately 1.5 km north of the mine, within the coticule layers, is a narrow finely banded, quartz-magnetite-sodic plagioclase-biotite-muscovite-garnet \pm pyrite rock interpreted as a BIF (Toteff, in press). Where present, garnets are very fine grained ($<100\mu\text{m}$), constitute approximately 1% of the rock and tend to form in the quartz rich bands which generally do not exceed 0.5 mm in width, and alternate with iron oxide-rich bands (Fig. 12c).

Field observations and petrology indicate a general decrease in garnet content in the andalusite-quartz-biotite-garnet \pm staurolite schist (herein termed the garnetiferous schist), towards the perimeter of the garnetiferous halo north of Kanmantoo mine. This halo has been interpreted by Toteff (in press) as a stratabound altered zone which has been metamorphosed to middle amphibolite grade producing the very coarse andalusite with staurolite only becoming apparent more proximal to the deposit.

Based on garnet size and content, the garnet lithologies of the Kanmantoo area can be grouped into two broad categories. Garnets from the garnetiferous schist are larger (~5-10mm) (Fig. 12d) and present in lesser amounts (~10%) than in the adjacent coticule layers. The coticule garnets range in size from 10 μm to 2 mm, and have a minimum garnet content of ~30% (Fig 12a).

4.3 Electron Microprobe Mineral Analyses of Garnet

Chemical compositions of garnets and staurolite from garnetiferous schist and coticules north and east of the Kanmantoo mine were obtained using standard electron microprobe techniques.

Garnets from all samples are primarily of almandine type, with lesser spessartine, pyrope and grossular type (Figs 4 & 5b). Garnets in interpreted coticules are slightly higher in spessartine component (10.0 wt % as compared to 4 wt % for surrounding metasediments).

4.4 Whole-rock Geochemistry

4.4.1 Results

Major and trace element whole rock analyses were conducted on 28 samples of garnet rich metasediments, cotiules and BIF with the intention of observing geochemical anomalies or trends that might allude to possible sources for the garnetiferous assemblages, and to observe similarities and/or differences in geochemistry when compared to the Scotts Creek and Angas deposits.

Whole-rock analyses indicate that the cotiules have less $\text{Fe}_2\text{O}_3\text{T}$, but increased amounts of Cu, Zn, Pb, Mn and Au than the surrounding metasediments ($\text{Fe}_2\text{O}_3\text{T}$ – cotiule-10.5, metasediments-13.4 wt %; Cu - 440, 68 ppm; Zn – 1125, 126 ppm; Pb - 400, 10 ppm; MnO – 1.6, 0.15 wt %; Au – 1470 ppb). (Table 2, Appendix B).

The bulk composition of the Kanmantoo BIF is dominated by Fe_2O_3 and SiO_2 . Al_2O_3 , MgO and TiO_2 contents are minor when compared to surrounding metasediments (refer to Table 2, Appendix C for analyses). Trace element analyses record a high Cu content (1502 ppm) associated with the BIF. The sulphide bearing garnet-muscovite-quartz-biotite rock stratigraphically above the BIF also shows anomalous levels of Cu (334 ppm), and also anomalous amounts of Au (1010 ppb).

4.5 REE Geochemistry

Five samples were taken from cotiules north and east of the Kanmantoo Cu orebody (1113-24K, 25K, 26K, 18K, and 283). Three samples were taken from the BIF, north along strike from the Kanmantoo Cu orebody (1113-01K, 22K, 23K). Refer to Figure 11 for sample locations, Appendix B for REE geochemistry and Figures 6b, 6c and 6d for REE chondrite normalised patterns.

4.5.1 Results

The coticles sampled have REE patterns that resemble the coticule unit sampled at Scotts Creek - enriched in LREE, and depleted in HREE with nil or negative Eu anomalies when compared to primitive chondrite (Fig.6a).

Chondrite-normalised REE patterns for BIF in the Kanmantoo region typically show enriched LREE, and substantially depleted HREE signature. Sample 1113-22K exhibits a positive Eu anomaly, whereas the REE pattern for BIF 1113-1K shows a positive Ce anomaly (Fig. 6d).

The coticule REE patterns are similar to the normal Tapanappa Formation sediments, and the unmineralised background sample (1113-282) (Fig 6a) however, the BIF exhibits a unique REE pattern to all of the above mentioned REE signatures, with more pronounced Eu and Ce anomalies. The BIF REE signatures are similar to REE patterns observed in BIF from Olary and Broken Hill, and coticule REE signature are similar to REE patterns observed in Broken Hill coticles (Figs. 6d and 6b).

4.6 Interpretation and Discussion

The garnetiferous lithologies east and north of the Kanmantoo Cu mine exhibit greater variation in mineralogy than those observed at Scotts Creek. The outcrop of a fine grained pale pink coticule (sample 1113-283) with anomalous levels of Pb, Zn and Ba and with a garnet composition higher in spessartine endmember than surrounding garnetiferous assemblages shows some similarities with the Scotts Creek coticule.

Anomalous Au levels in the garnet-muscovite-quartz-biotite rock stratigraphically above the BIF (which is devoid of precious metal mineralisation) reflects variation in physico-chemical conditions of the fluid from which it was deposited. The underlying BIF is anomalous in Cu, suggesting a genetic link with the base metal deposition.

In attempting to determine source components, the BIF, and coticules have been plotted on the ternary plot of Fe-Mn-(Cu+Co+Ni) x 10 (Fig. 6a). The plotted sample points illustrate a significant hydrothermal component in the source composition for the BIF, metasediments and coticules. The outlier is a sample of the coticule (sample 1113-283) from the Kanmantoo Cu mine vicinity, and has increased levels of Ni, Co, Cu and Mn (refer to Appendix B for whole rock analytical values). The plot of Al/(Al+Fe+Mn) versus Fe/Ti (Fig. 8a) illustrates a considerable hydrothermal component for the Kanmantoo BIF (>75%) and a chemical composition close to East Pacific Rise and Red Sea metalliferous sediments with minor contamination from terrigenous/pelagic sediments.

Sample points plotted from coticules show a significantly higher detrital source contribution and display similarities in source composition with the coticule from Scotts Creek.

The REE analyses from this field area, including a BIF and coticules indicate concentrations 1 to 400 times those of chondrite values which incorporates REE signatures of hydrothermal, hydrogenous and seawater source. The Kanmantoo coticule REE signatures are very similar to coticule REE patterns from Scotts Creek, suggesting a similar source of a hydrothermal and detrital sediment mix (Figs. 10a, 10b).

Negative REE Eu anomalies in some samples of the Kanmantoo BIF can be explained if the BIF contains an appreciable proportion (>30%) of detritus. However, this is not always evident in the BIF from Kanmantoo suggesting that the Eu anomaly is a reflection of the physico-chemical conditions of the fluid. Positive Eu anomalies are a more common signature of BIF (Spry *et al.*, in press) and is observed in sample 1113-22 from Kanmantoo. A positive Eu anomaly may indicate a significant contribution from high temperature (>250° C), reduced hydrothermal fluids (Sverjensky, 1984). The positive Ce anomaly in sample 1113-1K, is atypical of iron-formations (Spry *et al.*, in press); it commonly characterises modern Fe-Mn crusts (Elderfield *et al.*, 1981), which are the largest known Ce repository in modern oceans.

The major and trace element compositions and REE signatures of coticules from the Kanmantoo area (Fig. 6b) are similar to unaltered Tapanappa Formation (Fig. 6a), the Scotts Creek coticules (Fig. 6b) and coticules of similar composition from Broken Hill (Fig. 6b).

The Kanmantoo BIF displays slightly different patterns to unaltered Tapanappa, which may be due to the BIF containing less detrital sediment (Fig. 6c). The BIF has similar geochemical affinities with BIF from Olary and Broken Hill, Willyama Complex (Spry *et al.*, in press) (Fig 6d).

Chapter 5

ANGAS Pb-Zn DEPOSIT AND GARNET RICH BANDS

5.1 Introduction

The Angas lead-zinc deposit, hosted by metagreywackes was discovered by Aberfoyle Resources in 1992 (Anderson, 1993). The Pb-Zn deposit is situated on the east dipping limb of the Strathalbyn Anticline and forms a stratiform body parallel to compositional layering and sub-parallel to the dominant schistosity (S_2 of Spry *et al.*, 1988) (Fig.14).

Surrounding the mineralisation is an outer envelope of garnet-staurolite-sillimanite-chlorite-biotite-muscovite-andalusite-quartz schist, with minor cordierite, pyrite, pyrrhotite and chalcopyrite, and an inner envelope characterised by the additional presence of gahnite (McElhinney, 1994; Both *et al.*, 1995). Garnet abundance within the inner envelope is typically between 5-15% (Toteff, in press) and is usually ~1% in the outer envelope. Finely disseminated garnet (up to 10%) is also present in a zone in the footwall. Within the hanging wall, rare garnet rich bands (up to 90% garnet) ranging from a few mm up to 10mm have been reported (Toteff, pers. comm., 1998), along with a garnet-quartz-gahnite band (~40mm) observed in a railroad cutting and a garnet-quartz rock (~70% garnet) described by Toteff (in press) as a cotecule, discovered in a roadside Telstra trench.

5.2 Petrological Investigation of Garnet Rich Bands

Only one example of a cotecule was found in the drill core examined in this study (Fig 12f sample 1113-90 from DDH 28, 194.4m depth). This sample was located stratigraphically above the ore horizon and is a 10 mm wide band of fine grained dense pale pink euhedral garnet (>80%) with a mineralogically simple matrix of with quartz + muscovite + apatite and minor staurolite and biotite, located within the inner garnet envelope, and aligned parallel to compositional layering (Fig. 12g).

This study has been concentrated on the thin garnet band, which has previously been interpreted as a meta-exhalite (Toteff, pers. comm., 1998). Comparisons were made with garnets in the surface sample of an interpreted cotichule (1113-281, Fig. 12h) with garnets from a sample taken from the disseminated zone in the footwall (1113-2An) and data from McElhinney (1994) on samples containing disseminated garnet from within the outer and inner garnet envelopes. This study was aimed at establishing whether a common or unique origin exists for the band, in relation to the immediate garnet envelope and to similar rock types from Scotts Creek and Kanmantoo.

5.3 Electron Microprobe Mineral Analyses of Garnet

5.3.1 Results

Three samples; sample 1113-90 from the inner envelope above the mineralisation, sample 1113-281 from the Telstra trench and sample 1113-2An from the footwall directly below mineralisation were analysed by electron microprobe for their garnet composition. A traverse across the garnet rich band in sample 1113-90, and spot analyses of garnets from samples 1113-281 and 1113-2An were conducted to investigate similarities and differences between garnets in a multi-mineral matrix of the garnet envelope and a quartz matrix of the cotichule. These results were then compared to previous microprobe work by McElhinney (1994) on the Angas deposit, and cotichules from Scotts Creek, Kanmantoo and from Broken Hill (Wonder *et al.*, 1989), to illustrate similarities or differences in garnet compositions collected from Angas, with the underlying aim of establishing a mode of origin for the garnetiferous rocks.

Both within the garnet rich band consisting of predominantly garnet-quartz and biotite and within the surrounding multi-mineral matrix, the garnet compositions are of almandine type (~78 wt %, Fig 4, 5c). Zoning within garnet grains is not significant.

Sample 1113-2An and the surface cotichule sample 1113-281 have much larger components of spessartine (36 wt % and 37 wt % respectively) when compared to the cotichule band, 1113-90 (Fig 5c) and surrounding samples from the garnet envelope, which are predominantly almandine rich (~80 wt %). The spessartine cotichules have similar garnet compositions to cotichule garnet compositions from Broken Hill.

When compared to garnet compositions from garnet in the garnetiferous background rock (1113-282), the Angas samples are all depleted in almandine and enriched in spessartine (Fig. 5c).

5.4 Whole-rock Geochemistry

A total of 21 samples of the inner and outer garnet envelopes and footwall and hanging wall metasediments from 4 representative drillholes (DDH 4, DDH 9, DDH 14, DDH 18), were analysed by McElhinney (1994). In general the most abundant components in the metasediments are SiO_2 (47.8-72.9 wt %), Al_2O_3 (11.4-19.1 wt %) and $\text{Fe}_2\text{O}_3\text{T}$ (4.31-15.6 wt %). A garnet rich zone in the footwall of the garnetiferous envelope is enriched in Fe, Al, Mg and Ca and deplete in Si, when compared to the surrounding samples (refer to Appendix B for geochemical values). This may be a reflection of a higher garnet content in this sample, and may indicate alteration of the wall rock. The surface cotecule sample 1113-281 has abundant components of SiO_2 (58.56 wt %), Al_2O_3 (16 wt %) and Fe_2O_3 (20.45 wt %) which is within the elemental component range for cotecules reported by Spry *et al.* (in press). Refer to Chapter 3 for these values.

5.5 REE Geochemistry

The surface cotecule (sample 1113-281) was analysed for REE composition. The cotecule is enriched in light REE, depleted in heavy REE, and shows a distinctive negative Eu anomaly when compared to primitive chondrite (Fig. 9b). The LREE and HREE signature for the Angas cotecule is similar to LREE and HREE signatures from Scotts Creek and Kanmantoo, and closely resembles unaltered Tapanappa Formation metasediments, and the background sample (Fig. 9a). The Angas cotecule also resembles cotecules analysed from Broken Hill (Figs. 9b) (Spry *et al.*, in press). The distinctive negative Eu anomaly is not as pronounced in either the Scotts Creek, Kanmantoo or the background signatures.

5.6 Interpretation and Discussion

The coticule band previously interpreted as a meta-exhalite (Toteff, pers.comm., 1998) is almandine rich and when compared to garnet analyses from Scotts Creek and Kanmantoo, presented on a ternary plot of the garnet endmembers (Fig. 4) the garnets plot closest to the Kanmantoo garnet composition. The Fe content of the garnets in the coticule band is similar to the surrounding envelope garnets. This, and the position of the band, stratigraphically above the ore horizon lead to the implication that the garnet band and surrounding envelope have formed from similar precursor sediments. Garnet compositions from Angas samples are all depleted in Fe, and enriched in Mn when compared to the background garnet composition, a feature commonly associated with base metal deposits (Spry *et al.*, in press). The spessartine rich garnets from samples 1113-281 and -2An have similar garnet compositions to Scotts Creek and Broken Hill coticules (Figs. 5a, 5c) which leads to the implication of a similar precursor sediment high in Mn. The stratigraphic position of sample 1113-2An in the footwall of the Angas Pb-Zn deposit is also similar to the coticule observed at Scotts Creek, but is found in a disseminated garnet zone below a garnet rich envelope which is not observed at Scotts Creek, but is similar to surrounding garnetiferous rocks and coticules at Kanmantoo.

On a plot of Fe/Ti versus Al/(Al + Fe + Mn) (Bostrom, 1973), the Angas prospect garnet rocks from the representative drillholes and associated coticules, plot on or close to mixing lines between pelagic/terrigenous sediments and hydrothermal precipitates from the EPR and the Red Sea (Fig. 8a). The coticule contains a significant hydrothermal component (> 40%) (Fig. 6a), whereas the garnet envelope samples plot closer to a terrigenous source value (Bonatti *et al.*, 1972; Toth, 1980).

Exhalites formed in modern hydrothermally active areas e.g. the Red Sea, are enriched in both LREE and Eu, which is similar to hydrothermal solutions from the East Pacific Rise. REE patterns for metalliferous Fe-Mn sediments precipitated on the sea floor exhibit flat profiles and negative Ce and Eu anomalies similar to that of seawater. If the coticule had a hydrothermal source as was demonstrated in the above plot then a LREE enriched profile and positive Eu would be expected, yet a negative Eu anomaly is present. It is possible that these REE profiles will be modified depending on time of exposure to seawater, degree of subaqueous oxidation and degree of mixing (Lottermoser, 1992).

Chapter 6

DISCUSSION AND CONCLUSIONS

6.1 Comparative Discussion of Garnetiferous Assemblages

Garnetiferous assemblages observed within the three field areas exhibit considerable variation in mineralogy between each of the locations and within each location. Coticules from Scotts Creek, Angas and Kanmantoo consist of fine-grained (10 μm to 100 μm), in a simple matrix of quartz \pm apatite \pm chlorite \pm biotite \pm rutile \pm magnetite \pm ilmenite. Garnet and quartz make up the predominant matrix with accessory minerals occurring only in trace amounts. Garnet contents in the coticules range from 30% disseminated garnet up to 100% garnet in some bands. However, garnets in the surrounding metasediments, are larger (3 –10mm), and occur in a multi mineral matrix of biotite \pm quartz \pm feldspar \pm andalusite \pm actinolite \pm fibrolite \pm staurolite \pm chlorite \pm magnetite \pm ilmenite \pm apatite. Observations show that size and content of garnets are dependent on precursor mineralogy, which leads to the inference that the precursor sediments from which the garnets grew, were sourced from different origins.

The main chemical components in the garnetiferous rocks from the three field areas are SiO_2 , Al_2O_3 , Fe_2O_3 , and MnO with their proportions largely determined by the modal percentage of quartz and garnet, and the composition of the garnets. The Scotts Creek coticules exhibit a significantly higher Mn content than garnetiferous rocks from the other two deposits, and a relationship between Fe and Mn content of the coticules and proximity to mineralisation has been noted from this deposit. Coticules from Angas and Kanmantoo exhibit more variation in mineralogy, with an increased Mn and/or Fe content prevalent in samples associated with Pb-Zn mineralisation. This is also apparent in microprobe data, with Kanmantoo and Angas coticule garnets being predominantly of almandine type and those from Scotts Creek of spessartine type.

Increased levels of Ba were observed in the coticules associated with Ag-Pb-Zn mineralisation at Scotts Creek and from Kanmantoo.

On ternary plots of Fe-Mn-(Co+Ni+Cu) x10 (Figs 6a and 6b) the cotiules from Scotts Creek, Kanmantoo and Angas, and the BIF from Kanmantoo, plot in the hydrothermal field and have chemical signatures characteristic of metalliferous sediments from the Red Sea and other hydrothermal sediments. These features are consistent with garnet-rich rocks from Broken Hill, Australia (Spry *et al.*, 1990).

In the plot of Fe/Ti versus Al/(Al+Fe+Mn) (Figs. 8a and 8b), the cotiules and BIF plot close to the mixing curve of pelagic clays or terrigenous sediments and hydrothermal metalliferous precipitates. Most of the cotiules possess ~30% hydrothermal sediment input, suggesting contamination from terrigenous sources. The BIF samples indicate > 70% hydrothermal sedimentary input, suggesting less contamination from terrigenous sources.

The REE patterns of cotiules from Scotts Creek, Kanmantoo and Angas are similar to those for mixed hydrothermal and pelagic/terrigenous sediments from the Bauer Basin and Juan de Fuca ridge (Toth, 1980; Elderfield and Greaves, 1981). The similarity of Scotts Creek cotiule REE patterns with that for normal Tapanappa metasediments suggests that the patterns reflect the original bulk chemistry of the sediments. Pelitic rocks exhibit characteristic REE signatures of enriched LREE and depleted HREE, with minor to nil Eu anomalies (Peter and Good fellow 1996). This is preserved in the cotiules when the detrital component is >30%. These signatures are unlike those for typical metamorphic garnets (Gravuch, 1989). The moderate enrichment in LREE and substantial depletion in HREE, when compared to primitive chondrite, may be the result of seawater mixing with hydrothermal fluids. Although the REE signatures for the cotiules lack a distinctive positive Ce anomaly that is observed in seawater REE signatures, this is not uncommon. Mills and Elderfield (1995) pointed out that, for modern seafloor hydrothermal systems, negative Ce anomalies are only observed in mixtures of >90 % seawater. The cotiule REE signatures of all three deposits and BIF from Kanmantoo are similar to those observed for meta-exhalites in the Willyama Complex, as is the BIF, which also exhibits similar patterns to BIF from the Olary Block, Australia. The Angas cotiule signature with a distinctive negative Eu anomaly may indicate changing physico-chemical conditions in the fluid. An interpretation similar to that was used to explain negative Eu anomalies in cotiules from Broken Hill (Lottermoser, 1989).

Although interpretations concerning the origin of coticules and BIF based on major-and trace-element analyses do not yield an unequivocal answer, these data, when considered in conjunction with data on similar rock types described in the literature, are consistent with an origin in which hydrothermal ferromanganiferous sediments mixed with aluminous material of terrigenous origin.

6.2 Petrogenesis of the Garnetiferous Rocks

Various models have been put forth to explain the origin of manganese garnet-rich rocks. Stanton (1976) suggested that they formed *in situ* from manganiferous beds, viewing pennantite (a chlorite species), as the precursor to the spessartine garnets. Spry and Wonder (1989) argued that while pennantite could possibly produce variations in Mn, Fe, and Mg contents in garnets by this process, it does not account for the Ca content observed in garnets from Broken Hill. It is, therefore, also not suitable for the explanation of Mn content in the Tapanappa Formation garnets, as Ca, although minor, is present in the garnets from all three field areas studied.

Similarly, it is unlikely that the large amount of manganese-bearing clean detrital sands needed to support the proposal by Haydon and McConachy (1987) for the origin of garnet-rich rocks at Broken Hill were present, as no modern equivalents of these extensive detrital sand units have been recognised.

Garnet development at Broken Hill has also been suggested to have been a consequence of prograde metamorphism, with a reaction between Mn-Ca-rich fluids from the orebodies and the Al-rich wall rock (Hodgson, 1975; Lee, 1977). This theory must also come under question as it wrongly suggests that the garnet-rich rocks would only form adjacent to base metal mineralisation (Spry and Wonder, 1989).

Other interpretations of the genetic implications of manganese-bearing garnet-rich rocks include: isochemical metamorphism of a precursor Mn-rich sediment (Segnit, 1961); derivation from manganiferous chemical sediments (Richards, 1966; Stanton, 1976; Spry, 1979); development from Mn-rich sand layers (Clifford, 1960); marine cherts derived in part from Mn-rich nodules (Schiller and Taylor, 1965; Doyle, 1984); spessartine placer deposits (Richter, 1969); diagenetic replacement of marly sediments (Lamens *et al.*, 1986);

diagenesis of manganese-carbonate concretions (Bennett, 1989); chemically precipitated MnCO_3 (Woodland, 1939), Mn-rich volcanic tuffs (Kramm, 1976); and Mn-rich detrital sediments (Roy and Purkait, 1968).

For the Broken Hill deposit, Spry and Wonder (1989) suggested that garnet-formation occurred close to hydrothermal vents on the ocean floor from Mn precursor minerals such as manganite, pyrolusite, hausmannite, veradite and pyrochroite. The Fe required in the system may have been present as Fe-oxides in calcium carbonates on the sea floor (Bostrom and Peterson, 1969). Mixing of these minerals and detrital Al-Mg-bearing clays was used by Spry and Wonder to explain the presence of all the elemental components required to produce the coticles at Broken Hill. A similar process may have resulted in the formation of the coticles from this study.

The BIF could have formed by exhalation of Fe rich hydrothermal fluids with a higher ratio of hydrothermal : terrigenous components.

Oliver *et al.* (1998) recognised the presence of garnet-rich rocks in the ore envelope associated with sulphides at the Kanmantoo Cu mine and considered that they formed by syn-metamorphic metasomatic processes because the high garnet content (up to 95%) would be “very difficult to attain from metamorphism of normal sediments” (Oliver *et al.*, 1998, p. 185). Oliver *et al.* (1998) based their metasomatic model on the presence of sillimanite in altered rocks, suggesting that this indicated higher peak temperatures in the mine area compared to the surrounding rocks, and a gradient in whole rock oxygen isotopes. With this they proposed channelised fluid flow towards the Kanmantoo mine area. Marshall & Spry (in press) argued, however, that sillimanite (also found at Scotts Creek) is more likely to be a reflection of sillimanite-forming compositions of the host rocks, and that the $\delta^{18}\text{O}$ depletion zone need not be metamorphogenic, but could alternatively have formed in association with syngenetic exhalations (e.g., Green *et al.*, 1983) and been preserved during subsequent amphibolite facies metamorphism. They conclude that oxygen isotope studies neither confirm nor rule out metamorphosed syngenetic and metamorphogenic models.

6.3 Conclusions

Overprinting effects of the Delamerian Orogeny have masked and confused evidence of earlier mineralisation, although there are some features which have survived, and provide reasonable evidence for pre-metamorphic base metal mineralisation.

The stratigraphic position of the Scotts Creek deposit in the sequence is marked by an abrupt reduction in sediment input, probable local deepening of the basin and onset of reducing conditions (Toteff, in press), all of which are well documented controls of SEDEX (sedimentary exhalative) mineralisation (e.g. Large, 1981). Further evidence of exhalative activity within the Scotts Creek vicinity is provided by a coticule which forms the immediate host to the mineralisation and a coticule in the footwall to the deposit which can be recognised as thin bedding-parallel bands that extend for tens of metres north of the Ag-Pb-Zn deposit. The compositional changes in the coticule as the ore is approached, indicate a genetic link between the coticule and the mineralisation. The coticules are much finer grained than enclosing metasediments, a common feature of meta-exhalites described in the literature (Spry *et al.*, in press) with which they also have chemical affinities (Figs. 5, 6, 7 & 9). Other evidence of a pre-metamorphic origin lies in the relationship between the coticules and the prominent schistosity, where thin bands are tightly folded around high-grade schistosity which acts as the axial planar structure. Within this schistosity, the bands can also be seen to be boudinaged, reflecting competency differences with the enclosing quartz-biotite schists during the high-grade deformation. While the schistosity is largely sub-parallel to coticule layering, there are neither indications of replacement or alteration around the coticule bands themselves, even where they are tightly folded. These features also eliminate the possibility of a syn-tectonic origin with the shear zone acting as a conduit for the sulphide bearing fluids. However, evidence of rare sulphides aligned to the axial planar foliation provide evidence that the shear zone has contributed to modification of the deposit.

A BIF, with anomalous levels of Cu is observed at Kanmantoo and lies adjacent to, and stratigraphically above, the Cu mine. It has chemical and lithological affinities analogous with marine hydrothermal metalliferous deposits and BIF in the Olary Block and Broken Hill Block (Stanton, 1976; Lottermoser and Ashley, 1989), and is interpreted as an exhalative deposit. The sulphide rich garnet-muscovite-quartz-biotite layer immediately overlying the BIF is also anomalous in Cu and Au, and exhibits a similar REE pattern to the BIF and is evidence that garnet rich assemblages originated from similar fluids as the BIF.

The presence of the meta-exhalite layers in the hanging wall rocks to the Cu deposit is circumstantial evidence of sub-seafloor deposition of the Cu deposit in a feeder zone which also acted as a conduit for the fluids from which the ferromanganiferous exhalites were precipitated.

Footwall alteration observed at the Angas deposit as a zone of subtle garnet enrichment in normally garnet-free metagreywacke indicate that this zone needed to gained iron, manganese and magnesium to produce this mineralogy. The enriched spessartine component in garnet in the footwall is analogous with that observed at Scotts Creek. The composition of garnets between samples of Angas coticles is highly variable. Garnets in the coticule from the surface trench are spessartine rich, as for Scotts Creek. However, garnets in a coticule in the hanging wall inner garnet envelope are spessartine-poor and chemically similar to garnets in the garnet envelope, and Kanmantoo coticles. The similar garnet compositions observed in the fine coticule band and surrounding envelope indicate an identical original bulk rock composition. The above observations, along with the stratigraphic position of the coticles above the main ore horizon, and parallelism to compositional banding, suggest the origin of the garnet rich band is pre-metamorphic and formed by an exhalative process. It is not possible, on the basis of the present limited study of the Angas deposit, to determine whether the surrounding garnet envelope is also of exhalative origin (Both *et al.*, 1995) or a metamorphosed alteration zone as favoured by Toteff (pers.comm. 1998).

Remobilisation of sulphides is apparent as irregular stringers aligned along the shear planes (Toteff, in press). The shears are subparallel to the high-grade schistosity, but are composed of a retrograde assemblage, indicating that these structures have formed under different conditions to the metamorphosed ore (Toteff, in press).

On evidence presented in this study, combined with previous work and comparisons drawn with rocks of similar mineralogical and geochemical affinities from the literature, it is concluded that the garnet rich assemblages associated with base metal sulphide deposits studied in the Kanmantoo Trough are of essentially the same fluid source.

A sub-seafloor alteration/exhalation model is proposed for the Kanmantoo Cu mine and Angas Pb-Zn mine, and a SEDEX model is invoked for the origin of the Scotts Creek Ag-Pb-Zn deposit.

This is similar to the syn-sedimentary model proposed by Seccombe et al. (1985) for the Pb-Zn deposits in the Kanmantoo Group and a sub-seafloor origin for the Kanmantoo Cu deposit. This is, however, in conflict with the metamorphogenic model by Oliver *et al.* (1998) who suggested a different origin for the Kanmantoo Cu deposit than the Pb-Zn deposits in the Kanmantoo Group. The interpretation of meta-exhalite units above the Kanmantoo Cu deposit makes it difficult to explain the association of metamorphically derived metasomatic fluids with exhalative fluids.

The conclusion to this study has established similarities between Pb-Zn deposits and the Kanmantoo Cu deposit situated in the Tapanappa Formation. It is proposed that a common origin is possible for the base metal deposits, based on the similarity of the host rock sequences, and evidence of meta-exhalites within those host sequences. These meta-exhalites also exhibit geochemical and mineralogical affinities with each other and known exhalite deposits in literature.

It is envisaged that mineralisation was generated by large-scale hydrothermal convective systems driven by a thermal perturbation during crustal extension that occurred in the early Cambrian. Growth faults activated at this time in the subsiding Kanmantoo Trough acted as conduits for the upwelling hydrothermal fluid, although undetected igneous activity within the Kanmantoo Group is also a speculative heat source.

6.3.1 Further investigations

Suggested topics for further research into the origin of the garnetiferous rocks described in this thesis are:

- A more detailed study of cotecules with the Angas deposit in an attempt to determine if the garnet envelope and the cotecules have the same or different origins, this may also include a comprehensive REE geochemical study of the garnetiferous envelope to determine if there are variations in REE signatures that may further allude to the origin of the deposit.
- If further exploration in the vicinity of the Kanmantoo mine provide drill core samples of the cotecules and/or BIF, a more detailed study of their composition and relationships to the Cu mineralisation will be possible.

REFERENCES

- Addy, S. K., 1979. Rare earth patterns in manganese nodules and micronodules from northwest Atlantic. *Geochimica et Cosmochimica Acta*. Vol. 43, pp 1105 - 1115.
- Anderson, J. A., 1993. Kanmantoo Trough. Resources South Australia: Technical Session: Abstracts, 1993, Adelaide, South Australia.
- Appel, P. W. U., 1979. Stratabound copper sulphides in a banded iron-formation and in basaltic tuffs in the early Precambrian Isua Supracrustal Belt, West Greenland. *Economic Geology*. Vol. 74, pp 45 - 52.
- Askins, P. W., 1968. Geochemical exploration around the Aclare mine and mineral deposits of the surrounding region. *Unpublished Honours Thesis, University of Adelaide*.
- Barnes, R. G., Stroud, W. J., Willis, I. K., and Bradley, G. M., 1983. Zinc, manganese, and iron-rich rocks and various minor rock types. Geological Survey of New South Wales Records. Vol. 21, pp 289 - 323.
- Barnes, R. G. and Willis, I. L., 1989. The stratigraphic setting of Pb-Zn-Ag mineralization at Broken Hill; discussion. *Economic Geology*. Vol. 84, pp 188 - 191.
- Barrett, T. J., 1981. Chemistry and mineralogy of Jurassic bedded chert overlying ophiolites in the north Appenines, Italy. *Chemical Geology*. Vol. 34, pp 289 - 317.
- Bender, M., Broecker, W., Gornitz, V., Middel, U., Kay, R., Sun, S., and Biscaye, P., 1971. Geochemistry of three cores from the East Pacific Rise. *Earth Planetary Science Letters*. Vol. 12, pp 425 - 433.

- Bollenhagen, W. J., 1993. The influence of bulk rock MnO on garnet development in metamorphic rocks of andalusite-staurolite grade; Kanmantoo, South Australia. *Unpublished Honours Thesis, University of Adelaide*.
- Bonatti, E., 1975. Metallogensis at oceanic spreading centres. *Earth Planetary Science Annual Review*. Vol. 3, pp 401 - 431.
- Bonatti, E., Kraemer, T., and Rydell, H., 1972. Classification and genesis of sub-marine iron manganese deposits. *In* Ferromanganese deposits on the ocean floor: Washington (Ed. D. Horn). *National Science Foundation*, pp 149 - 165.
- Bonatti, E., Zerbi, M., Kay, R., and Rydell, H., 1976. Metalliferous deposits from the Apennine ophiolites: Mesozoic equivalents of modern deposits from oceanic spreading centres. *Geological Society of America Bulletin*. Vol. 87, pp 83 - 94.
- Boström, K., 1973. The origin and fate of ferromanganoan active ridge sediments: Stockholm University. *Contributions to Geology*. Vol. 27, pp 129 - 243.
- Boström, K., and Peterson, M. N. A., 1969. The origin of aluminium – poor ferromanganoan sediments in areas of high heat flow on the East Pacific Rise. *Marine Geology*. Vol. 7, pp 427 - 447.
- Both, R. A., 1990. Kanmantoo Trough - geology and mineral deposits. *In: Geology of the Australia and Papua New Guinean Mineral Deposits* (Ed. F. E. Hughes), pp 1195-1203 (The Australasian Institute of Mining and Metallurgy: Melbourne).
- Both, R. A., McElhinney, R., and Toteff, S., 1995. The Angas Zn-Pb-Ag deposit in the Kanmantoo Group, South Australia: Synsedimentary or Metamorphic? *In: Mineral Deposits: From Their Origins to Their Environmental Impacts* (Eds. J. Pasava, B. Kribek, and K. Zac, K), Rotterdam, A.A. Balkema, p. 847-850.

- Boynton, W.V., 1984. Cosmochemistry of the rare earth elements - meteorite studies. *In*: Rare Earth Element Geochemistry (Ed. P. Henderson). *Developmental Geochemistry 2*, Elsevier, Amsterdam, pp 63 - 114.
- Brookins, D. G., 1989. Aqueous geochemistry of rare earth elements. *In*: Geochemistry and mineralogy of rare earth elements (Eds. B. R. Lipin and G. A. McKay). *Reviews in Mineralogy*. Vol. 21, pp 201 - 225.
- Brown, H. Y. L., 1908. Record of the mines of South Australia, 4th edition: Adelaide, South Australia Dept. Mines, pp 135 - 136.
- Campbell, I. H., Lesheer, C. M., Coad, P., Franklin, J. M., Gorton, M. P., and Thurston, P. C., 1984. Rare earth element mobility in alteration pipes below massive Cu-Zn sulfide deposits. *Chemical Geology*. Vol. 45, pp 181 - 202.
- Chilman, J. K., 1982. Silver and a trace of gold- a history of the Aclare mine: Department of Mines and Energy South Australia, Special Education 1.
- Dickinson, S.B., 1942. The structural control of ore deposition in some Australian copper fields, *Geological survey of South Australia, Bulletin*, 20.
- Dymoke, P., and Sandiford, M., 1992. Phase relations of Buchan facies series pelitic assemblages - calculations and applications to the Mount Lofty Ranges, South Australia: *Contributions to Mineralogy and Petrology*. Vol. 110, pp 121 - 132.
- Elderfield, H., and Greaves, M. J., 1981. Negative cerium anomalies in the rare earth element patterns of oceanic ferromanganese nodules. *Earth Planetary Science Letters*. Vol. 55, pp 163 - 170.

- Elderfield, H., Hawkesworth, C. J., Greaves, M. J., and Calvert, S. E., 1981. Rare earth element geochemistry of oceanic ferromanganese nodules. *Earth and Planetary Science Letters*. Vol. 55, pp 163 - 170.
- Elderfield, H. and Mills, R. A., 1995. Rare earth element geochemistry of hydrothermal deposits from the active TAG Mound, 26 degrees N Mid-Atlantic Ridge. *Geochimica et Cosmochimica Acta*. Vol. 59, pp 3511 - 3524.
- Faulkner, I.L., 1996. Investigation of the exhalative horizon in the Kanmantoo area University of South Australia. B.Applied Sc. (Hons) thesis (unpublished).
- Fleming, P. D. and White, A. J. R., 1984. Relationships between deformation and partial melting in the Palmer migmatites, South Australia. *Australian Journal of Earth Sciences*. Vol. 31, pp 351 - 360.
- Flöttmann, T., James, P. R., Rogers, J., and Johnson, T., 1994. Early Palaeozoic foreland thrusting and basin reactivation at the southeastern Paleo-Pacific margin of the Australian Precambrian Craton – a reappraisal of the structural evolution of the Southern Adelaide Fold-Thrust Belt. *Tectonophysics*. Vol. 234 pp 95 - 116.
- Flöttmann, T., and Cockshell, C. D., 1996. Palaeozoic basins of southern South Australia – new insight to their structural history from regional seismic data. *Australian Journal of Earth Sciences*. Vol. 43, pp 45 - 55.
- Flöttmann, T., and James, P., 1997. Influence of basin architecture on the style of inversion and fold-thrust belt tectonics- the southern Adelaide Fold-Thrust Belt, South Australia. *Journal of Structural Geology*. Vol.19, No. 8, pp 1093-1110.
- Foden, J. D., Turner, S. P., and Morrison, R., 1990. The tectonic implications of the Delamerian magmatism in South Australia and western Victoria. *Geological Society of Australia, Special Publication*. Vol. 165, pp 483 - 495.

- Foden, J.D., Turner S. P., Sandiford M., Williams I.S., Compston, W., and Michard A., 1993. The nature, timing and duration of the Delamerian-Ross Orogeny. *Journal of the Geological Society of London*.
- Foden J.D., Sandiford M., Dougherty-Page J. and Williams I., 1999. (in press). The geochemistry and geochronology of the Rathjen Gneiss: Implications for the early tectonic evolution of the Delamerian Orogen. *Australian Journal of Earth Sciences.*, 46.
- Graf, J. L., 1977. Rare earth elements as hydrothermal tracers during the formation of massive sulfide deposits in volcanic rocks. *Economic Geology*. Vol. 72, pp 527 - 548.
- Green, G. R., Ohmoto, H., Date, J. and Takahashi, T., 1983. Whole-rock oxygen isotope distribution in the Fukazawa - Kosake area, Hokuroku District, Japan, and its potential application to mineral exploration. *In*: The Kuroko and related volcanic hosted massive sulphide deposits. *Economic Geology Monographs*. Vol. 5, pp 395 - 411.
- Haines, P. W., Flöttmann, T., Gum, J. C., Jago, J. B., and Gatehouse, C. G., 1996. Integrated approach to the reinterpretation of the Cambrian Kanmantoo Group type section, South Australia. *Geological Society of Australia Abstracts*. Vol. 41, p 177.
- Henderson, Q. J., 1953. North Broken Hill mine. *In*: Geology of Australian ore deposits (Ed. A. B. Edwards). *Australian Institute of Mining and Metallurgy*. Vol. 1, pp 627 - 649.
- Hodgson, C. J., 1975. The geology and geological development of the Broken Hill lode in the Broken Hill Consolidated Mine, Australia part 3 – petrology and petrogenesis. *Geological Society of Australia*. Vol. 22, pp 195 - 213.
- Holdaway, M. J., Dutrow, B. L., and Shore, P., 1986. A model for the crystal chemistry of staurolite. *American Mineralogist*. Vol. 71, pp 1142 - 1159.
- Hollister, L. S., 1996. Garnet zoning, an interpretation based on the Rayleigh fractional model. *Science* 154 (3757), pp 1647 - 1651.

- Hoy, T., Gibson, G., and Berg, N. W., 1984. Copper-Zinc deposits associated with basic volcanism, Goldstream area, southeastern British Columbia. *Economic Geology*. Vol. 79, pp 789 - 814.
- Huston, D. L., and Patterson, D. J., 1995. Zincian staurolite in the Dry River South volcanic-hosted massive sulfide deposit, northern Queensland, Australia – An assessment of its usefulness in exploration. *Applied Geochemistry*. Vol. 10, pp 329 - 336.
- Jenkins, R. J. F., 1990. The Adelaide Fold Belt: Tectonic reappraisal. In: The Evolution of a Late Precambrian-Early Palaeozoic Rift Complex: The Adelaide Geosyncline (Eds. J. B. Jago and P. S. Moore). *Geological Society of Australia, Special Publication*. No.16, pp 396 - 420.
- Jenkins, R. F. J., and Sandiford, M., 1992. Observations on the tectonic evolution of the southern Adelaide Fold Belt. *Tectonophysics*. Vol. 214, pp 27 - 36.
- Kennan, P. S., 1978. The origin of sulphide deposits in the Leinster Granite. *Journal of Earth Science Royal. Dupl. Soc.* 1. p. 41 – 47.
- Laing, W. P., 1977. Structural and metamorphic geology of a critical area adjacent to the Broken Hill orebody, Willyama Complex, Australia. *Unpublished PhD Thesis, The University of Adelaide*.
- Lee, S. D., 1977. Metasomatic alteration associated with the Broken Hill orebody, N.S.W.. *Second Australian Geological Convention Abstracts*. No. 45.
- Lottermoser, B. G., 1988. Rare earth element composition of garnets from the Broken Hill Pb-Zn-Ag orebodies, Australia. *Neues Jahrbuch fur Mineralogie Monatshefte*. Vol. H9, pp 423 - 431.
- Lottermoser, B. G., 1989. Rare earth element study of exhalites within the Willyama Supergroup, Broken Hill block, Australia. *Mineralium Deposita*. Vol. 24, pp 92 - 99.

- Lottermoser, B. G., 1992. Rare earth elements and hydrothermal ore processes. *Ore Geology Reviews*. Vol. 7, pp 25 - 41.
- Lottermoser, B.G., and Ashley, P.M., 1995. Exhalites within the Proterozoic Willyama Supergroup, Olary Block, South Australia, in Pasava, J., Kribek, Bl, and Zak, K., eds., *Mineral deposits: From their origin to their environmental impacts*: Rotterdam, A.A. Balkema, p. 237-240.
- Mancktelow, N. S., 1979. The structure and metamorphism of the southern Adelaide Fold belt. *Unpublished PhD. Thesis, The University of Adelaide*.
- Mancktelow, N. S., 1990. The structure of the southern Adelaide Fold Belt, South Australia. *Geological Society of Australia, Special Publication*. Vol. 16, pp 483 - 495.
- McElhinney, R., 1994. Style and genesis of base metal sulphide mineralisation of Angus prospect – Strathalbyn area, South Australia. *Unpublished Honours Thesis, The University of Adelaide*.
- Marlow, P. C., and Etheridge, M. A., 1977. Development of a layered crenulation cleavage in mica schists of the Kanmantoo Group near Macclesfield, South Australia. *Bulletin of the Geological Society America*. Vol. 88, pp 873 - 882.
- Marshall, M., and Spry, P.G., 1998. Discriminating between Regional Metamorphic Remobilisation and Syn-tectonic emplacement in the Genesis of Massive sulphide ores. *Reviews in Economic Geology*. Vol. 10, (in press).
- Milnes, A. R., Compston, W. W. and Daily, B., 1977. Pre- to Syn-tectonic emplacement of Early Palaeozoic granites in south eastern South Australia. *Geological Society of Australia*. Vol. 24, pp 87 - 106.
- Offler, R. and Fleming, P. D., 1968. A synthesis of folding and metamorphism in the Mt. Lofty Ranges, South Australia. *Geological Society of Australia*. Vol. 15, pp 245 - 266.

- Ohmoto, H. and Goldhaber, M. B., 1997. Sulfur and carbon isotopes. In: Geochemistry of hydrothermal ore deposits, 3rd edition: New York, Wiley, pp 517 - 611.
- Oliver, H. S., Dipple, G. M., Cartwright, I. and Schiller, J., 1998. Fluid flow and metasomatism in the genesis of the amphibolite-facies, pelite hosted Kanmantoo copper deposit, South Australia. *American Journal of Science*. Vol. 298, pp 181 - 218.
- Parker, A. J., 1986. Tectonic development and metallogeny of the Kanmantoo Trough in South Australia. *Ore Geology Review*. Vol.1, pp 203 - 212.
- Parr, J. M., 1992. Rare-earth element distribution in exhalites associated with Broken Hill-type mineralisation at the Pinnacles deposit, New South Wales. *Chemical Geology*. Vol.100, pp 73 - 91.
- Peter, J.M., and Goodfellow, W.D., 1996. Final report on Geological Survey of Canada – Noranda industrial partners program (IPP) on Development of new geochemical exploration techniques for deeply buried volcanogenic massive sulphide deposits in northeastern New Brunswick: Unpublished report for the Geological Survey of Canada, 569p.
- Piper, D. A., 1974. Rare earth elements in ferromanganese nodules and other marine phases. *Geochimica et Cosmochimica Acta*. Vol. 38, pp 1007 - 1022.
- Preiss, W. V., 1987. The Adelaide Geosyncline – late Proterozoic stratigraphy, sedimentation, palaeontology and tectonics. *Geological Survey of South Australia Bulletin*. No. 53.
- Preiss, W. V., 1995. Delamerian Orogeny. In: The Geology of South Australia. Adelaide: Geological Survey of South Australia (Eds. J. F. Drexel and W. V. Preiss), pp 45 - 61.
- Renard, A., 1878. Sur la structure et la composition mineralogique du coticule et sur ses rapports avec le phyllade oligistifere: *Memoires couronnes de l'Academie Royale Belgique*, Vol. 41.

- Richards, S.M., 1966. The banded iron formations at Broken Hill, Australia, and their relationship to the lead-zinc orebodies, Part 2: *Economic Geology*, Vol. 61, p. 72-96.
- Rozendaal, A., and Stumpfl, E.F., 1984, Mineral chemistry and genesis of Gamsberg zinc deposit, South Africa: *Institute of Mining and Metallurgy Transactions*, Vol 93, p. 161-175.
- Ruhlin, D. E., and Owen, R. M. 1986. The rare earth element geochemistry of hydrothermal sediments from the East Pacific Rise- Examination of a seawater scavenging mechanism. *Geochimica et Cosmochimica Acta*. Vol. 50, pp 393 - 400.
- Ryan, P. J., Lawrence, A. L., Lipson, A. L., Moore, J. M., Paterson, A., Stedman, D. P. and Van Zyl, D., 1986. The Aggeneys base metal sulphide deposits, Namaqualand district. In: Mineral deposits of Southern Africa (Eds. C. R. Anhaeusser and S. Maske). *Geological Society of South Africa*. Vol. 2, pp 1447 - 1474.
- Sandiford, M., Foden, J., Zhou, S and Turner, S. P., 1992. Granite genesis and the mechanics of convergent orogenic belts with application to the southern Adelaide Fold Belt. *Transactions of the Royal Society of Edinburgh: Earth Sciences*. Vol. 83, pp 83 - 93.
- Sandiford, M., Fraser, G., Arnold, J., Foden, J and Farrow, T., 1995. Some causes and consequences of High-T, Low-P metamorphism, Mt Lofty Ranges. *Australian Journal of Earth Sciences*. Vol. 42, pp 241 - 247.
- Sangster, D. F., 1990. Mississippi Valley type SEDEX lead-zinc deposits: a comparative examination. *Institute of Mining and Metallurgy Transactions*. Vol B99, pp B21 - B42.
- Seccombe, P. K., Spry, P. G., Both, R. A., Jones, M. T. and Schiller, J. C., 1985. Base metal mineralization in the Kanmantoo Group, South Australia: a regional sulphur isotope study. *Economic Geology*. Vol. 80, pp 1824 - 1841.

- Segnit, E. R., 1961. Petrology of the zinc lode, New Broken Hill Consolidated Ltd., Broken Hill, New South Wales. *Australasian Institute of Mining and Metallurgy Proceedings*. Vol. 199, pp 87 - 112.
- Slack, J. F., Shaw, D. R., Leitch, C. H. B., and Turner, R. J. W., 1998. Tourmalinites and cotiules from the Sullivan Pb-Zn-Ag deposit and vicinity, British Columbia, geochemistry, and genesis. *In*: The Sullivan deposit and its geological environment (Eds. J. F. Lydon, T. Hoy and M. E. Knapp). *Geological Survey of Canada Bulletin*.
- Solomon, M., and Groves, D. I., 1994. The Geology and Origin of Australia's Mineral Deposits. Clarendon Press, Oxford, pp 713 - 715.
- Spry, P. G., 1979. Manganese anomalies associated with volcanic exhalative sulphide deposits- the Broken Hill example. *Geological Association of Canada - Mineralogical Association of Canada, Programs and Abstracts*. Vol.4, p 80.
- Spry, P. G., 1987. The chemistry and origin of zincian spinel associated with the Aggeneys Cu-Pb-Zn-Ag deposits, Namaqualand, South Africa. *Mineralium Deposita*. Vol. 22, pp 262 - 268.
- Spry, P. G., 1988. Manganese anomalies as guides in the exploration for metamorphosed massive sulphide deposits- The Aggeneys example, Namaqualand, South Africa. *Geological Society of America, Programs and Abstracts*. Vol. 20, A300.
- Spry, P. G., 1990. Geochemistry and origin of cotiules (spessartine-quartz rocks) associated with metamorphosed massive sulfide deposits. *In*: Regional Metamorphism of Ore Deposits (Eds. P. G. Spry and Bryndzia). VSP, pp 49 - 75.
- Spry, P. G. and Scott, S. D., 1986a. The stability of zincian spinels in sulphide systems and their potential as exploration guides for metamorphosed massive sulfide deposits. *Economic Geology*. Vol. 81, pp 1146 - 1163.

- Spry, P. G., and Scott, S. D., 1986b. Zincian spinel and stauralite as guides to ore in the Appalachians and Scandinavian Caledonides. *Canadian Mineralogist*. Vol. 24, pp 147 - 163.
- Spry, P.G., Schiller, J.C., and Both, R.A., 1988. Structure and Metamorphic setting of base metal mineralisation in the Kanmantoo Group, South Australia: *The AusIMM Bulletin and Proceedings*, Vol. 293, p. 57-66.
- Spry, P. G., and Wonder, J. D., 1989. Manganese-rich rocks associated with the Broken Hill lead-zinc-silver deposit, New South Wales, Australia. *Economic Geology*. Vol. 27, pp 275-292.
- Spry, P. G., Sulfidation and oxidation haloes as guides in the exploration for metamorphosed massive sulfide ores. *Reviews in Economic Geology*, Vol. 10. (in press).
- Spry, P. G., Peter, J. M., and Slack, J. F., Meta-exhalites as exploration guides to ore. *Reviews in Economic Geology*, Vol.10, (in press).
- Stanton, R. L., 1976. Petrochemical studies of ore environment at Broken Hill, New South Wales, 3 Banded iron formations and sulfide orebodies- constitutional and genetic ties. *Australasian Institute of Mining and Metallurgy Transactions*. Vol. B85, pp 132 - 141.
- Stanton, R. L., and Vaughan, J. P., 1979. Facies of ore formation- A preliminary account of the Pegmont deposit as an example of potential relations between small 'iron formations' and stratiform sulphide ores. *Australasian Institute of Mining and Metallurgy Proceedings*. Vol. 270, pp 25 - 38.
- Stanton, R. L., 1983. The place of the Appalacian Province in the development of stratiform ore genesis. In: *Program and Abstracts; Symposium on stratabound sulphides of the Appalacian - Caledonian Orogen*.
- Steinhardt, C., 1989. Stop 31 - The nose of the Strathalbyn anticline. In: *Structural geology of the Fleurieu Peninsula* (Ed. P. R. James), Australasian Tectonics Conference, 1989. *Geological Society of Australia, Specialist Group in Tectonics and Structural Geology*, pp 86 - 90.

- Stumpfl, E. F., 1979. Manganese haloes surrounding metamorphic stratabound base metal deposits. *Mineralium Deposita*. Vol. 14, pp 207 - 217.
- Sverjensky, D. A., 1984. Europium redox equilibria in aqueous solution. *Earth and Planetary Science Letters*. Vol. 67, pp 70 - 78.
- Thomson, B.P. 1969. Palaeozoic Era. In: Handbook of South Australia geology. *Geol. Surv. South Australia* (Ed. L. W. Parkin), pp 97 - 108.
- Thomson, B. P., 1975. Kanmantoo Trough-regional geology and comments on mineralization. In: *Economic Geology of Australia and Papua New Guinea, Vol.1 metal* (Ed. C. L. Knight), pp 555 - 560 (The Australasian Institute of Mining and Metallurgy: Melbourne).
- Toteff, S., Cambrian sediment-hosted exhalative base metal mineralisation, Kanmantoo Trough, South Australia: *MESA - Report of Investigations* (in press).
- Toth, J. R., 1980. Deposition of submarine crusts rich in manganese and iron. *Geological Society of America Bulletin*. Vol. 91, pp 44 - 54.
- Troop, D. G., 1984. The petrology and geochemistry of Ordovician banded iron formations and associated rocks at the Flat Landing Brook massive sulphide deposit, northern New Brunswick. *Unpublished Masters Thesis, University of Toronto*.
- Turner, S. P, Foden, J. B., Sandiford, M., and Bruce, D, 1992. Sm-Nd isotopic evidence for the provenance of sediments from the Adelaide Foldbelt and southeastern Australia with implications for crustal growth models. *Geological Society of Australia Abstracts*. Vol. 32, pp 153 - 154.

- Turner, S. P., Foden, J. B., Sandiford, M., and Bruce, D., 1993. Sm-Nd isotopic evidence for the provenance of sediments from the Adelaide Fold Belt and southeastern Australia with implications for episodic crustal addition. *Geochimica Cosmochimica Acta*. Vol. 57, pp 1837 - 1856.
- Vaughan, J. P., and Stanton, R. L., 1986. Sedimentary and metamorphic factors in the development of the Pegmont stratiform Pb-Zn deposit, Queensland. *Australia: Institution of Mining and Metallurgy*. Vol. 95, sec. B, pp B94 - B121.
- Verwoerd, P. J., and Cleghorn, J. H., 1975. Kanmantoo copper orebody. In: *Economic geology of Australia and Papua New Guinea, I. Metals* (Ed. C. L. Knight). Australasian Inst. Mining Metallurgy Mon. Vol. 5, p. 560 - 565.
- Wade, M. L., and Cochrane, G. W., 1954. Wheal Ellen mine. *South Australia Dept. Mines, Mining Review*. Vol. 97, p. 68 - 81.
- Wonder, D. J., Spry, P. G., and Windom, K. E., 1988. Geochemistry and origin of manganese-rich rocks related to iron-formation and sulfide deposits, Western Georgia. *Economic Geology*. Vol. 83, pp 1070 - 1081.

ACKNOWLEDGEMENTS

I would like to take this opportunity to acknowledge the unlimited supply of guidance, support, advice and patience I have received from Dr. Ross Both of the Department of Geology and Geophysics, Adelaide University during the preparation of this thesis.

I must also acknowledge the work of Wayne Mussared, not only for his preparation of thin sections, but also for his provision of constant humour which was always appreciated and John Stanley for his assistance in understanding the ropes of analytical geochemistry.

Thanks also to Gerald Buttfeld for the logistical support and anything else that doesn't fall into this category - my heartfelt appreciation goes out to you.

Special thanks go to Pasminco Pty. Ltd. For making this project available and providing financial support.

Thankyou to Dr. Paul Spry for providing unpublished transcripts. Many thanks also, to Dr. Steve Toteff for sharing his vast knowledge of the field areas at any time. Thanks also to PIRSA – a useful source of information, and PIMA for providing essential core log data.

Access to private properties around the Kanmantoo area has been vital in the preparation of this thesis and thanks must go to the landholders who unhesitatingly allowed inspections to be carried out on their land.

Thanks to Pat James, for sharing his expertise in structural geology and to Robin Oliver for his expertise in petrology. To post docs, Geoff Fraser for field and microprobe assistance, Justin Gum for sharing knowledge and geochemistry data on Kanmantoo Group stratigraphy and Betina Bendall for teaching me how to question everything I did, and when I had the answer, how to question this as well!!

To my fellow peers, in particular Nicole Radzik, Nicole Nasev and Ben Till, your encouragement, support, friendship and stress eradication techniques have contributed immensely to making this a rewarding journey.

To my family, thankyou dearly for your support.

Lastly, and mostly, this honours thesis is dedicated to my nanna, Vinjie Smith, you are the gem of my life and my Rock of Gibraltar – Thankyou for everything!

APPENDICES:

Appendix A: Hand Specimen and petrological description of samples

Appendix B: XRF analysis – major and trace elements

Appendix C: Electron microprobe analysis of garnet

Sample number: 1113-282

Location: 5kms north of Kanmantoo mine.

Tapanappa Formation

Biotite-quartz-staurolite-garnet-andalusite schist

Hand specimen:

Medium grained poikiloblastic schist with large andalusite grains. Platy biotite crystals align to form dominant foliation. Sample is light grey/maroon in colour, and of medium hardness.

Thin section:

Biotite	35%
Quartz	30%
Staurolite	20%
Garnet	10%
Andalusite	5%

Idioblastic grains of garnet with inclusion rich cores are present wrapped by platy biotite crystals defining foliation. Staurolite and andalusite are present in poikiloblastic forms and are also wrapped by biotite foliation. This sample is free of mineralisation yet enriched in garnet and has been used in the study as a background sample to compared other garnetiferous rocks to.

Sample number: A1113-25, A1113-32, A1113-37, A1113-35

Location Scotts Creek, west of main shaft from thin (20cm) cotecule layer

Tapanappa Formation

Garnet-quartz cotecule

Hand Specimen

This specimen is pale cream, pale pink in colour, massive, extremely fine grained and very hard. The sample possesses fine banding (approx. 1mm thick) and is homogeneous in grain size. Visible minerals include quartz, and pale pink spessartine garnet.

Thin section

Garnet	60%
Quartz	20%
Opagues	10%
Felspar	5%
Biotite	5%

In thin section the specimen is very fine grained and consists of idioblastic grains of garnet and annealed sub-idioblastic recrystallised quartz, with subidioblastic grains of biotite and feldspar. The arrangement of the quartz and garnet results in a granoblastic texture, with the quartz and garnet separated into distinct bands defining layering in the rock.

Sample number: 1113-38

Location: in lower boundary of Scotts Creek thrust zone

Tapanappa Formation

Mica-feldspar-quartz-garnet-staurolite-andalusite schist

Hand specimen:

This schist is a coarse grained rock with biotite forming well defined foliation. The schist is soft and friable and dark grey-maroon in colour due to garnet content.

Thin section

Biotite	20%
Muscovite	20%
Feldspar	10%
Quartz	10%
Garnet	10%
Andalusite	8%
Staurolite	5%
Fibrolite	5%
Chlorite	5%
Opagues	5%

Xenoblastic biotite present with idioblastic quartz in matrix forming compositional layering with adjacent muscovite rich layer. The muscovite rich layer is much coarser grained and exhibits recrystallisation and deformation of all minerals. Deformation present in the form of crenulation of muscovite minerals and folding of biotite exhibiting original foliation. Lenticular fibrolite is most common as nucleated fibrous crystals in muscovite, where the K⁺ of muscovite has been replaced by H⁺ ions (A. Purvis, pers. comm). The fibrolite may have formed due to aluminous sediments being metamorphosed under conditions of intense strain provided by the shearing event. The fibrolite formed late in the sequence of mineral growth. Association of chlorite and andalusite together suggests a low temperature shearing event (If the event was a high temperature, these minerals would have broken down to cordierite and staurolite). The low quartz content could be due to either the original composition being devoid of silica, or the quartz was removed by increased fluid activity during the shearing event. Andalusite is breaking down in the presence of muscovite indicating that muscovite growth was later than andalusite growth.

Sample number: 1113-40

Location: Scotts Creek, overturned folded zone

Tapanappa Formation

Quartz-mica-andalusite-schist

Hand Specimen

The hand specimen is light grey in colour, medium grained and medium hardness. An intensely foliated texture is present. Visible minerals in the specimen include quartz, biotite and porphyroblasts of andalusite ranging from 5mm to 15 mm in size.

Thin section

Biotite	30%
Andalusite	25%
Quartz	20%
Muscovite	15%
Fibrolite	5%
K-feldspar	5%

The thin section shows a medium grained prophyroblastic texture. The specimen consists of idioblastic grains of biotite and muscovite, xenoblastic to subidioblastic grains of quartz, and acicular fibrolite grains. The andalusite has a poikiloblastic texture with inclusions of biotite, k-feldspar and quartz. Alignment of the mica grains results in a strong foliated texture with occasional kink banding evident across the mica grains equated to D₃ deformation event. (Following Spry et al. (1988) nomenclature)

Sample number: 1113-41

Location: Scotts Creek, overturned folded zone

Tapanappa Formation

Quartz-Mica Schist

Hand Specimen

A medium grained sample light grey in colour, homogeneous with medium hardness. Minerals present include quartz, biotite and muscovite. The specimen has an intensely foliated texture defined by the biotite minerals.

Thin section

Quartz	40%
Biotite	30%
Muscovite	20%

The thin section is medium grained with subidioblastic to xenoblastic quartz crystals and idioblastic biotite and muscovite. Generally the quartz forms a granoblastic texture and the alignment of the mica grains results in a foliated texture.

Sample Number 1113-43

Location: Scotts Creek, east of main shaft

Tapanappa Formation

Quartz-Mica-Garnet-Feldspar Schist

Hand Specimen

A fine to medium grained relatively homogeneous rock, also termed a greywacke by other authors. Medium to dark grey in colour with medium hardness, this rock exhibits subtle foliation determined by the alignment of the biotite grains.

Thin Section

Quartz	30%
Biotite	20%
Albite	20%
Garnet	10%
Muscovite	10%
Fibrolite	5%

In thin section, this rock exhibits a fine to medium grained homogeneous texture. Iodioblastic to subidioblastic quartz and feldspar grains form a granoblastic texture.

Veins of predominantly k-Feldspar and quartz exhibit undulose extinction suggesting a high strain ratio in the area.

Iodioblastic and xenoblastic grains of biotite and muscovite form a subtle foliation, and also cross-cut this foliation in places suggesting two stages of growth.

Garnet is iodioblastic, very fine, pale pink and predominantly of spessartine type. It is distributed evenly throughout the rock and contributes to the granoblastic texture.

Specimen number: 1113-45

Location: north of Scotts Creek main shaft

Tapanappa Formation

Quartz-mica-garnet feldspar-Schist

Hand Specimen

This fine to medium grained homogeneous rock is dark grey in handspecimen, and of medium hardness. A subtle foliation is observed. Visible minerals include quartz, biotite and garnet.

Thin Section

Quartz	30%
Biotite	25%
Garnet	15%
Muscovite	10%
Fibrolite	10%
K-Feldspar	5%

The thin section reveals of fine to medium grained granoblastic texture with idioblastic grains of garnet and biotite and subidioblastic grains of quartz which exhibits undulose extinction. Foliated texture is seen in the alignment of the biotite grains. The feldspar is present as coarse grained xenoblastic, recrystallised grains in a vein, and as very fine grained crystals within the matrix. The feldspar type is microcline exhibiting annealed and crosshatched twinning. The idioblastic fine grained garnets are present only around the quartz vein, along with an altered band which is present as the deformed matrix with increased garnet content, and the formation of large recrystallised muscovite grains which overgrow all other minerals, suggesting they are a post deformation product.

Sample number: 1113-50

Location: 20m north of Scotts Creek main shaft.

Tapanappa Formation

Biotite-quartz-garnet-muscovite schist

Hand specimen:

A folded sample of very fine grained laminated quartz biotite quartz-biotite schist of medium hardness.

Thin section:

Biotite	30%
Quartz	30%
Garnet	20%
Muscovite	20%

Thin section shows folded compositional banding with biotite and garnet rich layers alternating with quartz and biotite layers. Xenoblastic biotite is aligned parallel to axial plane and forms dominant foliation. Very fine grained idioblastic garnet and sub idioblastic to idioblastic quartz forms a very fine grained matrix. Muscovite exhibits crenulated twinning indicating two deformation events. Large recrystallised muscovite also crosscuts foliation and compositional banding, thus is a post deformation mineral.

Sample number: 1113-283

Location: 150m south east of Kanmantoo mine

Tapanappa Formation

Garnet-quartz-chlorite coticule

Hand specimen:

A very fine grained light grey rock with minor fine grained bands.

Thin section:

Garnet	50%
Quartz	40%
Chlorite	10%

Very fine grained idioblastic garnet with inclusion rich/altered cores. Garnet and sub idioblastic – idioblastic quartz make up granoblastic matrix. Garnet is also present in minor garnet rich bands. Very fine grained chlorite is not aligned nor does it make up a prominent foliation as is observed in other rock types from the close vicinity.

Sample number: 1113-2An

Location: Angas prospect, DDH 28 depth

Tapanappa Formation

Quartz-biotite-muscovite-garnet-schist

Hand specimen:

A very fine grained hard greywacke, of predominantly quartz and biotite.

Thin section:

Quartz	40%
Biotite	25%
Muscovite	15%
Garnet	15%

Idioblastic garnet is present in a disseminated form and exhibits inclusion rich/altered cores. Garnet and idioblastic quartz make up granoblastic matrix. Xenoblastic biotite and muscovite align to form a weak foliation.

Sample Number 1113-1K, 1113-22K, 1113-23K

Location north along strike of Kanmantoo mine

Tapanappa Formation

Banded Iron Formation

Hand Specimen

Very fine grained massive maroon rock with an extremely high density. Very hard banded rock.

Thin Section

Magnetite	60%
Quartz	20%
Biotite	10%
Garnet	4%
Muscovite	3%
Chlorite	2%

In thin section this rock is very fine grained with alternating bands of granoblastic quartz exhibiting undulose extinction and opaques (predominantly magnetite). Minor muscovite is present in interlaying pelite layers with the banded iron formation that define a foliation by alignment of xenoblastic muscovite crystals and are parallel to magnetite banding. Sample 1113-23K contains garnets, all of which have been oxidised considerably. Very minor chlorite present within thin pelite layer.

Sample number: 1113-24K, -25K, -26K

Location: 150m east of Kanmantoo mine

Tapanappa Formation

Garnet-quartz-muscovite coticule

Hand specimen:

A hard fine to medium grained maroon rock, with 1cm bands of garnet present, and garnet crystals disseminated throughout matrix.

Thin section:

Quartz	40%
Garnet	30%
Muscovite	10%
Opaques	2%
Biotite	5%
Feldspar	5%
Staurolite	5%
Andalusite	2%

Idioblastic garnet ranges from 50 μ m to 2mm in size. The garnet is stained by oxides and is present in folded bands. Feldspar present in veins as xenoblastic grains that exhibit annealed twinning, and are large grains suggesting recrystallisation. Idioblastic quartz is present as the granoblastic matrix. The garnets within the matrix are much fine grained than within the garnet rich layers. Minor xenoblastic poikiloblastic andalusite and staurolite are coarse grained and present in minor amounts.

Sample number: 1113-18K

Location: 700m north of Kanmantoo mine

Tapanappa Formation

Garnet-quartz-biotite-staurolite coticule

Hand specimen

A manganese stained very fine grained hard sample within a biotite quartz schist.

Thin section

Garnet	40%
Quartz	30%
Biotite	20%
Staurolite	10%

In thin section, this rock exhibits very fine grained pale pink idioblastic garnet grains with altered cores. The garnet is present in bands and disseminated through out the matrix. Granoblastic matrix of fine grained idioblastic to sub-idioblastic quartz grains with garnet. Compositional banding is present indicated by staurolite-biotite rich layer. Staurolite exists in xenoblastic grains, with no inclusions or poikiloblastic varieties present as is common in surrounding garnetiferous schist. This may be an indication of the higher zinc content within the staurolite that stabilises the mineral during metamorphism. Garnets present in this layer (5mm) are larger than surrounding matrix and may be a reflection of multimineral matrix from which it has grown. Biotite wraps the staurolite and garnet forming the foliation of the rock. Andalusite is present in both porphyroblastic and poikiloblastic forms.

Sample Number 1113-8K

Location: 1 km north of Kanmantoo mine

Tapanappa Formation

Quartz-Mica-Andalusite-Staurolite Schist

Hand Specimen

This rock is medium to coarse grained, with medium hardness and is slightly friable. The colour is light to dark grey. The overall texture of the rock shows intense foliation. Visible minerals include quartz, andalusite, biotite and staurolite. The andalusite porphyroblasts have a size range of 5-10 mm.

Thin Section

Quartz	30%
Biotite	25%
Andalusite	15%
Staurolite	10%
Garnet?	10%

The thin section reveals a medium to coarse grained porphyroblastic texture consisting of subidioblastic grains of quartz, and garnet, idioblastic grains of biotite, staurolite and muscovite and xenoblastic grains of andalusite. The quartz grains form a grainoblastic texture. The andalusite grains have an intense poikiloblastic texture with inclusions of quartz, and mica grains. The alignment of the mica grains results in an overall foliated texture.

Sample Number 1113-12K

Location Kanmantoo, north of mine

Tapanappa Formation

Quartz-mica-garnet-andalusite-staurolite Schist

Hand Specimen

The rock is fine to medium grained, with medium hardness and is slightly friable.

The colour is light grey with yellow porphyroblasts of staurolite ranging in size from 2 mm to 5mm, and white porphyroblasts of andalusite ranging in size from 1mm to 5mm. The overall texture of the rock shows intense foliation.

Thin Section

Quartz	25%
Biotite	20%
Andalusite	20%
Garnet	15%
Staurolite	10%
Muscovite	10%

The thin section consists of an overall medium grained porphyroblastic texture.

Quartz and feldspars form a granoblastic texture. Idioblastic garnet grains are distributed throughout the rock. Staurolite is subidioblastic with inclusions of mica, quartz and k-feldspar. Andalusite porphyroblasts contain inclusions of staurolite, quartz, mica and k-feldspar. The alignment of mica grains results in an overall foliated texture.

Sample number: A1113-5K, A1113-2K, A1113-34K, A1113-27K, A11113-28K

Location: north of Kanmantoo mine

Tapanappa Formation

Quartz-Mica-Andalusite-Garnet Schist

Hand Specimen

This medium grained rock is dark grey to maroon in colour and is relatively friable. Visible minerals include quartz, biotite, garnet and abundant andalusite porphyroblasts which range in size from 3 mm to 10 mm. Overall a foliated texture is present.

Thin Section

Quartz	30%
Biotite	25%
Andalusite	15%
Garnet	15%
Muscovite	5%
Fibrolite	5%

The thin section reveals a medium grained prophyroblastic texture with idioblastic grains of biotite, andalusite, garnet and muscovite: subidioblastic grains of quartz and k-feldspar. There are trace quantities of acicular fibrolite grains surrounding the large poikiloblastic andalusite grains with inclusions of quartz, k-feldspar, staurolite and mica. The biotite grains bifurcate around the andalusite grains resulting in flaser structures. Overall alignment of the biotite grains results in a foliated texture. The quartz exhibits undulose extinction and generally forms a granoblastic textural arrangement. Decomposition of the garnet grains is relatively common, with fractures iron stained. Garnets usually exhibit inclusions of quartz, biotite and K-feldspar. Deformation and elongation has occurred to the majority of the andalusite grains resulting in a sigmoidal shape.

Sample Number: 1113-102K

Location: north of Kanmantoo mine

Tapanappa Formation

Breccia

Hand Specimen

Thin section is light grey to maroon in colour and is relatively hard. The rock consists of breccia clasts up to 10 mm in size. The individual clasts are predominantly quartz.

Thin Section

Quartz	30%
Opaques	30%
Andalusite	20%
Staurolite	10%
Muscovite	10%

The thin section reveals a fine grained porphyroblastic texture. The breccia clasts range in size from 3 mm to 15 mm and are predominantly quartz with some brecciated andalusite grains. Fine grained quartz contributes to a granoblastic textural arrangement. The andalusite has a poikiloblasti texture with inclusions of muscovite and idioblastic staurolite. Opaques surround and crosscut quartz breccia clasts that represent the intrusion of later iron rich fluids. Staurolite has inclusion trails of idioblastic opaques and mica grains. Any textural foliation present has been obliterated by the iron rich fluids.

Sample number: 1113-281

Location: surface coticule found near effluent pond, in a telecom trench, Strathalbyn
Tapanappa Formation
Garnet-quartz-andalusite-staurolite coticule

Hand specimen:

Very fine grained pale pink dense massive rock of predominantly quartz and garnet. Very hard crystallised specimen.

Thin section:

Garnet	50%
Quartz	20%
Andalusite	20%
Staurolite	5%
Chlorite	5%

Very fine grained idiomorphic garnet present in minor bands (2mm) but mostly disseminated throughout the matrix. Garnet along with fine grained idiomorphic quartz makes up granoblastic matrix. The garnet overgrows large xenoblastic poikiloblastic andalusite grains and xenoblastic chlorite grains.

Sample Number A1113-90, DDH No. 31

Location: Angas drillcore

Tapanappa Formation

Garnet-Biotite-Quartz-Schist with trace Staurolite and disseminated fine grained sulphide.

Hand Specimen

A hard, fine to medium grained light grey rock, with 1cm dense pale pink very fine grained garnet bands present.

Thin Section

Quartz	20%
Biotite	20%
Garnet	20%
Andalusite	10%
Staurolite	5%
Muscovite	10%
Opaques	5%

In thin section, this rock is finely layered with a distinct garnet band with greater than 90% garnet in places aligning the layers. Garnet is pale pink, very fine grained idioblastic to subidioblastic grains congealing as clumps of undistinguishable grains to being finely disseminated throughout the matrix. Idioblastic quartz grains and subidioblastic euhedral biotite grains form a granoblastic texture. A generally massive homogeneous rock with subtle foliation represented by alignment of biotite grains. Very anhedral staurolite grains appear to have reacted to form some of the sulphides present which are predominantly pyrrhotite, pyrite, sphalerite and galena, which are disseminated throughout the matrix. Garnets are predominantly inclusion free, with minor amounts having inclusions of quartz and biotite.

Appendix B

ANALYTICAL PROCEDURES – PREPARATION AND ANALYTICAL TECHNIQUES

SAMPLE PREPARATION:

1. Whole rock samples were cleaned of weathered and organic material. This was followed by crushing of the samples in a jaw crusher to gravel size pieces (~10mm size).
2. Crushed samples were milled for 30-45 seconds in a W₂C (tungsten carbide) mill vessel, to produce a fine powder suitable for analysis.

Major elements

The powdered samples were dried in an oven at 110°C for over 2 hours to remove absorbed moisture. They were then weighed into alumina crucibles and ignited overnight in a furnace at 960°C, to yield the Loss on Ignition (LOI) values. This comprises organic material, CO₂ from carbonate minerals, H₂O (water in combination with the crystal structure), and possible S, Cl and other volatiles depending on the mineralogy of the samples.

Trace elements

About 5-10g of sample powder was mixed with nominally 1ml of binder solution (Poly Vinyl Alcohol) and pressed to form a pellet in a 30mm aluminium cup. This was allowed to dry in air and was heated for a further 1 to 2 hours in a 60°C oven to ensure that the pellet was completely dry before analysis.

ANALYSIS:

Major elements

The samples were analysed using a Philips PW 1480 Xray Fluorescence Spectrometer (XRF), using an analysis program calibrated against several international and local Standard Reference Materials (SRM's). A dual-anode (Sc-Mo) Xray tube was used, operating at 40kv, 75mA.

Trace elements

Samples from Kanmantoo were analysed at Adelaide University, using a Philips PW 1480 CRF Spectrometer, using several analysis programs covering suites of from 1 to 7 trace elements, with conditions optimised for the elements being analysed. The programs were calibrated against many (30 or more in some cases) local and international SRM's. The dual-anode Sc-Mo tube (operated at sufficient voltage to excite the Mo) and a Au tube were used for the analyses. Matrix corrections are made using either the Compton Scatter peak, or mass absorption calculated from the major element data.

Samples from Scotts Creek were analysed at Australian National University, Canberra, using a SPECTRO X-lab energy dispersive XRF spectrometer. This spectrometer uses secondary targets to minimise background radiation and therefore minimise detection limits. Boron carbide and alumina targets are used to produce polarised X-rays for excitation of elements of atomic number > Fe, a Co target is used to excite K-Mn with Co-K α radiation and a graphite target is used to reflect Fh L radiation for the excitation of Na-S. All elements in a sample are used in a fundamental parameters scheme for matrix correction. The powders were also measured on a PW1400 wavelength dispersive XRF spectrometer for Sc, V and C.

To detect Au limits, the samples were fused with litharge and flux. The resultant lead button is cupelled and digested in aqua regia and determined by AAS.

Rare earth elements

Samples were analysed at Amdel Laboratories using ICP-AAS methods. A total digest method was used on the milled powder to give total elemental concentrations in varying matrices. A multi acid digest with HF is used to dissolve the refractory minerals. Some chromite, spinels, rutile, barite and zircon may not be completely dissolved.

RESULTS

Major elements

The results are presented on a 'dry basis' in a tabular form as oxides in weight %, which is the traditional form for silicate analyses. The analyses are on the 'whole' sample, including any organic material that may be present. The iron is analysed as total Fe (combining the ferrous and ferric forms, expressed as Fe₂O₃T).

The oxides analysed were: SiO₂, Fe₂O₃, MnO, MgO, Na₂O, K₂O, TiO₂, P₂O₃, SO₃.

Trace elements

The results are presented as elements in tabular form, expressed as ppm. The calibrations assume trace levels of the elements, usually up to one to several thousand ppm.

The elements analysed were: Sr (1.0), Rb (1.0), Y (1.0), Zr (2.0), Nb (1.5), Pb (2.5), Th (1.5), U (1.5), Ba (3), Sc (2), Ga (2), B (2), Cr(1.5), Ce (5), Nd (3), La (2), Ni (3), Cu (4), Zn (3), Co (2). The detection limits are in brackets and represent the analytical technique used by Adelaide University.

Gold (Au) was measured from one to several thousand ppb.

Rare earth elements

The results are presented as elements in tabular form, expressed as ppm.

The elements analysed were: Ce, Eu, Gd, La, Lu, Nd, Sm, Tb, Yb and Au.

Abbreviations used for Scotts Creek analytical results:

q- quartz; b - biotite; an - andalusite; g - garnet; sch - schist;

Abbreviations and descriptions of samples from Kanmantoo field area:

1113-01K	BIF - dk br/red vfg layered dense
1113-22K	BIF - dk br/red vfg + garnet, dense
1113-23K	BIF - dk br/red vfg + garnet, dense
1113-02K	pl pk/gy vfg gt-qtz,chl + qtz vns,S
1113-03K	and,bi,qtz,gt sch. Cg, v fol. ~1%gt
1114-04K	qtz,bi, gt ~10%, chl, mag,hem
1113-05K	qtz S staining, pitted
1113-06K	mg, layered, fe,qtz,msv, some gt
1113-07K	mg, Fe stain, S rich, qtz rich
1113-13K	vfg qtz,bi schist, no gt, fol
1113-14K	vfg mica,qz,and,st schist <1%gt
1113-21K	vfg qtz rich g/wacke, <1%gt
1113-15K	vfg gy/pink qt,bi, gt<5%, pitted S
1113-16K	vfg qtz,bi,and schist ~1% gt
1113-17K	cg qtz+and+bi+st+chl+gt schist
1113-18K	vfg dense lgt gy rock w c vns + garnet
1113-32K	mg sulphide rich,garnet rich quartz rock
1113-24K	mg garnet-quartz rock + biotite
1113-25K	mg garnet-quartz rock + biotite
1113-26K	mg garnet-quartz rock + biotite
1113-19K	fg-cg, fol, qtz,bi,and,qt ~5% qt vns
1113-20K	qtz,bi,and,gt,st,schist dk gy,folS
1113-08K	gossan,Fe rch,qtz breccia, and
1113-09K	qz-gt schist +st+and+fe stain
1113-10K	fg layered lgt gy dense qtz rock,S
1113-11K	gt <5%,banded greywacke
1113-12K	gt rich,S, msv mg-cg pink qtz vns
1113-283	vfg gry siltstone + garnet,feldspar,quartz
1113-282	background garnet-quartz-biotite-andalusite-schist

vfg - very fine grained; mg - medium grained; cg - coarse grained; fol - foliated; vns - veins;
 msv - massive; S - sulphide; and - andalusite; bi - biotite; gt - garnet; qtz - quartz; st - staurolite
 fspr - feldspar; mag - magnetite; hem - hematite; chl - chlorite; g/wacke - greywacke; lgt - light;
 dk - dark; pl - pale; br - brown; gy - grey; w - with.

E-W trav-di - east-west distal traverse; E-W trav-pr - east-west proximal traverse.

Abbreviations used for Angas analytical results:

FWS	Footwall sequence
HWS	hanging wall sequence
LHU	lower host unit
UHU	upper host unit
MHU	main host unit

Table 1

Major, trace element and REE data for various rock types from Scotts Creek

E-W PROXIMAL TRAVERSE THROUGH SCOTT'S CREEK MINE								
	1113-59	1113-60	1113-61	1113-62	1113-63	1113-64	1113-65	1113-66
	main shaft				foot wall			
	q b sch		coticule	host rock	q b sch	host rock	q b and sch	q b sch
SiO ₂	66.12	67.59	63.41	64.57	62.51	48.22	68.32	61.78
Al ₂ O ₃	15.05	14.65	14.64	13.01	17.66	14.17	14.22	17.23
Fe ₂ O ₃	6.24	5.65	5.76	5.69	6.44	6.99	5.59	7.19
MnO	0.18	0.42	5.04	6.30	0.24	12.49	0.07	0.09
MgO	2.25	2.55	1.11	1.23	2.48	2.07	3.46	4.44
CaO	1.44	2.14	0.51	0.84	0.97	12.83	2.21	1.67
Na ₂ O	2.13	1.51	0.35	0.29	1.04	0.08	1.48	1.63
K ₂ O	4.40	3.51	6.04	5.30	5.03	0.05	2.91	3.38
TiO ₂	0.78	0.71	0.73	0.57	0.82	0.45	0.73	0.78
P ₂ O ₅	0.19	0.17	0.17	0.13	0.16	1.07	0.18	0.16
SO ₃	0.00	0.00	0.01	0.01	0.01	0.08	0.00	0.01
LOI	1.00	1.05	0.44	0.24	2.34	1.23	1.10	1.52
Total	99.79	99.96	98.21	98.18	99.69	99.72	100.26	99.89
Sc	22.0	20.0	16.0	12.0	26.0	8.0	20.0	28.0
V	100.0	94.0	92.0	78.0	112.0	90.0	94.0	120.0
Cr	96.0	94.0	84.0	70.0	110.0	48.0	92.0	116.0
Ni	38.0	40.0	14.0	8.0	56.0	10.0	38.0	50.0
Cu	21.5	34.1	23.5	786.3	119.0	46.9	12.1	18.8
Zn	77.1	508.1	176.9	170.3	627.1	39.8	65.8	76.6
Ga	17.7	14.1	18.3	15.7	18.4	17.2	17.0	20.8
Ge	1.2	2.3	1.1	0.9	2.2	1.8	1.4	1.7
As	-0.6	9.4	48.5	12.5	17.6	-0.6	0.6	3.2
Se	-0.2	-0.2	-0.2	-0.2	-0.2	-0.2	-0.2	-0.2
Br	0.6	0.6	0.9	1.2	0.6	3.2	0.7	0.3
Rb	136.0	132.7	259.1	188.4	201.7	0.3	131.9	151.3
Sr	166.7	123.0	132.6	136.7	79.6	71.9	80.0	80.4
Y	28.4	26.1	29.3	14.4	34.4	32.8	27.6	30.6
Zr	220.5	175.2	221.5	113.6	172.4	87.8	219.5	144.0
Nb	15.2	14.1	14.2	12.4	15.8	10.2	14.0	15.2
Mo	0.5	-0.4	1.0	0.5	-0.4	1.8	-0.4	0.3
Ag	-0.1	0.1	1.7	5.7	-0.1	0.6	-0.1	0.2
Cd	-0.1	0.6	0.7	3.9	2.1	0.7	1.4	-0.1
In	-0.1	-0.1	-0.1	-0.1	-0.1	-0.1	-0.1	-0.1
Sn	4.8	4.1	5.2	2.1	5.8	4.4	4.5	3.7
Sb	-0.1	-0.1	5.8	6.9	0.3	-0.1	-0.1	-0.1
Te	-0.2	-0.2	-0.2	-0.2	-0.2	-0.2	-0.2	-0.2
I	-0.3	-0.3	-0.3	-0.3	-0.3	-0.3	-0.3	-0.3
Cs	6.3	3.2	2.3	2.0	10.5	0.0	5.6	4.7
Ba	1373.0	708.5	735.7	1059.0	1000.0	191.6	370.0	375.8
La	15.9	3.0	44.6	6.8	21.4	25.9	44.6	42.2
Ce	68.1	23.3	105.6	46.9	67.1	58.0	93.4	90.6
Pr	8.9	-1.5	8.9	2.9	4.7	-1.5	7.4	5.1
Nd	38.7	12.7	48.0	26.2	42.5	19.1	39.3	38.8
Hf	8.9	7.4	21.6	-0.1	7.9	8.8	8.3	6.2
Tl	1.1	0.8	-0.5	-0.5	2.2	-0.5	0.8	1.1
Pb	19.7	93.0	2278.0	3223.0	88.5	4.1	67.3	42.4
Bi	-0.3	-0.3	-0.3	-0.3	-0.3	1.3	-0.3	-0.3
Th	19.0	18.0	21.0	14.0	20.0	13.0	16.0	18.0
U	3.0	3.0	4.0	3.0	3.0	3.0	3.0	3.0
Co	n/a	n/a	3	4	14	23	n/a	n/a

Table 1

Major, trace element and REE data for various rock types from Scotts Creek

	1113-23	1113-24	1113-25	1113-284	1113-285	1113-286
	coticule layer 12m west of main shaft garnet-quartz coticule + apatite + biotite + rutile					
SiO2	61.59	67.12	62.80	58.29	62.49	64.62
Al2O3	15.72	11.23	14.91	16.79	14.99	14.76
Fe2O3	4.63	8.33	5.79	6.20	5.84	4.86
MnO	6.34	8.56	5.17	7.72	5.43	6.43
MgO	1.16	0.83	1.12	1.34	1.12	0.91
CaO	2.05	2.53	0.53	2.53	0.57	1.70
Na2O	0.98	0.39	0.34	0.89	0.37	0.59
K2O	5.02	0.23	6.11	3.64	6.20	3.71
TiO2	0.79	0.46	0.72	0.81	0.74	0.75
P2O5	0.15	0.14	0.13	0.23	0.16	0.14
SO3	0.01	0.01	0.02	0.02	0.02	0.01
LOI	0.46	-0.15	0.33	0.32	0.56	0.67
Total	98.90	99.66	97.96	98.77	98.49	99.15
Sc	17.6	14.2	13.5	15.3	15.3	15.0
V	144	101	131	146	141	129
Cr	n/a	n/a	n/a	n/a	n/a	n/a
Ni	37	8	16	16	20	13
Cu	472	90	21	22	64	31
Zn	132	108	207	205	162	66
Ga	23.1	7.4	27.4	29.2	23.9	17.4
Rb	187.8	16.4	299.8	291.9	108.4	92.6
Sr	151.6	42.2	140.7	151.0	126.2	105.6
Y	31.0	27.6	34.6	35.1	32.8	28.6
Zr	170.8	114.7	198.7	224.8	205.2	195.9
Nb	17.5	12.9	14.9	16.7	16.6	16.5
Ba	1248	76	950	1077	1739	1406
La	67	35	65	69	16	38
Ce	129	100	139	163	57	90
Pr	n/a	n/a	n/a	n/a	n/a	n/a
Nd	34	9	45	45	0	20
Hf	n/a	n/a	n/a	n/a	n/a	n/a
Tl	n/a	n/a	n/a	n/a	n/a	n/a
Pb	105.8	87.0	2137.5	2434.0	1394.6	110.0
Bi	n/a	n/a	n/a	n/a	n/a	n/a
Th	20.3	13.6	23.4	24.7	24.0	18.8
U	2.0	1.1	4.7	2.9	1.5	3.2
Co	6	3	2	3	3	5
Rare earth element analyses		Au in ppb, REE in ppm				
La	53	28	n/a	63	15.5	32.5
Ce	96	50	n/a	120	26	58
Nd	36.5	23	n/a	45.5	12	25
Sm	7	4.8	n/a	8.5	4.6	6
Eu	1.95	1.25	n/a	1.8	1.8	1.85
Gd	7	6	n/a	8	5.5	6.5
Tb	0.93	0.82	n/a	1	0.85	0.87
Yb	2.7	2.3	n/a	2.8	2.7	2.6
Lu	0.41	0.34	n/a	0.42	0.41	0.4
Au	-	-	-	2	-	-

Table 2

Major, trace-element and REE data for various rock types from the Kanmantoo field area.

Sample Name	1113-1K	1113-22K	1113-23K	1113-2K	1113-3K	1113-4K	1113-5K
LOCATION	E-W trav-pr	E-W trav-di	E-W trav-di	E-W trav-pr	E-W trav-pr	E-W trav-pr	E-W trav-pr
wt%							
SiO ₂	20.33	58.43	64.86	61.79	66.81	69.00	73.38
Al ₂ O ₃	2.12	4.41	4.46	9.40	9.13	7.92	8.15
Fe ₂ O ₃ T	74.56	26.06	25.4	25.07	18.62	19.18	14.25
MnO	0.07	0.03	0.04	0.16	0.08	0.15	0.10
MgO	0.34	0.17	0.87	2.04	2.24	1.80	0.26
CaO	0.03	0.04	0.07	0.15	0.03	0.03	0.34
Na ₂ O	0.02	0.1	0.01	0.00	0.01	0.01	0.00
K ₂ O	0.12	2.16	1.4	0.06	0.28	0.02	0.01
TiO ₂	0.11	0.34	0.25	0.41	0.47	0.39	0.30
P ₂ O ₅	0.01	0.08	0.15	0.05	0.02	0.04	0.01
SO ₃	0.00	0.29	0.02	0.00	0.00	0.01	0.00
LOI	0.93	8.06	2.16	1.12	1.96	1.73	3.33
Total %	98.63	100.17	99.68	100.25	99.65	100.27	100.13
ppm							
Zr	30.1	77.2	71.7	127.9	127.9	127.1	81.1
Nb	9.2	9.4	6.7	10.7	13.0	10.6	8.5
Y	3.3	6.3	12.9	16.2	24.4	23.9	10.0
Sr	9.4	43.9	123.8	2.6	1.0	6.9	5.8
Rb	18.7	25.1	149.7	5.1	19.4	2.0	1.6
U	4.6	2	2.9	2.9	3.7	1.6	3.4
Th	61.2	22.9	8.4	10.1	9.8	7.4	4.7
Pb	4.6	17.8	3.1	1.9	1.1	3.1	1.9
Ga	11.9	13.7	11.5	13.3	13.9	8.7	6.9
Cu	1502	69	80	550	603	133	848
Zn	30	62	58	102	88	104	7
Ni	29	9	38	33	27	17	7
Ba	37	195	326	34	48	14	40
Sc	1.0	4.9	4.4	6.5	10.8	5.8	21.8
Co	20	11	53	73	55	61	49
V	125	54	63	70	59	42	44
Ce	70	51	192	44	19	24	26
Nd	5	10	66	12	5	1	7
La	1	10	104	9	1	1	6
Cr	19	145	118	69	78	49	64
Rare earth element analyses							
La	6.5	20.5	105				
Ce	23	34.5	165				
Nd	7.5	16.5	71				
Sm	1.6	3.1	11				
Eu	0.39	2.1	2.3				
Gd	1.6	2.8	9.5				
Tb	0.26	0.32	0.85				
Yb	1.15	0.4	1				
Lu	0.16	0.06	0.17				
Au -ppb	<1	0.027	0.011				

Table 2

Major, trace-element and REE data for various rock types from the Kanmantoo field area.

Sample Name	1113-6K	1113-7K	1113-13K	1113-14K	1113-21K	1113-15K	1113-16K	1113-17K
LOCATION	E-W trav-pr	E-W trav-pr	E-W trav-pr	E-W trav-pr	E-W trav-pr	E-W trav-pr	E-W trav-pr	E-W trav-pr
wt%								
SiO ₂	58.40	64.47	68.33	61.37	76.39	76.28	66.66	66.26
Al ₂ O ₃	4.12	11.99	12.67	16.80	10.30	10.26	13.14	12.04
Fe ₂ O ₃ T	35.02	17.33	7.79	11.00	4.73	4.71	10.70	15.11
MnO	0.07	0.11	0.12	0.11	0.12	0.12	0.20	0.14
MgO	0.35	0.39	2.46	3.22	1.74	1.73	2.42	2.74
CaO	0.05	0.59	1.50	0.24	2.13	2.11	0.12	0.03
Na ₂ O	0.01	0.01	2.04	0.73	1.68	1.66	0.14	0.10
K ₂ O	0.07	0.01	2.78	3.46	1.80	1.79	4.54	2.00
TiO ₂	0.17	0.41	0.73	0.75	0.52	0.51	0.72	0.53
P ₂ O ₅	0.01	0.02	0.18	0.11	0.17	0.17	0.09	0.04
SO ₃	0.00	0.00	0.00	0.00	0.00	0.00	0.00	0.00
LOI	1.51	4.55	0.87	1.78	0.36	0.38	1.09	0.98
Total %	99.77	99.87	99.46	99.57	99.93	99.71	99.84	99.97
ppm								
Zr	40.8	113.6	297.0	148.0	234.5	282.2	206.7	92.2
Nb	4.9	8.7	15.2	15.5	11.0	11.8	16.3	14.4
Y	4.8	4.9	25.0	34.4	24.7	30.7	30.7	13.1
Sr	4.7	2.4	104.0	35.3	68.4	26.5	25.9	12.1
Rb	3.4	0.7	122.8	166.6	99.6	204.4	114.9	94.0
U	1.9	1.9	1.9	4.4	3.7	3.6	3.6	3.2
Th	4.2	9.4	16.9	16.8	14.7	13.9	13.9	12.8
Pb	5.8	3.1	15.6	4.7	9.0	9.7	6.4	2.9
Ga	6.1	11.8	18.7	23.0	11.6	18.7	18.4	14.1
Cu	137	755	25	60	35	6	19	36
Zn	26	10	79	45	52	83	74	82
Ni	18	88	37	52	19	32	27	42
Ba	117	29	987	491	472	894	370	374
Sc	6.3	19.5	12.5	18.7	9.6	12.5	11.6	11.0
Co	45	40	36	35	44	32	70	63
V	148	45	104	131	68	103	103	86
Ce	39	29	60	74	93	69	76	19
Nd	2	5	25	29	40	25	27	2
La	4	3	27	30	43	30	34	0
Cr	30	295	106	136	68	106	99	96

Table 2

Major, trace-element and REE data for various rock types from the Kanmantoo field area.

Sample Name	1113-18K	1113-32K	1113-24K	1113-25K	21113-26K	1113-19K	1113-20K	1113-8K
LOCATION	W-prox	W-prox	E-prox	E-prox	E-prox	E-W trav-pr	E-W trav-pr	E-W trav-di
wt %								
SiO ₂	65.02	63.02	65.59	66.19	67.74	63.96	67.91	42.52
Al ₂ O ₃	10.00	3.37	13.62	12.5	11.3	14.45	13.35	9.01
Fe ₂ O ₃ T	17.38	18.77	13.85	13.17	14.18	12.71	10.41	44.14
MnO	1.68	0.05	0.17	0.17	0.23	0.14	0.11	0.05
MgO	0.63	0.11	1.69	1.49	1.29	2.64	2.97	0.25
CaO	0.26	0.03	0.15	0.18	0.2	0.08	0.19	0.22
Na ₂ O	0.16	0.76	0.07	0.1	0.07	0.10	0.41	0.04
K ₂ O	0.49	1.19	2.94	2.3	2.82	2.89	2.58	0.11
TiO ₂	0.51	0.33	0.69	0.72	0.61	0.68	0.68	0.51
P ₂ O ₅	0.16	0.07	0.14	0.19	0.21	0.11	0.12	0.04
SO ₃	0.05	0.38	0	0.01	0	0.00	0.00	0.01
LOI	3.05	11.78	1.07	2.67	1.32	1.68	0.74	2.32
Total %	99.39	99.85	99.97	99.67	99.95	99.44	99.47	99.22
ppm								
Zr	142.6	138.4	220.1	387.3	312.4	160.8	221.6	127.8
Nb	10.3	11.1	15.2	16.5	15	14.9	14.7	12.9
Y	19.9	7.5	26.4	44.3	28.3	31.7	30.7	10.8
Sr	15.3	16.8	35	132.3	122.7	9.9	15.7	30.1
Rb	13.0	20.3	157.1	92.4	151.7	140.1	132.7	7.6
U	2.4	2.4	2.4	5	2.9	4.1	2.2	2.3
Th	213.4	39.0	16.1	19.7	14.8	16.2	13.7	35.4
Pb	400.3	6.1	8.1	40.7	32.8	19.8	5.2	12.3
Ga	12.0	5.6	20	20.3	14.2	22.0	18.6	20.3
Cu	334	349	173	132	75	767	34	209
Zn	2378	9	139	47	121	76	63	59
Ni	8	10	50	48	50	45	43	17
Ba	106	21	423	514	290	417	402	185
Sc	9.5	3.3	12.2	12.2	9.1	14.9	13.1	10.4
Co	32	8	17	16	17	46	44	19
V	69	32	111	108	91	117	106	173
Ce	64	47	68	85	75	73	74	48
Nd	12	14	29	30	26	25	30	6
La	17	12	30	34	28	29	31	2
Cr	72	n/a	223	175	177	117	107	134
Rare earth element analyses								
La	26.5	28	44	51	41.5			
Ce	43.5	49.5	76	90	72			
Nd	18.5	22	37	43.5	34.5			
Sm	3.5	4.2	6.5	7.5	6			
Eu	1.55	2.4	1.4	1.4	1.05			
Gd	4.3	3.4	6	6.5	5.5			
Tb	0.64	0.31	0.83	0.8	0.77			
Yb	2.1	0.4	2.3	2.1	2.1			
Lu	0.3	0.06	0.41	0.44	0.42			
Au	1470	1010	n/a	n/a	n/a			

Table 2

Major, trace-element and REE data for various rock types from the Kanmantoo field area.

Sample Name	1113-9K	1113-10K	1113-11K	1113-12K	1113-283	1113-282
LOCATION	E-W trav-di	E-W trav-di	E-W trav-di	E-W trav-di	mine site	background
wt%						
SiO ₂	62.30	65.86	74.50	76.42	75.37	66.51
Al ₂ O ₃	13.92	5.80	8.64	5.50	10.49	13.30
Fe ₂ O ₃ T	18.55	24.11	13.40	15.18	5.01	13.38
MnO	0.02	0.08	0.02	0.04	1.60	0.15
MgO	0.57	0.15	0.19	0.17	1.66	1.86
CaO	0.04	0.19	0.03	0.03	0.51	0.19
Na ₂ O	0.02	-0.01	0.00	0.00	0.06	0.08
K ₂ O	0.53	0.01	0.01	0.03	2.84	3.00
TiO ₂	0.71	0.34	0.52	0.30	0.53	0.71
P ₂ O ₅	0.04	0.15	0.03	0.03	0.10	0.16
SO ₃	0.00	0.00	0.00	0.00	0.02	0.01
LOI	2.77	3.19	2.70	2.14	1.27	0.69
Total %	99.48	99.88	100.04	99.84	99.45	100.04
ppm						
Zr	138.7	88.8	212.7	62.1	159.1	232.6
Nb	16.7	8.6	11.1	7.2	10.2	16.0
Y	14.2	6.8	9.6	9.3	93.5	25.9
Sr	3.7	5.8	4.7	2.6	179.1	13.5
Rb	95.8	1.3	4.8	9.3	155.5	166.1
U	1.9	0.5	2.5	0.8	1.5	2.5
Th	14.6	10.3	12.4	8.2	14.9	13.6
Pb	12.8	2.0	8.4	2.6	161.8	10.0
Ga	22.4	5.1	14.5	7.6	11.2	18.9
Cu	64	56	29	32	512	68
Zn	84	9	75	34	221	126
Ni	37	8	11	9	35	52
Ba	171	24	52	8	992	334
Sc	13.1	5.1	5.6	2.6	9.1	11.3
Co	38	31	54	45	31	17
V	119	81	70	60	67	105
Ce	42	21	20	13	202	65
Nd	12	3	7	3	84	23
La	11	0	4	0	93	23
Cr	201	53	81	59	n/a	n/a
Rare earth element analyses						
La					94	41.5
Ce					180	82
Nd					71	32
Sm					14	6
Eu					3.1	1.4
Gd					14	6
Tb					2.2	0.8
Yb					9.5	2.2
Lu					1.35	0.34
Au					2	n/a

table 3:

Major, trace and REE data for various rock types from Angas Pb-Zn prospect

SAMPLE	1113-281	4 - FWS	4 - HWS	4 - LHU	4 - UHU	4 - MHU	9 - HWS
SiO ₂	58.56	72.93	71.68	70.13	61.53	58.44	70.56
Al ₂ O ₃	16.04	0.61	0.61	0.64	0.76	0.71	0.67
Fe ₂ O ₃ T	20.45	11.44	13.21	13.51	15.45	15.74	13.41
MnO	0.77	4.73	4.56	4.91	8.12	12.41	4.46
MgO	2.97	0.18	0.06	0.11	0.28	0.43	0.21
CaO	0.28	1.98	2.03	2.37	4.058	3.14	1.94
Na ₂ O	0.08	2.71	1.84	2.12	1.01	0.31	1.62
K ₂ O	0.66	2.08	1.71	1.44	0.64	0.53	1.68
TiO ₂	0.70	1.85	2.78	2.98	4.55	3.31	3.36
P ₂ O ₅	0.15	0.18	0.17	0.17	0.17	0.15	0.19
SO ₃	0.02	0.03	0.02	0.02	0.11	0.05	0.04
LOI	0.00	0.86	1.11	1.26	3.14	2.13	1.31
Total	100.38	99.58	99.77	99.65	99.65	97.37	99.43
traces ppm							
Zr	145.2						
Nb	16.8						
Y	33.9						
Sr	15.0						
Rb	39.5						
U	5.1						
Th	17.2						
Pb	59.1						
Ga	30.3						
Cu	10	112.9	120.2	102.2	76.2	57.4	81.8
Zn	1570						
Ni	80	33	18	36	48	67	40
Ba	385						
Sc	10.3						
Co	4	41	32	15	91	192	26
V	113						
Ce	81						
Nd	30						
La	32						
Cr	-						
Rare earth elements							
Ce	89						
Eu	0.49						
Gd	7						
La	44.5						
Lu	0.43						
Nd	35						
Sm	6						
Tb							
Yb							
Au	93						

Major data from McElhinney,(1994); trace element data from Both, (1998)

table 3:

Major, trace and REE data for various rock types from Angas Pb-Zn prospect

SAMPLE	9 - MHU	9 - FWS	9 - UHU	9 - LHU	14 - MHU	14 - LHU	14 - FWS	14 - HWS
SiO ₂	59.24	62.46	65.12	71.38	67.91	47.81	72.02	66.61
Al ₂ O ₃	0.77	0.69	0.68	0.57	0.61	0.79	0.61	0.61
Fe ₂ O ₃ T	18.53	16.59	14.88	12.44	14.16	19.07	12.39	13.27
MnO	10.81	6.48	6.27	5.14	9.11	15.58	4.47	4.92
MgO	0.54	0.08	0.21	0.28	0.57	0.35	0.07	0.14
CaO	3.95	3.67	3.08	2.27	2.38	5.82	2.04	1.92
Na ₂ O	0.58	2.63	2.87	2.86	0.52	3.78	2.22	3.07
K ₂ O	0.31	2.22	1.59	0.58	0.33	0.38	2.41	1.38
TiO ₂	3.51	3.48	2.89	2.75	2.51	2.69	2.57	2.31
P ₂ O ₅	0.15	0.16	0.16	0.14	0.15	0.18	0.17	0.15
SO ₃	0.06	0.03	0.06	0.05	0.03	0.13	0.02	0.15
LOI	1.35	1.35	1.61	1.42	0.82	3.21	0.73	4.84
Total	99.81	99.84	99.87	99.81	99.06	99.77	99.71	99.35
traces ppm								
Zr								
Nb								
Y								
Sr								
Rb								
U								
Th								
Pb								
Ga								
Cu	96.4	145.5	117	117.7	102.6	72.5	145.4	169.2
Zn								
Ni	75	27	37	26	40	39	24	29
Ba								
Sc								
Co	15	32	20	55	21	241	31	12
V								
Ce								
Nd								
La								
Cr								

Major data from McElhinney,(1994); trace element data from Both, (1998)

table 3:

Major, trace and REE data for various rock types from Angas Pb-Zn prospect

SAMPLE	14 - UHU	18 - LHU	18 - UHU	18 - MHU	18 - HWS
SiO ₂	59.11	67.23	65.01	45.72	74.23
Al ₂ O ₃	0.76	0.64	0.68	0.64	0.51
Fe ₂ O ₃ T	16.89	14.49	15.57	14.96	11.58
MnO	7.56	5.72	6.01	17.17	4.31
MgO	0.38	0.11	0.56	1.48	0.07
CaO	3.91	2.74	2.88	3.26	2.02
Na ₂ O	1.05	1.84	3.06	1.06	2.11
K ₂ O	1.54	2.58	0.85	1.63	2.34
TiO ₂	4.87	2.95	2.81	2.64	1.86
P ₂ O ₅	0.16	0.16	0.17	0.16	0.16
SO ₃	0.09	0.04	0.08	0.26	0.02
LOI	3.16	1.23	1.94	2.91	0.82
Total	99.46	99.73	99.61	91.88	100.02
traces ppm					
Zr					
Nb					
Y					
Sr					
Rb					
U					
Th					
Pb					
Ga					
Cu	70.9	111.3	116.3	62	116.8
Zn					
Ni	52	37	37	53	45
Ba					
Sc					
Co	12	18	42	275	14
V					
Ce					
Nd					
La					
Cr					

Major data from McElhinney,(1994); trace element data from Both, (1998)

Appendix C

ELECTON MICROPROBE ANALYSES

Electron microprobe is an analytical technique applied to minerals to determine their chemical composition using the emission of characteristic X-rays by atoms for the specific mineral.

For a given sample the number of the photons of any particular characteristic energy (wavelength) emitted is related to the concentration of the element present (Battey and Pring, 1997). Analysis by the electron microprobe is not a form of absolute analysis, but rather a comparison of the X-ray emissions of an unknown sample with the emissions from a series of standards (Battey and Pring, 1997).

Electron microprobe analyses were conducted on polished thin sections, carbon coated with a standard carbon coating, and analysed using a CAMECA 5X51 MICROANALYSER using 15KeV voltage and a 20mA beam current on a standard package called miscgn.

Garnets were recalculated to 24 oxygens using a computer generated program called probe recalculation.

TABLE 1: ELECTRON MICROPROBE ANALYSES OF GARNETS FROM SCOTTS CREEK (BASED ON 24 OXYGENS)

Sample # Wt. % cations	1113-11 traverse						1113-32							
	1	2	3	4	5	6	1c	1r	2c	2r	3c	3r	4c	4r
SiO ₂	36.110	36.464	36.318	36.223	36.642	36.650	36.259	41.104	36.377	36.014	36.045	37.251	35.524	36.144
TiO ₂	0.032	0.035	0.001	0.066	0.154	0.010	0.136	0.055	0.025	0.274	0.224	0.009	0.008	0.014
Al ₂ O ₃	20.296	20.442	20.388	20.300	20.554	20.477	20.388	20.342	20.839	20.147	20.067	21.017	20.675	20.642
V ₂ O ₃	0.004	0.013	0.010	0.008	0.010	0.000	0.000	0.000	0.000	0.000	0.000	0.000	0.000	0.000
Cr ₂ O ₃	0.000	0.011	0.000	0.000	0.029	0.000	0.036	0.063	0.015	0.025	0.000	0.000	0.000	0.006
MgO	1.435	2.848	2.879	2.736	2.744	2.543	1.312	1.152	1.447	1.488	1.457	1.272	1.507	1.430
CaO	2.409	0.690	0.767	1.121	0.915	0.640	5.437	4.609	2.068	3.853	3.864	4.381	5.099	4.243
MnO	11.127	3.264	3.409	3.494	3.294	3.911	19.863	20.100	22.384	21.052	21.124	20.889	21.339	21.466
FeO	28.333	35.239	34.944	35.151	35.027	35.271	14.140	14.136	15.917	15.030	14.708	13.871	13.350	14.213
ZnO	0.000	0.000	0.000	0.003	0.000	0.000	0.000	0.000	0.000	0.000	0.000	0.000	0.000	0.000
Na ₂ O	0.008	0.029	0.001	0.000	0.025	0.036	0.012	0.001	0.021	0.000	0.011	0.150	0.000	0.021
K ₂ O	0.002	0.000	0.008	0.010	0.000	0.009	0.001	0.012	0.000	0.000	0.009	0.026	0.013	0.000
total	99.768	99.045	98.739	99.128	99.393	99.564	97.585	101.574	99.093	97.882	97.506	98.864	97.515	98.179
Atomic proportions														
Si	5.9353	5.9769	5.9717	5.9502	5.9793	5.9894	5.9573	5.9925	5.9571	5.9577	5.9854	5.9644	5.9566	5.9773
Ti	0.0039	0.0043	0.0001	0.0081	0.0188	0.0013	0.1	0	0.002	0.0011	0	0	0	0
Al	3.9316	3.949	3.9509	3.9301	3.953	3.9438	3.9763	3.9247	3.9622	3.9536	3.9465	3.9543	3.959	3.9432
V	0.0006	0.0016	0.0014	0.0011	0.0014	0	0	0	0.0016	0.0008	0.0006	0.0019	0.0029	0.0012
Cr	0	0.0014	0	0	0.0037	0	0.48	0.0042	0	0	0	0.0014	0.0019	0.0019
Mg	0.3516	0.6959	0.7055	0.6698	0.6674	0.6195	0.6661	0.5359	0.5522	0.5207	0.6382	0.6798	0.6872	0.6686
Ca	0.4242	0.1211	0.1351	0.1972	0.16	0.1121	0.181	0.1214	0.1138	0.112	0.1149	0.1177	0.1305	0.1643
Mn	1.5491	0.4531	0.4748	0.4862	0.4552	0.5413	0.4237	0.6811	0.6649	0.6751	0.5298	0.456	0.5044	0.519
Fe	3.8945	4.8305	4.8051	4.8289	4.78	4.8204	4.8369	4.7803	4.7884	4.8193	4.8097	4.8738	4.802	4.766
Zn	0	0	0	0.0003	0	0	0.5	0	0.0048	0.0076	0.0137	0	0	0
Na	0.0026	0.0091	0.0002	0	0.0079	0.0115	0.94	0.0024	0.0058	0.0131	0.0027	0.0084	0.0012	0
K	0.0004	0	0.0016	0.0022	0	0.002	0.15	0.0025	0	0.0059	0.0018	0	0.0007	0.0004
pyrope (Mg)	5.925	11.669	11.821	11.250	11.156	10.387	5.384	4.838	5.938	6.122	6.006	5.282	6.327	5.908
almandine (Fe)	60.819	78.702	77.961	77.272	78.561	78.658	32.247	33.298	35.758	33.256	33.056	32.328	27.372	31.093
spessartine (Mn)	26.106	7.598	7.955	8.165	7.608	9.076	46.328	47.953	52.203	49.225	49.488	49.308	50.911	50.398
grossular (Ca)	7.150	2.031	2.263	3.312	2.675	1.879	16.041	13.911	6.101	11.396	11.450	13.082	15.390	12.601

TABLE 1: ELECTRON MICROPROBE ANALYSES OF GARNETS FROM SCOTTS CREEK (BASED ON 24 OXYGENS)

Sample #	1113-37				1113-50				1113-45				
	1	2	3c	3r	1c	1r	2c	2r	1	2	3c	3r	4
Wt.% cations													
SiO ₂	36.1621	38.8422	35.9449	37.1087	35.9465	36.2916	36.3146	36.2191	36.3634	36.4069	36.2836	36.486	36.2467
TiO ₂	0.0887	0.191	0.05	0.1695	0.0238	0.0042	0	0.0745	0.3321	0.3123	0.1474	0.1054	0.1855
Al ₂ O ₃	20.4589	19.2183	20.3986	20.8725	20.3316	20.3452	20.2792	20.2703	20.1505	20.075	20.4848	20.491	20.3383
V ₂ O ₃	0	0	0	0	0	0	0	0	0	0	0	0	0
Cr ₂ O ₃	0	0.0115	0.0132	0.0823	0	0.0073	0.0055	0	0.0131	0.0767	0.0318	0	0.0374
MgO	1.4814	1.3014	1.5129	1.4117	1.1501	1.158	1.253	1.2188	1.2537	1.2495	1.1468	1.0772	1.2401
CaO	3.4269	3.7311	2.2682	4.9724	1.7401	1.9572	2.1866	2.0521	5.3804	5.0942	4.746	4.3712	4.3821
MnO	28.1341	27.3927	28.407	27.2386	15.8174	15.4217	15.4136	15.6406	14.9965	15.4465	15.8663	16.5996	15.7282
FeO	7.1531	6.1064	9.028	7.2211	23.2475	22.817	22.6536	22.9008	19.2933	19.673	19.3363	19.491	20.0152
ZnO	0	0	0	0	0	0	0	0	0	0	0	0	0
Na ₂ O	0.0141	0.0286	0.0285	0.0302	0.0261	0	0.0374	0.0084	0.0361	0	0.0129	0.0334	0.0205
K ₂ O	0.0158	0.0086	0.0192	0.0021	0.0179	0	0	0.0397	0.0017	0.0077	0.0103	0	0.0086
total	96.9351	96.8318	97.6704	99.1092	98.301	98.0021	98.1434	98.4243	97.8207	98.3418	98.066	98.6548	98.2025
Atomic proportions													
Si	6.0128	6.3746	5.9751	6.0159	5.9775	6.0263	6.0218	6.0018	6.0034	5.996	5.9864	5.9962	5.9829
Ti	0.0111	0.0236	0.0063	0.0207	0.003	0.0005	0	0.0093	0.0412	0.0387	0.0183	0.013	0.023
Al	4.0092	3.7172	3.9964	3.988	3.9847	3.9817	3.9632	3.9588	3.9208	3.8966	3.9833	3.9689	3.9565
V	0	0	0	0	0	0	0	0	0	0	0	0	0
Cr	0	0.0015	0.0017	0.0105	0	0.001	0.0007	0	0.0017	0.01	0.0042	0	0.0049
Mg	0.3671	0.3184	0.3748	0.3411	0.2851	0.2866	0.3097	0.301	0.3085	0.3067	0.282	0.2639	0.3051
Ca	0.6105	0.6561	0.404	0.8637	0.31	0.3482	0.3885	0.3643	0.9517	0.8989	0.839	0.7697	0.775
Mn	3.9622	3.8077	3.9996	3.7402	2.2279	2.169	2.1649	2.1952	2.097	2.1547	2.2173	2.3106	2.1989
Fe	0.9947	0.8381	1.255	0.979	3.2329	3.1686	3.1415	3.1736	2.6638	2.7096	2.668	2.6788	2.7629
Zn	0	0	0	0	0	0	0	0	0	0	0	0	0
Na	0.0045	0.0091	0.0092	0.0095	0.0084	0	0.012	0.0027	0.0116	0	0.0041	0.0106	0.0066
K	0.0033	0.0018	0.0041	0.0004	0.0038	0	0	0.0084	0.0004	0.0016	0.0022	0	0.0018
pyrope (Mg)	6.18686	5.66456	6.21318	5.758565	4.785827	4.79923	5.1632679	5.026272	5.124122	5.085218	4.706314	4.406416	5.093885
almandine (Fe)	16.7602	14.9117	20.8008	16.52575	52.60885	53.0527	52.269092	52.23951	44.24033	44.29134	44.29472	44.15677	45.25701
spessartine (Mn)	66.7656	67.7504	66.2904	63.13618	37.40056	36.3176	36.091031	36.65123	34.82871	35.72112	36.99904	38.5841	36.71074
grossular (Ca)	10.2874	11.6734	6.6956	14.5795	5.204757	5.83046	6.4766097	6.082987	15.80684	14.90233	13.99993	12.85271	12.93837

TABLE 1: ELECTRON MICROPROBE ANALYSES OF GARNETS FROM SCOTTS CREEK (BASED ON 24 OXYGENS)

Sample # Wt.% cations	1113-35 - coticule host rock					1113-38 - garnet biotite schist					
	1c	1r	2	3c	3r	4c	4r	2	3c	3r	1
SiO ₂	35.53	36.10	36.89	35.85	44.32	35.98	36.07	36.12	36.29	36.61	36.36
TiO ₂	0.17	0.20	0.13	0.29	0.07	0.02	0.01	0.00	0.01	0.00	0.00
Al ₂ O ₃	19.71	20.15	20.62	20.10	18.26	20.34	20.80	20.47	20.56	20.80	20.59
V ₂ O ₃	0.00	0.00	0.00	0.00	0.00	0.00	0.00	0.00	0.00	0.00	0.00
Cr ₂ O ₃	0.01	0.00	0.05	0.00	0.03	0.00	0.00	0.03	0.04	0.00	0.04
MgO	1.55	1.44	1.64	1.19	1.47	2.52	2.41	2.72	2.60	2.37	2.73
CaO	4.38	4.11	4.51	5.84	3.13	0.79	0.66	0.69	0.97	0.63	1.03
MnO	23.43	24.17	23.30	24.87	20.93	3.27	3.87	2.90	3.55	3.81	3.05
FeO	10.68	10.98	11.54	8.81	10.20	35.26	34.75	35.73	34.86	34.78	35.30
ZnO	0.00	0.00	0.00	0.00	0.00	0.00	0.00	0.00	0.00	0.02	0.00
Na ₂ O	0.02	0.00	0.04	0.01	0.01	0.03	0.00	0.02	0.00	0.01	0.03
K ₂ O	0.00	0.02	0.00	0.00	0.02	0.00	0.00	0.00	0.00	0.00	0.01
total	95.49	97.19	98.73	96.96	98.44	98.20	98.58	98.69	98.87	99.03	99.14
Atomic proportions											
Si	6.0059	6.0021	6.0154	5.9693	6.9579	5.9621	5.9472	5.9577	5.9636	5.9571	5.9573
Ti	0.0214	0.0255	0.0159	0.0363	0.008	0.2	0.16	0.0011	0.11	0.002	0.1
Al	3.9261	3.9488	3.9629	3.9438	3.3787	3.973	4.405	3.9536	3.9821	3.9622	3.9763
V	0	0	0	0	0	0	0	0.0008	0	0.0016	0
Cr	0.001	0	0.0059	0	0.0033	0	0	0	0.47	0	0.48
Mg	0.3908	0.3564	0.3989	0.2959	0.3428	0.6221	0.5927	0.5207	0.6356	0.5522	0.6661
Ca	0.7941	0.7327	0.7876	1.0418	0.5271	0.1403	0.1171	0.112	0.17	0.1138	0.181
Mn	3.355	3.4035	3.2179	3.5078	2.7826	0.4589	0.5406	0.6751	0.4948	0.6649	0.4237
Fe	1.5103	1.527	1.5736	1.2264	1.3392	4.8869	4.7905	4.8193	4.79	4.7884	4.8369
Zn	0	0	0	0	0	0	0	0.0076	0	0.0048	0.5
Na	0.008	0.0005	0.0125	0.0022	0.0033	0.81	0.12	0.0131	0	0.0058	0.94
K	0.0008	0.0037	0	0.0005	0.0034	0	0.4	0.0059	0	0	0.15
pyrope (Mg)	6.50	5.92	6.67	4.93	6.87	10.46	9.97	11.26	10.66	9.66	11.22
almandine (Fe)	24.46	25.37	26.32	19.25	26.83	79.47	78.97	79.87	78.20	79.65	78.59
spessartine (Mn)	55.82	56.54	53.83	58.45	55.74	7.71	9.09	6.82	8.29	8.84	7.14
grossular (Ca)	13.21	12.17	13.17	17.36	10.56	2.36	1.97	2.05	2.85	1.85	3.05

TABLE 1: ELECTRON MICROPROBE ANALYSES OF GARNETS FROM SCOTTS CREEK (BASED ON 24 OXYGENS)

Sample #	1113-38 garnet 1 scan										1113-38 garnet 2 scan			
	1	2	3	4	5	6	7	8	9	10	1	2	3	4
Wt.% cations														
SiO ₂	36.1898	36.4211	36.3127	36.3239	36.4922	36.2589	36.3065	36.4829	36.1382	36.3269	36.4696	36.4472	36.4123	36.5402
TiO ₂	0	0.0034	0.0362	0	0.0306	0	0.0408	0	0.0159	0.0091	0	0	0	0
Al ₂ O ₃	20.5112	20.4924	20.5453	20.4506	20.3421	20.4399	20.578	20.2737	20.3946	20.4543	20.4032	20.503	20.5342	20.453
V ₂ O ₃	0.0146	0.0065	0.0162	0	0	0.0211	0	0	0.0125	0.006	0.0049	0.0147	0.0218	0.0093
Cr ₂ O ₃	0	0.0143	0	0.0285	0.0321	0	0.0107	0.0321	0	0	0	0.0107	0.0143	0.0143
MgO	2.092	2.0851	2.1742	2.2392	2.2228	2.2005	2.1569	2.1891	2.2474	2.1301	2.6091	2.7869	2.8185	2.7421
CaO	0.6053	0.6113	0.6751	0.7561	0.8065	0.7341	0.6918	0.6899	0.6446	0.6373	0.6536	0.6713	0.7446	0.9375
MnO	5.0599	4.8569	4.812	4.7721	4.7315	4.8297	4.767	4.8956	4.762	4.8599	3.8109	3.2901	3.6402	3.7457
FeO	34.8061	34.4631	34.7558	34.7021	34.5295	35.1867	34.4715	34.7997	34.7353	35.1375	35.043	35.6132	35.1006	34.8391
ZnO	0.047	0	0	0.0026	0	0.0288	0.0706	0	0.0392	0.0628	0.1129	0	0	0
Na ₂ O	0.0479	0.0273	0.0137	0.0243	0.0243	0.0343	0.025	0.0076	0.0182	0.0412	0.0084	0.0266	0.0038	0
K ₂ O	0.0325	0.0077	0.018	0.0068	0	0.0214	0.0146	0.012	0	0.0283	0.0086	0	0.0034	0.0017
total	99.4551	99.0401	99.3591	99.3951	99.2158	99.768	99.1717	99.3854	99.0513	99.7188	99.1241	99.3763	99.3568	99.318
Atomic proportions														
Si	5.9498	5.9907	5.963	5.9622	5.9938	5.9461	5.9668	5.9925	5.9571	5.9577	5.9854	5.9644	5.9566	5.9773
Ti	0	0.0004	0.0045	0	0.0038	0	0.005	0	0.002	0.0011	0	0	0	0
Al	3.9743	3.9726	3.9763	3.9562	3.9378	3.9505	3.9858	3.9247	3.9622	3.9536	3.9465	3.9543	3.959	3.9432
V	0.0019	0.0009	0.0021	0	0	0.0028	0	0	0.0016	0.0008	0.0006	0.0019	0.0029	0.0012
Cr	0	0.0019	0	0.0037	0.0042	0	0.0014	0.0042	0	0	0	0.0014	0.0019	0.0019
Mg	0.5127	0.5112	0.5322	0.5478	0.5442	0.5379	0.5283	0.5359	0.5522	0.5207	0.6382	0.6798	0.6872	0.6686
Ca	0.1066	0.1077	0.1188	0.133	0.1419	0.129	0.1218	0.1214	0.1138	0.112	0.1149	0.1177	0.1305	0.1643
Mn	0.7046	0.6767	0.6693	0.6635	0.6583	0.6709	0.6636	0.6811	0.6649	0.6751	0.5298	0.456	0.5044	0.519
Fe	4.7855	4.7407	4.773	4.7635	4.743	4.8256	4.7378	4.7803	4.7884	4.8193	4.8097	4.8738	4.802	4.766
Zn	0.0057	0	0	0.0003	0	0.0035	0.0086	0	0.0048	0.0076	0.0137	0	0	0
Na	0.0153	0.0087	0.0044	0.0077	0.0077	0.0109	0.008	0.0024	0.0058	0.0131	0.0027	0.0084	0.0012	0
K	0.0068	0.0016	0.0038	0.0014	0	0.0045	0.0031	0.0025	0	0.0059	0.0018	0	0.0007	0.0004
pyrope (Mg)	8.68857	8.56169	8.94165	9.216723	9.09632	9.09772	8.8925874	8.957961	9.291468	8.805344	10.70339	11.42892	11.54427	11.18616
almandine (Fe)	77.5632	78.3019	77.8175	77.38497	77.529	77.3744	77.889543	77.62942	77.60592	77.88552	78.4859	78.92546	77.79137	77.38219
spessartine (Mn)	11.9413	11.3322	11.2452	11.1613	11.00236	11.3463	11.16773	11.38338	11.18703	11.41551	8.883415	7.666804	8.47218	8.682651
grossular (Ca)	1.80702	1.80423	1.99568	2.237009	2.372327	2.18158	2.0501398	2.029245	1.915575	1.89363	1.927293	1.978815	2.19218	2.748994

TABLE 1: ELECTRON MICROPROBE ANALYSES OF GARNETS FROM SCOTTS CREEK (BASED ON 24 OXYGENS)

Sample #	1113-38 garnet 2 scan									1113-38 garnet 3 scan								
	Wt.% cations	5	6	7	8	9	1	2	3	4	5	6	7	8	9			
SiO2	36.4111	36.3619	36.2732	36.228	36.3389	36.6399	36.3298	36.4006	36.5181	36.4151	36.2178	36.4022	36.5108	36.2224				
TiO2	0.041	0	0.0148	0	0	0	0	0	0.0362	0	0	0.0147	0	0				
Al2O3	20.4475	20.3807	20.4169	20.2998	20.4454	20.5519	20.4606	20.5802	20.4251	20.6695	20.5407	20.5695	20.5857	20.4625				
Y2O3	0	0	0.0327	0.0114	0	0	0.0027	0.0304	0.0087	0	0.006	0	0.0108	0				
Cr2O3	0	0	0.0358	0	0	0	0.0143	0.0571	0.0179	0	0	0.0036	0.025	0				
MgO	2.7782	2.7518	2.8097	2.742	2.7432	2.568	2.4058	2.4862	2.3147	2.2275	2.2173	2.2439	2.3469	1.9758				
CaO	0.8856	0.8571	0.8877	0.7415	0.631	0.6541	0.6464	0.8178	0.8355	0.9131	0.9445	0.9768	0.8906	0.7738				
MnO	3.6205	3.6476	3.6811	3.7361	3.5135	3.8554	4.3956	4.7786	5.942	6.6124	6.7197	6.3656	6.0824	4.8663				
FeO	34.6698	34.5181	35.0554	35.0666	35.4456	35.0751	34.7594	34.781	33.8318	33.1536	33.0823	32.9539	34.2143	35.2563				
ZnO	0.0788	0.0394	0	0.0131	0.0262	0.0314	0.0078	0.0235	0	0	0	0.0576	0	0.1125				
Na2O	0.0235	0.0061	0.025	0.0137	0.0122	0.0355	0.0023	0.0076	0.0106	0.025	0.022	0.031	0.0091	0.0252				
K2O	0.0077	0	0.0052	0	0.006	0.012	0.0051	0	0.0034	0	0	0.0034	0.0137	0.0094				
Total	98.9636	98.5627	99.254	99.003	99.4491	99.4373	99.0999	100.0394	100.0655	100.0163	99.7545	99.6223	100.7162	99.7235				
Atomic proportions																		
Si	5.9744	5.9869	5.9481	5.9557	5.9452	5.9891	5.9704	5.9369	5.9583	5.9445	5.9351	5.959	5.9317	5.9491				
Ti	0.0051	0	0.0018	0	0	0	0	0	0.0044	0	0	0.0018	0	0				
Al	3.9542	3.9549	3.9458	3.9331	3.9423	3.9593	3.9629	3.956	3.9277	3.9767	3.9671	3.9685	3.9417	3.9608				
V	0	0	0.0043	0.0015	0	0	0.0004	0.004	0.0011	0	0.0008	0	0.0014	0				
Cr	0	0	0.0046	0	0	0	0.0019	0.0074	0.0023	0	0	0.0005	0.0032	0				
Mg	0.6794	0.6753	0.6867	0.6719	0.6689	0.6257	0.5893	0.6044	0.5629	0.542	0.5416	0.5475	0.5683	0.4837				
Ca	0.1557	0.1512	0.156	0.1306	0.1106	0.1146	0.1138	0.1429	0.1461	0.1597	0.1658	0.1713	0.155	0.1362				
Mn	0.5032	0.5087	0.5113	0.5202	0.4869	0.5338	0.6119	0.6601	0.8212	0.9143	0.9327	0.8826	0.837	0.6769				
Fe	4.7574	4.7529	4.8073	4.821	4.8497	4.7947	4.7772	4.744	4.6163	4.5261	4.5338	4.5113	4.6486	4.8425				
Zn	0.0095	0.0048	0	0.0016	0.0032	0.0038	0.001	0.0028	0	0	0	0.007	0	0.0136				
Na	0.0075	0.0019	0.008	0.0044	0.0039	0.0113	0.0007	0.0024	0.0034	0.0079	0.007	0.0099	0.0029	0.008				
K	0.0016	0	0.0011	0	0.0013	0.0025	0.0011	0	0.0007	0	0	0.0007	0.0028	0.002				
pyrope (Mg)	11.4156	11.2958	11.5765	11.30039	11.27673	10.5011	9.8774477	10.19304	9.453049	9.141363	9.146261	9.228053	9.599014	8.176069				
almandine (Fe)	77.5156	77.6672	77.1762	77.75389	78.65172	78.618	77.960186	76.26453	74.30538	72.74551	72.30294	73.00912	73.64662	78.07977				
spessartine (Mn)	8.45325	8.50804	8.61823	8.749158	8.207057	8.95837	10.254748	11.13243	13.78896	15.41963	15.75037	14.87536	14.13607	11.44253				
grossular (Ca)	2.61563	2.52893	2.629	2.196555	1.86449	1.922259	1.9076178	2.410013	2.45261	2.693496	2.800438	2.887467	2.618301	2.301628				

TABLE 2: ELECTRON MICROPROBE ANALYSES OF GARNETS FROM KANMANTOO AREA (BASED ON 24 OXYGENS)

Sample #	1113-18K		1113-18K		1113-18K		1113-282		1113-282		1113-8K		1113-8K		1113-100K		1113-100K	
	1c	1t	2c	2t	3c	3t	1c	1t	2	1	2	1c	1t	1c	1t	1c	1t	
SiO2	36.34	36.30	36.380	36.384	36.009	35.975	36.586	36.153	35.989	36.313	36.018	35.554	35.894					
TiO2	0.00	0.00	0.012	0.025	0.025	0.004	0.033	0.008	0.000	0.000	0.041	0.004	0.063					
Al2O3	20.39	20.41	20.377	20.522	20.289	20.265	20.803	20.632	20.606	20.380	20.374	20.065	20.000					
V2O3	0.00	0.00	0.000	0.000	0.000	0.000	0.000	0.000	0.000	0.000	0.002	0.000	0.000					
Cr2O3	0.05	0.00	0.027	0.027	0.018	0.000	0.005	0.022	0.000	0.025	0.014	0.030	0.041					
MgO	2.17	2.08	2.013	1.852	2.237	2.100	1.629	1.672	1.620	1.725	1.797	0.580	0.523					
CaO	0.43	0.25	1.096	0.269	0.429	0.335	1.526	0.443	0.323	0.930	0.211	0.951	1.305					
MnO	4.55	4.56	4.181	4.406	4.460	4.328	1.247	1.277	1.306	1.619	1.682	0.533	0.444					
FeO	35.49	35.43	35.393	35.320	34.306	34.906	38.219	39.175	38.851	38.332	38.949	40.686	40.827					
ZnO	0.00	0.00	0.000	0.000	0.000	0.000	0.025	0.000	0.018	0.000	0.008	0.000	0.000					
Na2O	0.02	0.02	0.001	0.010	0.034	0.045	0.032	0.000	0.006	0.028	0.019	0.015	0.000					
K2O	0.00	0.01	0.019	0.013	0.030	0.007	0.004	0.002	0.004	0.006	0.012	0.009	0.006					
total	99.4474	99.0576	99.498	98.8279	97.8368	97.9638	100.1071	99.3836	98.7229	99.3679	99.1448	98.427	99.1017					
Atomic Proportion																		
Si	5.9723	5.985	5.9736	6.0034	5.9907	5.9886	5.9676	5.9581	5.9656	5.981	5.958	5.967	5.9829					
Ti	0	0	0.0015	0.0031	0.0032	0.0005	0.004	0.001	0	0.000	0.005	0.0005	0.0079					
Al	3.949	3.9651	3.9435	3.9909	3.9781	3.9758	3.9992	4.0074	4.0256	3.956	3.972	3.9689	3.9289					
V	0	0	0	0	0	0	0	0	0	0.000	0.000	0	0					
Cr	0.0065	0	0.0035	0.0035	0.0024	0	0.0006	0.0028	0	0.003	0.002	0.004	0.0054					
Mg	0.532	0.5115	0.4926	0.4554	0.5547	0.521	0.396	0.4107	0.4003	0.423	0.443	0.1451	0.13					
Ca	0.0756	0.0446	0.1928	0.0475	0.0765	0.0597	0.2667	0.0783	0.0574	0.164	0.037	0.171	0.233					
Mn	0.6339	0.6372	0.5814	0.6158	0.6285	0.6102	0.1723	0.1782	0.1833	0.226	0.236	0.0757	0.0626					
Fe	4.8772	4.8858	4.8602	4.8738	4.7731	4.8594	5.2134	5.3991	5.3856	5.280	5.388	5.7104	5.691					
Zn	0	0	0	0	0	0	0.0032	0	0.0023	0.000	0.001	0	0					
K	0.017	0.005	0.001	0.008	0.026	0.033	0.023	0.000	0.005	0.000	0.000	0	0					
pyrope (Mg)	8.9281	8.57	8.26	7.600	9.308	8.745	6.66	6.89	6.719	7.103	7.451	2.437	2.170					
almandine (Fe)	79.165	80.0	78.8	81.33	78.863	80.01	85.96	88.80	89.24	86.35	87.96	93.418	92.894					
spessartine (Mn)	10.638	10.7	9.74	10.28	10.546	10.24	2.90	2.991	3.076	3.79	3.96	1.272	1.046					
grossular (Ca)	1.268	0.75	3.23	0.793	1.2832	1.001	4.484	1.313	0.964	2.75	0.628	2.872	3.890					

TABLE 2: ELECTRON MICROPROBE ANALYSES OF GARNETS FROM KANMANTOO AREA (BASED ON 24 OXYGENS)

Sample #	1113-100K		1113-100K		1113-27K		1113-27K		1113-27K		1113-27K		1113-27K		1113-27K		1113-28K		1113-28K		1113-28K		1113-28K		
Wt.% Cations	2c	2r	1	2c	2r	3c	3r	4	1c	1r	2c	2r	1c	1r	2c	2r	1c	1r	2c	2r	1c	1r	2c	2r	
SiO ₂	35.472	35.840	36.494	36.164	36.113	36.289	36.652	35.956	36.060	36.157	35.461	35.446	36.060	36.157	35.461	35.446	36.060	36.157	35.461	35.446	36.060	36.157	35.461	35.446	
TiO ₂	0.022	0.052	0.025	0.000	0.038	0.041	0.037	0.017	0.034	0.000	0.022	0.035	0.034	0.000	0.022	0.035	0.034	0.000	0.022	0.035	0.034	0.000	0.022	0.035	
Al ₂ O ₃	20.077	19.951	20.588	20.323	20.425	20.423	20.472	20.324	20.131	20.228	20.245	19.994	20.131	20.228	20.245	19.994	20.131	20.228	20.245	19.994	20.131	20.228	20.245	19.994	
V ₂ O ₃	0.000	0.000	0.000	0.000	0.000	0.000	0.000	0.000	0.000	0.000	0.000	0.000	0.000	0.000	0.000	0.000	0.000	0.000	0.000	0.000	0.000	0.000	0.000	0.000	
Cr ₂ O ₃	0.004	0.025	0.014	0.000	0.025	0.004	0.014	0.016	0.015	0.033	0.000	0.000	0.015	0.033	0.000	0.000	0.015	0.033	0.000	0.000	0.015	0.033	0.000	0.000	
MgO	0.542	0.534	1.694	2.040	1.926	2.214	2.143	1.982	1.793	1.572	1.800	1.818	1.793	1.572	1.800	1.818	1.793	1.572	1.800	1.818	1.793	1.572	1.800	1.818	
CaO	1.260	1.459	0.214	0.258	0.237	0.980	0.222	0.275	1.083	0.283	1.107	1.184	1.083	0.283	1.107	1.184	1.083	0.283	1.107	1.184	1.083	0.283	1.107	1.184	
MnO	0.536	0.554	0.977	1.249	1.495	1.324	1.259	1.044	1.395	1.678	1.405	1.400	1.395	1.678	1.405	1.400	1.395	1.678	1.405	1.400	1.395	1.678	1.405	1.400	
FeO	41.262	40.382	38.765	38.904	39.028	37.789	38.589	39.385	37.541	38.367	37.648	37.221	37.541	38.367	37.648	37.221	37.541	38.367	37.648	37.221	37.541	38.367	37.648	37.221	
ZnO	0.000	0.000	0.000	0.000	0.000	0.000	0.000	0.000	0.000	0.000	0.000	0.000	0.000	0.000	0.000	0.000	0.000	0.000	0.000	0.000	0.000	0.000	0.000	0.000	
Na ₂ O	0.010	0.037	0.043	0.026	0.026	0.024	0.050	0.033	0.009	0.043	0.033	0.031	0.009	0.043	0.033	0.031	0.009	0.043	0.033	0.031	0.009	0.043	0.033	0.031	
K ₂ O	0.000	0.000	0.030	0.001	0.000	0.019	0.000	0.002	0.005	0.000	0.000	0.005	0.005	0.000	0.000	0.005	0.005	0.000	0.000	0.005	0.005	0.000	0.000	0.005	
total	99.184	98.8337	98.8445	98.9646	99.3142	99.1061	99.4385	99.0334	98.0661	98.3644	97.721	97.1327	98.0661	98.3644	97.721	97.1327	98.0661	98.3644	97.721	97.1327	98.0661	98.3644	97.721	97.1327	
Atomic Proportion																									
Si	5.9284	5.9861	6.0196	5.9779	5.9577	5.9711	6.009	5.9517	5.9651	5.9382	6.132	6.17	5.9651	5.9382	6.132	6.17	5.9651	5.9382	6.132	6.17	5.9651	5.9382	6.132	6.17	
Ti	0.0027	0.0065	0.0031	0	0.0048	0.0051	0.0046	0.0021	0.44	0.28	0	0.42	0.44	0.28	0	0.42	0.44	0.28	0	0.42	0.44	0.28	0	0.42	
Al	3.9545	3.9273	4.0024	3.9593	3.9713	3.9605	3.9557	3.965	3.9655	3.9955	3.9648	3.9489	3.9655	3.9955	3.9648	3.9489	3.9655	3.9955	3.9648	3.9489	3.9655	3.9955	3.9648	3.9489	
V	0	0	0	0	0	0	0	0	0	0	0	0	0	0	0	0	0	0	0	0	0	0	0	0	
Cr	0.0005	0.0033	0.0019	0	0.0032	0.0005	0.0018	0.0021	0	0	0.44	0.2	0	0	0.44	0.2	0	0	0.44	0.2	0	0	0.44	0.2	
Mg	0.1351	0.1329	0.4165	0.5027	0.4737	0.543	0.5237	0.489	0.4559	0.4494	0.3898	0.4447	0.4559	0.4494	0.3898	0.4447	0.4559	0.4494	0.3898	0.4447	0.4559	0.4494	0.3898	0.4447	
Ca	0.2257	0.2612	0.0378	0.0457	0.042	0.1728	0.039	0.0488	0.2135	0.1986	0.505	0.1931	0.2135	0.1986	0.505	0.1931	0.2135	0.1986	0.505	0.1931	0.2135	0.1986	0.505	0.1931	
Mn	0.0759	0.0784	0.1365	0.1748	0.2089	0.1845	0.1748	0.1463	0.1996	0.1992	0.2363	0.1967	0.1996	0.1992	0.2363	0.1967	0.1996	0.1992	0.2363	0.1967	0.1996	0.1992	0.2363	0.1967	
Fe	5.7671	5.6405	5.3475	5.378	5.3846	5.2001	5.291	5.4521	5.2383	5.2723	5.3361	5.2254	5.2383	5.2723	5.3361	5.2254	5.2383	5.2723	5.3361	5.2254	5.2383	5.2723	5.3361	5.2254	
Zn	0	0	0	0	0	0	0	0	0	0	0.2	0	0	0	0.2	0	0	0	0.2	0	0	0	0.2	0	
pyrope (Mg)	2.280	2.226	3.769	8.433	7.967	9.121	8.755	8.243	7.415	6.512	7.591	7.665	7.415	6.512	7.591	7.665	7.415	6.512	7.591	7.665	7.415	6.512	7.591	7.665	
almandine (Fe)	92.631	92.086	92.388	87.868	87.814	84.877	87.672	88.468	86.087	88.698	85.690	85.390	86.087	88.698	85.690	85.390	86.087	88.698	85.690	85.390	86.087	88.698	85.690	85.390	
spessartine (Mn)	1.281	1.313	2.946	2.932	3.514	3.099	2.922	2.466	3.279	3.948	3.365	3.355	3.279	3.948	3.365	3.355	3.279	3.948	3.365	3.355	3.279	3.948	3.365	3.355	
grossular (Ca)	3.809	4.375	0.897	0.766	0.706	2.903	0.652	0.822	3.219	0.843	3.354	3.590	3.219	0.843	3.354	3.590	3.219	0.843	3.354	3.590	3.219	0.843	3.354	3.590	

TABLE 2: ELECTRON MICROPROBE ANALYSES OF GARNETS FROM KANMANTOO AREA (BASED ON 24 OXYGENS)

Sample#	A1113-2K	A1113-2K	A1113-5K	A1113-5K	A1113-5K	A1113-5K	A1113-7K	A1113-7K	A1113-7K	A1113-7K	A1113-34K	A1113-34K
Wt%	core	rim	core	rim	core	rim	icore	irim	2core	2rim	rim	core
SiO ₂	36.6018	36.3213	36.2753	36.3129	36.2983	35.8557	36.4063	36.5353	36.7061	36.3856	36.1046	35.9348
TiO ₂	0.06	0.027	0.0203	0	0.0181	0.0214	0	0	0.0113	0	0.0369	0
Al ₂ O ₃	20.4455	20.5138	20.6798	20.3542	20.3952	20.4039	20.6966	20.6055	20.5891	20.3275	20.2794	20.3004
Y ₂ O ₃	0.0238	0	0	0.0167	0.0049	0.0043	0.0151	0.0151	0	0.0108	0	0
Cr ₂ O ₃	0.0036	0.0177	0.0634	0.0141	0	0.0211	0.1056	0	0	0	0.037	0.0388
MgO	1.9906	1.6312	1.7884	1.5123	1.85	1.6961	2.5367	2.3939	2.6818	2.6555	1.733	2.1367
CaO	1.3613	0.404	0.359	0.3324	0.5428	0.2224	0.1765	0.2338	0.2221	0.3414	0.2622	0.2888
MnO	4.3983	4.7243	1.5495	1.759	1.7202	1.7363	0.5761	0.6462	0.5084	0.5221	0.855	0.8652
FeO	35.52	36.4393	39.4508	39.5139	38.5807	39.3857	39.3048	39.3774	39.0582	38.936	39.102	38.6799
ZnO	0.0287	0	0.0782	0.0287	0.0287	0.0651	0	0.0339	0.0209	0	0	0
Na ₂ O	0.0327	0.0429	0.0338	0.0354	0.0076	0.0146	0.0228	0.0328	0.016	0.0312	0.0227	0.0242
K ₂ O	0.0085	0.0171	0	0	0	0.0102	0	0	0	0.0009	0.0073	0
total	100.4748	100.1454	100.3846	99.8795	99.4657	99.4368	99.8474	99.8976	99.8139	99.2125	98.44	98.2688
Atomic Proportions												
Si	5.9602	5.9556	5.9269	5.9755	5.9754	5.9311	5.9479	5.9687	5.9852	5.9779	5.9976	5.9725
Ti	0.0073	0.0033	0.0025	0	0.0022	0.0027	0	0	0.0014	0	0.0046	0
Al	3.9238	3.9643	3.9822	3.9475	3.957	3.9778	3.9851	3.9674	3.9567	3.936	3.9703	3.9765
V	0.0031	0	0	0.0022	0.0006	0.0006	0.002	0.002	0	0.0014	0	0
Cr	0.0005	0.0023	0.0082	0.0018	0	0.0028	0.0136	0	0	0	0.0049	0.0051
Mg	0.4832	0.3987	0.4355	0.3709	0.4539	0.4182	0.6177	0.5829	0.6518	0.6503	0.4291	0.5293
Ca	0.2375	0.071	0.0628	0.0586	0.0957	0.0394	0.0309	0.0409	0.0388	0.0601	0.0467	0.0514
Mn	0.6066	0.6561	0.2144	0.2452	0.2399	0.2433	0.0797	0.0894	0.0702	0.0727	0.1203	0.1218
Fe	4.8371	4.9968	5.3905	5.4378	5.3114	5.4485	5.3702	5.3799	5.3261	5.3497	5.4322	5.3763
Zn	0.0035	0	0.0094	0.0035	0.0035	0.008	0	0.0041	0.0025	0	0	0
Na	0.0103	0.0136	0.0251	0.0263	0.0057	0.0108	0.0169	0.0243	0.0118	0.0231	0.0073	0.018
K	0.0018	0.0036	0	0	0	0.0085	0	0	0	0.0007	0.0015	0
pyrope (Mg)	8.1335256	6.7287847	7.3833436	6.2343798	7.6040675	7.0729495	10.410355	9.8067128	10.909932	10.914598	7.1697349	8.8854812
almandine (Fe)	77.6566	80.999738	87.916341	88.660222	86.774573	88.146119	87.725562	88.000645	87.265384	86.857404	90.040557	88.206818
spessartine (Mn)	10.211776	11.073592	3.6349766	4.1204321	4.0176749	4.1142955	1.3434328	1.5042015	1.1752298	1.2193734	2.0099824	2.0444454
grossular (Ca)	3.9980984	1.1978862	1.0653386	0.9849657	1.6036843	0.6666539	0.5206501	0.688441	0.6494549	1.008625	0.779726	0.8632556

TABLE 3: ELECTRON MICROPROBE ANALYSES OF GARNETS FROM ANGAS PROSPECT (BASED ON 24 OXYGENS)

	Sample A1113-90 with garnet-quartz rich band from Angas Prospect, DDH 31.											
	1c	1r	3c	3r	2c	2r	4c	4r	7c	7r	5c	5r
Wt.%												
SiO ₂	36.274	36.2385	35.6304	36.1865	36.3597	72.8134	36.3378	36.1173	36.1325	35.9378	36.2451	36.1268
TiO ₂	0.0185	0.0149	0.7187	0.0328	0.061	0	0.0299	0	0.0472	0.0262	0.0442	0.0376
Al ₂ O ₃	20.3142	20.193	19.6055	20.2141	20.0201	9.4172	20.339	20.0785	20.1209	19.8954	20.1802	20.0847
V ₂ O ₃	0	0	0	0	0	0	0	0	0	0	0	0
Cr ₂ O ₃	0	0.0464	0	0	0.0234	0.0116	0	0.025	0.0071	0.0427	0	0
MgO	2.2272	2.1973	1.8418	2.076	1.9522	0.9589	1.9949	2.0471	2.0047	1.8708	1.8725	1.9393
CaO	1.0239	0.8481	2.2189	0.9009	2.0748	0.5615	1.8049	0.9691	1.0926	0.6931	1.7493	0.8127
MnO	5.3302	4.9643	7.0543	5.6777	5.9859	2.5213	5.1151	5.022	4.7558	4.2913	6.1563	4.7833
FeO	33.0985	33.221	30.8021	33.2014	31.6839	15.7777	32.7592	33.2992	34.3017	34.9521	32.272	34.2134
ZnO	0	0	0	0	0	0	0	0	0	0	0	0
Na ₂ O	0	0.0116	0.0201	0.0101	0.0231	0.0288	0.0085	0.0271	0	0.0389	0.0201	0.0233
K ₂ O	0.0021	0.0034	0.0196	0.0026	0.0064	0	0.0175	0	0.003	0.0201	0.0077	0.0175
total	98.2887	97.7385	97.9114	98.3022	98.1905	102.0903	98.4068	97.5852	98.4655	97.7685	98.5474	98.0387
Si	16.9561	16.9395	16.6553	16.9152	16.9962	34.0363	16.9859	16.8829	16.89	16.799	16.9426	16.8873
Ti	0.0111	0.0089	0.4309	0.0197	0.0366	0	0.0179	0	0.0283	0.0157	0.0265	0.0225
Al	10.7515	10.6874	10.3764	10.6985	10.5959	4.9841	10.7646	10.6268	10.6492	10.5298	10.6806	10.63
V	0	0	0	0	0	0	0	0	0	0	0	0
Cr	0	0.0317	0	0	0.016	0.008	0	0.0171	0.0049	0.0292	0	0
Mg	1.3433	1.3252	1.1108	1.2521	1.1774	0.5783	1.2031	1.2346	1.209	1.1283	1.1293	1.1696
Ca	0.7318	0.6062	1.5859	0.6439	1.4829	0.4013	1.29	0.6926	0.7809	0.4954	1.2502	0.5809
Mn	4.128	3.8446	5.4633	4.3972	4.6359	1.9526	3.9614	3.8893	3.6832	3.3235	4.7678	3.7045
Fe	25.728	25.8232	23.9429	25.808	24.6284	12.2643	25.4642	25.884	26.6632	27.1688	25.0856	26.5946
Zn	0	0	0	0	0	0	0	0	0	0	0	0
Na	0	0.0086	0.0149	0.0075	0.0171	0.0213	0.0063	0.0201	0	0.0289	0.0149	0.0173
K	0.0018	0.0028	0.0163	0.0021	0.0053	0	0.0146	0	0.0025	0.0167	0.0064	0.0146
pyrope (Mg)	9.1491018	9.0551563	7.4488168	8.4470039	7.9291586	8.2330674	8.116714	8.4315088	8.2629272	7.7983528	7.5706673	7.9361753
almandine (Fe)	75.385763	76.807799	69.889379	75.791023	72.19838	76.000784	74.778789	76.946003	77.361437	79.960436	73.202218	78.550421
spessartine (Mn)	12.441833	11.62482	16.211394	13.127118	13.815095	12.300832	11.825918	11.753428	11.138578	10.1645	14.143397	11.122835
grossular (Ca)	3.0233023	2.5122245	6.4504104	2.634855	6.0573662	3.4653165	5.2785793	2.86906	3.2370583	2.0767117	5.0837177	2.3905691

TABLE 3: ELECTRON MICROPROBE ANALYSES OF GARNETS FROM ANGAS PROSPECT (BASED ON 24 OXYGENS)

	A113-90	6c	6r	8c	8r	4c	4r	3c	3r	exhalite	exhalite	Ic	Ir
Wt.%													
SiO2	34.8716	37.2803	36.4009	38.0599	36.1524	36.2351	35.8171	34.7512	36.1187	36.3331	35.9409	36.082	
TiO2	0.0042	0.0078	0.0485	0.0367	0.0462	0.0287	0.4864	0	0.087	0.0084	0.0156	0.0264	
Al2O3	19.5633	21.1788	20.3191	22.0069	20.6098	20.5883	20.1968	19.6567	20.1899	20.311	20.4295	20.5434	
Y2O3	0	0	0	0	0	0	0	0	0	0	0	0	
Cr2O3	0.0198	0	0.0233	0.0433	0	0.0306	0.0082	0.0112	0.0297	0	0.0447	0.0226	
MgO	1.85	1.9664	1.9569	1.9682	1.8975	1.8285	1.7939	1.8989	1.7276	2.0653	2.1467	2.1154	
CaO	3.5979	0.746	1.525	0.7025	1.2042	0.7227	1.8113	0.7016	1.8923	0.8773	1.5873	0.6748	
MnO	4.5133	4.1904	5.9058	5.071	4.2201	4.345	6.3281	5.1606	7.6708	5.4768	5.1896	4.8091	
FeO	32.1017	34.968	32.3177	31.9784	34.1828	35.0354	31.7778	33.8309	30.9067	33.0877	32.8848	33.7207	
ZnO	0	0	0	0	0.028	0.0596	0.0228	0.0648	0.0123	0	0.0175	0	
Na2O	0.0193	0.0139	0.0316	0.0441	0.0205	0.0008	0.0174	0.0138	0	0	0.0121	0	
K2O	0.0017	0.0801	0.0167	0.6837	0	0.0136	0.0033	0.0318	0.0025	0	0	0.0174	
total	96.5428	100.4316	98.5455	100.5945	98.3615	98.8885	98.2633	96.1214	98.6375	98.1597	98.2687	98.0117	
Si	16.3006	17.4265	17.0154	17.7909	16.8993	16.9379	16.7425	16.2443	16.8835	16.9838	16.8004	16.8664	
Ti	0.0025	0.0047	0.029	0.022	0.0277	0.0172	0.2916	0	0.0522	0.005	0.0094	0.0158	
Al	10.3541	11.2091	10.7541	11.6474	10.9079	10.8966	10.6894	10.4035	10.6858	10.7498	10.8126	10.8728	
V	0	0	0	0	0	0	0	0	0	0	0	0	
Cr	0.0136	0	0.016	0.0296	0	0.0209	0.0056	0.0077	0.0203	0	0.0306	0.0154	
Mg	1.1158	1.186	1.1803	1.187	1.1444	1.1028	0.0819	1.1452	1.0419	1.2456	1.2947	1.2758	
Ca	2.5714	0.5332	1.0899	0.502	0.8606	0.5165	1.2946	0.5015	1.3525	0.627	1.1344	0.4823	
Mn	3.4954	3.2453	4.5738	3.9273	3.2683	3.3651	4.9009	3.9966	5.9408	4.2416	4.0191	3.7244	
Fe	24.9532	27.1811	25.121	24.8573	26.5708	27.2336	24.7014	26.2973	24.0243	25.7196	25.5618	26.2116	
Zn	0	0	0	0	0.022	0.0468	0.0179	0.0509	0.0096	0	0.0138	0	
Na	0.0143	0.0103	0.0235	0.0327	0.0152	0.0006	0.0129	0.0102	0	0	0.009	0	
K	0.0014	0.0665	0.0138	0.5675	0	0.0113	0.0027	0.0264	0.0021	0	0	0.0144	
pyrope (Mg)	7.3968215	8.0255288	7.9742979	8.448853	7.8369705	7.5336395	7.3160851	7.8093436	6.9700323	8.4743634	8.6960683	8.722787	
almadine (Fe)	72.009114	80.067932	73.883982	77.014284	78.684077	80.153721	72.709368	78.057028	69.956852	76.1687	74.736511	78.00912	
spessartine (Mn)	10.253904	9.7180446	13.6749	12.369261	9.9040035	10.172349	14.664777	12.059637	17.585466	12.769457	11.945576	11.268035	
grossular (Ca)	10.340161	2.1884943	4.4668201	2.1676025	3.574949	2.1402905	5.3097699	2.0739907	5.4876497	2.5874792	4.6218452	2.0000582	

TABLE 3: ELECTRON MICROPROBE ANALYSES OF GARNETS FROM ANGAS PROSPECT (BASED ON 24 OXYGENS)

Surface sample A1113-281 of garnet-quartz cotecule, Angas prospect												
A1113-281	1	1 2r	3c	3r	4c	4r						
Wt.%												
SiO2	36.6261	36.6919	43.5709	36.7814	36.9832	36.5114	36.6714					
TiO2	0.3279	0.2938	0.1458	0.2089	0.0279	0.2044	0.0985					
Al2O3	20.1299	19.9382	18.403	20.4377	20.9318	20.4315	20.5707					
V2O3	0	0	0	0	0	0	0					
Cr2O3	0.0137	0.083	0.0409	0.0485	0	0	0.0289					
MgO	1.9557	1.9169	1.6613	1.8353	1.9649	2.0258	1.8898					
CaO	4.5702	4.7671	3.5602	4.5376	3.6627	4.6918	4.7138					
MnO	15.5942	15.7023	14.9373	15.8224	16.2294	16.1641	16.0169					
FeO	19.605	19.3516	18.2862	19.2553	19.1651	18.9243	19.5245					
ZnO	0.0333	0	0	0.007	0.0529	0	0.0176					
Na2O	0	0.011	0.0036	0	0.0037	0.0162	0.0325					
K2O	0.0004	0.0078	0	0	0	0.0186	0.0335					
total	98.8565	98.7639	100.6093	98.9342	99.0214	98.9882	99.5981					
Si	17.1207	17.1515	20.367	17.1933	17.2876	17.0671	17.1419					
Ti	0.1966	0.1762	0.0874	0.1252	0.0167	0.1226	0.0591					
Al	10.654	10.5525	9.74	10.8169	11.0784	10.8136	10.8873					
V	0	0	0	0	0	0	0					
Cr	0.0094	0.0568	0.028	0.0332	0	0	0.0198					
Mg	1.1795	1.1561	1.002	1.1069	1.185	1.2218	1.1397					
Ca	3.2664	3.4071	2.5445	3.2431	2.6178	3.3533	3.369					
Mn	12.0771	12.1609	11.5684	12.2538	12.569	12.5185	12.4045					
Fe	15.2393	15.0423	14.2142	14.9674	14.8973	14.7101	15.1767					
Zn	0.0262	0	0	0.0055	0.0416	0	0.0139					
Na	0	0.0082	0.0027	0	0.0027	0.012	0.0241					
K	0.0003	0.0065	0	0	0	0.0155	0.0278					
pyrope (Mg)	7.9107161	7.7530978	7.2333494	7.406371	7.9965647	8.2597795	7.7124107					
almandine (Fe)	42.958971	42.299984	44.668449	43.149305	43.758267	40.54038	41.317102					
spessartine (Mn)	35.842499	36.087823	36.956012	36.282096	37.530736	37.449414	37.142778					
grossular (Ca)	13.287815	13.859095	11.14219	13.162228	10.714432	13.750427	13.827709					

TABLE 3: ELECTRON MICROPROBE ANALYSES OF GARNETS FROM ANGAS PROSPECT (BASED ON 24 OXYGENS)

Wt.%	Sample A1113-2An from inner garnite envelope of Angas Pb-Zn deposit (below A1113-90)											
	Ic	1r	2c	2r	3c	3r	4c	4r	1c	1r	2c	2r
SiO2	36.8219	36.3254	36.4392	36.9629	36.761	37.1719	36.9426	36.8511	36.1042	36.306	36.5084	36.4966
TiO2	0.0586	0.006	0.3785	0.0188	0.2851	0.0456	0.214	0.0319	0.0133	0.0043	0.2012	0.0494
Al2O3	20.7551	20.2458	19.799	21.0937	19.702	20.6356	20.2039	20.7997	20.6692	20.7267	19.8824	20.7739
V2O3	0	0	0	0	0	0	0	0	0	0	0	0
Cr2O3	0	0.0181	0.0387	0	0.0528	0.0289	0	0	0.0354	0.0093	0.0329	0.1091
MgO	2.0913	1.5317	0.4012	2.1971	0.3706	2.0812	2.1448	2.3052	2.1966	1.9309	0.6155	2.0566
CaO	3.7358	2.9077	7.3392	4.5497	8.6945	5.223	4.7314	2.1828	1.9069	2.3493	9.8358	6.4999
MnO	15.4233	16.6994	25.2309	15.7776	22.9369	15.5448	15.0321	15.9799	15.6209	15.5625	18.4947	15.868
FeO	21.0483	20.5641	9.7045	19.066	10.4996	18.2344	20.0123	21.0587	21.6194	21.3154	12.5918	16.5774
ZnO	0.0562	0.0649	0.0368	0.0176	0	0.0281	0.0176	0.0123	0	0	0	0
Na2O	0.0052	0	0.0022	0	0.016	0	0	0.0022	0.0315	0.0054	0	0.0277
K2O	0	0.0095	0	0	0.0119	0.0124	0	0	0	0.0039	0	0.026
total	99.9956	98.3728	99.3702	99.6833	99.3305	99.0059	99.2986	99.2239	98.1975	98.2136	98.1627	98.4846
Si	17.2122	16.9802	17.0333	17.2781	17.1838	17.3758	17.2687	17.2259	16.8767	16.8767	16.9711	17.0657
Ti	0.0351	0.0036	0.2269	0.0113	0.1709	0.0273	0.1283	0.0191	0.008	0.0026	0.1206	0.0296
Al	10.9848	10.7153	10.4789	11.1641	10.4275	10.9216	10.6932	11.0085	10.9394	10.9698	10.523	10.9948
V	0	0	0	0	0	0	0	0	0	0	0	0
Cr	0	0.0124	0.0265	0	0.0361	0.0198	0	0	0.0242	0.0064	0.0225	0.0746
Mg	1.2613	0.9238	0.242	1.3251	0.2235	1.2552	1.2935	1.3903	1.3248	1.1646	0.3712	1.2404
Ca	2.67	2.0781	5.2454	3.2517	6.214	3.7329	3.3816	1.5601	1.3629	1.6791	7.0297	4.6455
Mn	11.9448	12.9331	19.5403	12.2191	17.7638	12.0388	11.6418	12.3759	12.0978	12.0526	14.3234	12.2892
Fe	16.3612	15.9848	7.5434	14.8203	8.1615	14.1739	15.5558	16.3692	16.8051	16.5688	9.7878	12.8859
Zn	0.0442	0.051	0.0289	0.0138	0	0.0221	0.0138	0.0097	0	0	0	0
Na	0.0038	0	0.0016	0	0.0118	0	0	0.0016	0.0233	0.004	0	0.0206
K	0	0.0079	0	0	0.0098	0.0103	0	0	0	0.0032	0	0.0216
pyrope (Mg)	8.4690478	6.296363	1.6298657	8.8590555	1.4976002	8.3587438	8.6186748	9.321806	9.0962279	7.9328533	2.5023955	8.4302961
almandine (Fe)	45.165606	46.10547	18.695834	41.805256	20.579837	41.087026	43.391345	47.614822	48.470936	48.799052	26.027477	35.457718
spessartine (Mn)	35.490913	39.006639	58.243203	36.149322	52.667998	35.475943	34.323768	36.718685	36.756827	36.330437	42.726448	36.960412
grossular (Ca)	10.874434	8.5915285	21.431097	13.186367	25.254564	15.078287	13.666212	6.3446868	5.6760088	6.9376584	28.74368	19.151574

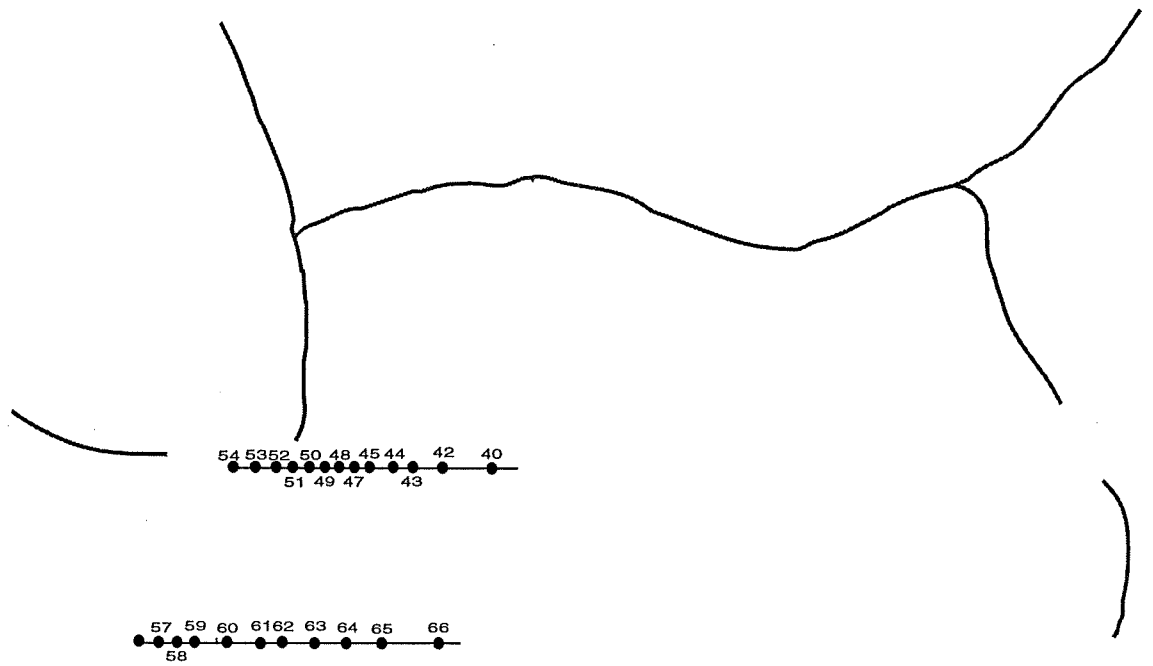


Figure 2. STRUCTURAL INTERPRETATION OF SCOTTS CREEK SHEAR ZONE